PHASE STABILITY AND DEFECT STRUCTURE DETERMINATION OF POLYTITANATE COMPOUNDS IN THE BaO-TiO_2 SYSTEM

Jafar Javadpour

B.Sc., SUNY at Stony Brook, 1980

M.Sc., SUNY at Stony Brook, 1983

A thesis presented to the faculty
of the Oregon Graduate Center
in partial fulfillment of the
requirements for the degree
Doctor of Philosophy
in
Materials Science and Engineering

January, 1988

The Thesis "Phase Stability and Defect Structure Determination of Polytitanate Compounds in the BaO-TiO_2 System" by Jafar Javadpour has been examined and approved by the following Examination Committee:

Nicholas G. Eror, Thesis Advisor
Professor
Department of Materials Science and Engineering

William E. Wood
Professor
Chairman
Department of Materials Science and Engineering

Jack H. Devletian
Professor
Department of Materials Science and Engineering

Paul R. Davis
Associate Professor
Department of Applied Physics and
Electrical Engineering

ACKNOWLEDGEMENTS

The author wishes to express his sincere gratitude to his advisor, Dr. Nicholas Eror and the other members of his thesis committee, Drs. William Wood, Jack Devletian and Paul Davis for their time and helpful discussions. The author also would like to thank Bonnie Comegys, Xuefeng Zhou and Dan Danks for their help in preparing this manuscript. Finally, the author would like to thank the support staff at the Oregon Graduate Center.

To my parents, for their endless

support from a far-away land.

TABLE OF CONTENTS

LIST OF ILLUSTRATIONS

LIST OF TABLES

Phase Stability and Defect Structure Determination of

Polytitanate Compounds in the BaO-TiO_2 System

Jafar Javadpour, Ph.D.

Oregon Graduate Center, 1988

Supervising Professor: Nicholas G. Eror

ABSTRACT

Polytitanates in the BaO-TiO_2 system with Ba:Ti ratios ranging from 1:2 to 1:5 were prepared using a low temperature technique developed by Pechini. The samples were heated at 600 to 1300°C in oxygen. Room temperature Raman spectroscopy was used to investigate the phase relations in this system. Results of this study indicate the following: except for $BaTi_4O_9$, the powders of these compounds were amorphous when heated at 600°C for 4hrs; the compound $BaTi_2O_5$ is a low temperature stable phase; $Ba_6Ti_{17}O_{40}$ forms only at temperatures above 1100°C; $Ba_4Ti_{13}O_{30}$ does not form below 1000°C; the single phase $BaTi_4O_9$ structure was observed at 1200°C; the $Ba_2Ti_9O_{20}$ phase is obtained only after

long heat treatment at 1200°; $BaTi_5O_{11}$ was stable up to 1200°C, at which it decomposes into $Ba_2Ti_9O_{20}$ and TiO_2. After determination of stability relationships in this system, the electrical conductivities of these compounds were examined as a function of temperature and oxygen partial pressure. For all the temperatures (850-1150°C) studied, the conductivities of these compounds increased with decreasing oxygen partial pressure resulting in n-type properties throughout the whole P_{O_2} range (10^{-19} - 1atm). The P_{O_2} dependencies of the electrical conductivity were found to be linear for an extensive range of oxygen partial pressures. On the basis of structural considerations the conductivity data was described by a majority defect model consisting of both singly and doubly ionized oxygen vacancies. For lower oxygen partial pressure values a drastic change in the electrical conductivity was observed. This is believed to result from increasing defect interaction for larger departures from stoichiometry. A defect model based on this interaction is proposed to account for the observed sharp change in the electrical conductivity values.

I. INTRODUCTION

The compositions of most dielectric materials utilized for ceramic capacitors are based on ferroelectric barium titanate ($BaTiO_3$). This is because this ceramic material has an exceptionally high dielectric constant. One of the most important properties of any dielectric material is the dependency of the dielectric constant on frequency. $BaTiO_3$ cannot be used as capacitors in circuits where microwave-frequency stability is needed [28]. Compounds in the system BaO-TiO_2 have been extensively studied for use in microwave-frequency applications [29-33]. These polytitanate materials have shown promising properties such as high dielectric constant, low temperature coefficient of the dielectric constant and low dielectric loss [36].

Rase and Roy [39] published the first comprehensive phase equilibria study of the BaO-TiO_2 system. They reported five intermediate compounds in this system; Ba_2TiO_4, $BaTiO_3$, $BaTi_2O_5$, $BaTi_3O_7$ and $BaTi_4O_9$. Several subsequent investigations have presented contradictory data on compound composition and stability. For example, Tillmanns [40] assigned $Ba_4Ti_{13}O_{30}$ to the compound previously designated as $BaTi_3O_7$ by Rase and Roy [39]. Jonker and Kwestroo [50] reported the existence of the phases $Ba_2Ti_5O_{12}$ and $Ba_2Ti_9O_{20}$ and questioned the ability of $BaTi_2O_5$ to form by solid state reaction. Their work also indicates that the single phase $Ba_2Ti_9O_{20}$ was obtained only when small amounts of SnO_2 or

ZrO_2 were present. The phase $Ba_2Ti_9O_{20}$ was confirmed by O'Bryan and Thomson [51]. However, they suggested that substitutions were not required in stabilizing the phase. In more recent work done on this system, Negas and Roth [38] have observed polytitanates at ratios of 6:17, 4:13, 1:4 and 2:9. In the same study they indicated that the compound reported as $Ba_2Ti_5O_{12}$ appears to have been mistaken for $Ba_6Ti_{17}O_{40}$. Because of all these inconsistencies, we re-examined the phase stability relations in this system using Raman spectroscopy. Results of this study have been compared with the most recent published data on BaO-TiO_2 phase diagram. It should be mentioned that the Raman spectra are being reported for the first time on these compounds. With knowledge of the spectra of the various polytitanates, they may be investigated by Raman spectroscopy with a spacial resolution of $\sim$ 1μm. Also, in view of the influence of defect structure upon transport properties, measurement of the high temperature electrical conductivity was chosen as a means of examining the role of point defects in these materials. The nature of predominant defects was determined by matching the experimental data to predictions based upon thermodynamic relations. The results of this study show that control of the oxygen pressure and temperature at which a crystal is equilibrated offers the possibility of varying the room temperature conductivity over several orders of magnitude.

II. LITERATURE REVIEW

A. Nonstoichiometric Compounds

Nonstoichiometric phases are found in many oxide systems at high temperatures. This behavior is observed especially in compounds where a cation can exist in several oxidation states. A good example is provided by ferrous oxide (FeO). The composition FeO is unstable under all conditions of temperature and pressure. Preparation at various oxygen pressures yields phases with the same structure, but the unit cell size varies smoothly with pressure, indicating change of composition. The phase varies in composition by leaving some divalent Fe sites vacant. To balance each Fe divalent vacancy, two cations must be oxidized to trivalent Fe. Hence FeO shows deficiency in the Fe sublattice. In systems such as TiO_2 and CeO_2, cation reduction from the tetravalent to the trivalent state is the basic cause of nonstoichiometry. The electronic species created on oxidation or reduction perturb the charge balance in a crystal. The charge balance may also be perturbed by aliovalent dopant ions (ones whose charge differs from that of the host lattice ions). In the majority of nonstoichiometric compounds, the charge balance is restored by creation of charge compensating point defects. These defects influence the physical properties of the solid to a high degree. Explanation of properties such as electrical transport, luminescence,

diffusion and ability to react chemically requires the knowlege of defect structures in materials. The nature of these defects is developed in the following section.

B. Defect Theories

i. Small Deviation From Stoichiometry

A crystal in thermodynamic equilibrium at a finite temperature always contains a finite concentration of defects. The introduction of such defects into a crystal increases the lattice energy. However, the existence of native defects in a lattice arises from a tendency of a crystal to increase its entropy. The number of defects will be limited, however, by the enthalpy necessary to form the defects. The actual number of defects present at any temperature is that which gives the minimum value of the thermodynamic potential of the system. In pure crystals lattice defects are referred to as native defects. The two principle inherent thermodynamic defects are:

(a) Schottky Defects. These involve the presence of vacant cation lattice sites and vacant anion lattice sites in equal numbers for charge compensation. Defects of this type are formed as a result of the diffusion of a certain number of cations and the equivalent number of anions from their lattice positions to the surface of the crystal, as shown in Fig. 1a.

(b) Frenkel Defects. These consists of equal numbers of vacant lattice sites and interstitial ions. These defects are formed by ions leaving their normal lattice site to take up interstitial positions, as illustrated in Fig. 1b. For a given crystal,

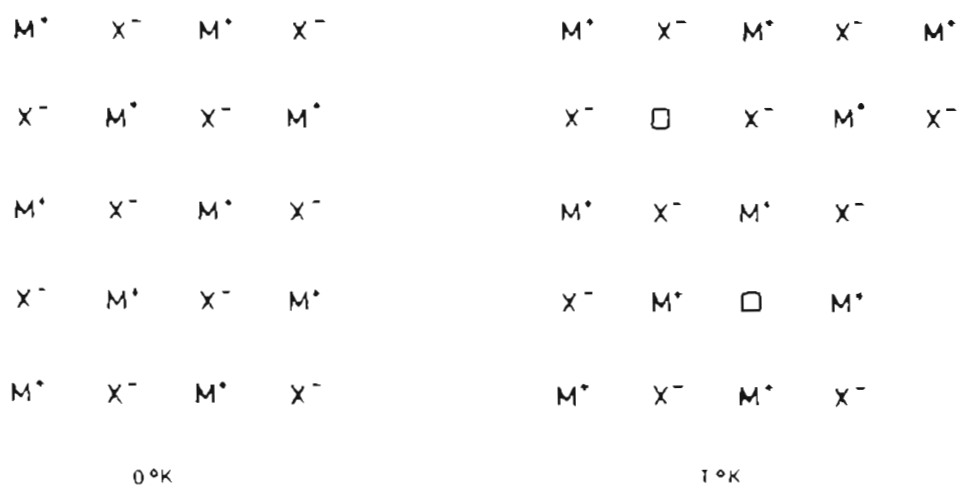

Figure-1a. Creation of a Schottky defect in a crystal MX. The ideal crystal at absolute zero is completely regular; above this temperature equal numbers of vacancies are formed in anion and cation sublattices.

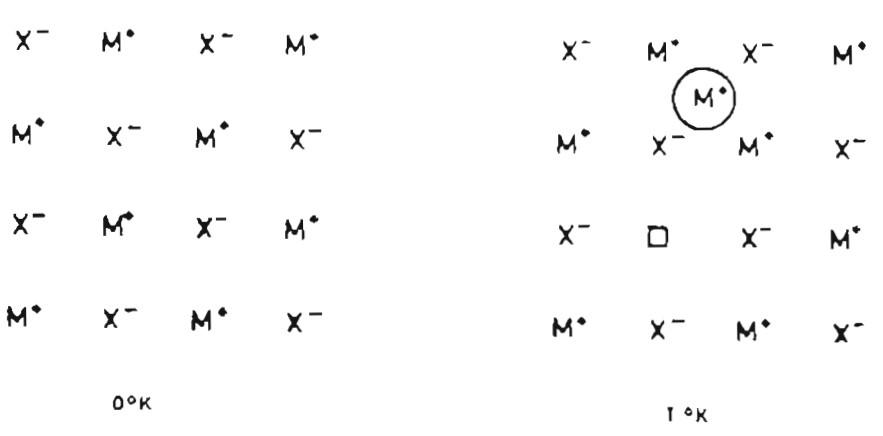

Figure-1b. Creation of a Frenkel defect in a crystal MX. The ideally regular crystal at absolute zero is disordered by having an interstitial ion with simultaneous formation of a vacancy.

the activation energies of the formation of Schottky and Frenkel are sufficiently different that one type is dominant.

Since point defects occur in thermal equilibrium within the material, they

the activation energies of the formation of Schottky and Frenkel are sufficiently different that one type is dominant.

Since point defects occur in thermal equilibrium within the material, they can be treated as chemical species in terms of equilibrium constants and the mass action law. The principles of this theory were created by Schottky & Wagner [1-2]. In later years considerable progress in the theory of point defects was made as a result of fundamental research carried out by Kroger & Vink [3]. Employing the laws of statistical thermodynamics, these authors derived general relationships between equilibrium concentrations of the point defects and dependence of these concentrations on temperature and partial pressures of crystal components present in the gas phase surrounding the crystal. In addition to the intrinsic defects mentioned above there may be defects formed on the crystal surface as a result of chemical reactions between the solid phase and the surrounding atmosphere. As a result of diffusion at sufficiently high temperatures, these surface defects migrate into the bulk of the lattice until a thermodynamic equilibrium between the defect crystal and its surrounding is established. In some oxide systems these defects create nonstoichiometric phases which extend over a considerable composition range. The deviations from stoichiometry are manifested as an excess or a deficit of a component of the compound. At small deviation from stoichiometry the interaction between these defects is ignored. In describing the defects the notation proposed by Kroger & Vink [3] is used throughout. In this system the type of imperfection is indicated by a capital letter, the location is described by a subscript and the charge of the defect relative to the normal lattice is indicated by a superscript. Vacancies or interstitials

in an oxide are thus written

V_o , oxygen vacancy

V_m , metal vacancy

O_i , oxygen interstitial

M_i , metal interstitial

The point defects may be neutral or charged. Singly and doubly ionized vacancies are, for instance written as $V_o^{\cdot}$ and $V_o^{\cdot\cdot}$, respectively. The superscript dot represents a positive charge. Similarly, singly & doubly ionized cation vacancies are written as $V_m^{'}$ and $V_m^{''}$, where the superscript primes indicate the negative effective charges. For an illustration of the defect formation let us take the simple case of an oxygen deficient oxide. An oxygen vacancy is formed by transfer of an oxygen atom on a normal site to the gaseous state. The defect reaction for this process may be written as

$$O_o = V_o + 1/2O_2 \tag{1}$$

Electrons may, depending on the temperature, be excited and freed from the vacancy. Thus, the oxygen vacancy acts as a donor and becomes singly or doubly ionized:

$$V_o = V_o^{\cdot} + e' \tag{2}$$

or

$$V_o = V_o^{\cdot\cdot} + 2e' \tag{3}$$

e′, in the above equations is an electron. The equilibrium constant for the latter

reaction is

$$K(T) = \frac{[e']^2[V_o^{\cdot\cdot}]P_{O_2}^{1/2}}{[O_o]} \tag{4}$$

If doubly ionized oxygen vacancies are the predominating defects in the oxygen deficient oxide, the electroneutrality condition requires that

$$[n] = 2[V_o^{\cdot\cdot}] \tag{5}$$

By combination of (4) and (5) an expression for the concentration of free electrons can be obtained

$$[e'] = [2k(T)]^{1/3}P_{O_2}^{-1/6} = 2^{1/3}P_{O_2}^{-1/6}\exp(-\Delta G/3RT) \tag{6}$$

where ΔG is the enthalpy to create an oxygen vacancy and two conduction band electrons. Therefore, in an oxygen deficient oxide where doubly ionized vacancies predominate, the concentration of electrons will be a function of the ambient oxygen partial pressure. The following rules must be obeyed in writing defect reactions:

(1) Mass Balance. The mass balance must be maintained; the number of atoms involved in the defect reaction must be the same before and after the defect formation. Vacancies have zero mass.

(2) Electrical Neutrality. The compounds must remain electrically neutral. This means that both sides of the equations have the same total effective charge.

(3) Lattice Site Relations. The site relation must always be maintained. Thus in a compound MO, the number of M sites should always be equal to the number of

O sites, regardless of whether the actual composition is stoichiometric or non-stoichiometric.

(4) Site-Relation. The total number of sites may change in a defect reaction; therefore, the defect equation may include the creation or annihilation of sites.

ii. Large Deviation From Stoichiometry

The presence of a high concentration of point defects in some compounds is unfavorable from the energy point of view and causes a decrease in their stability. These point defects could be eliminated from the lattice by the formation of planar defects known as shear planes (SP), first defined by Anderson et al [4] and later by a number of investigators, notably Bursill & Hyde [5], J. S. Anderson [6], and S. Anderson and A. D. Wadsley [7-8]. Shear planes are formed by a process known as crystallographic shear (CS). In oxide systems, in essence, this involves a rearrangement of the mode of linkage between coordination polyhedra so that the oxygen to metal ratio is modified. The schematic illustration of shear plane formation is given in Fig. 2a and 2b. As the number of shear planes increases they begin to interact with each other, leading to their consequent ordering along definite crystallographic direction. When the width of unperturbed portions of parent structure between the successive shear planes are the same, a new crystallographic structure is formed. The overall stoichiometric composition of the resulting crystals depends upon the thickness of parent lattice between the shear planes and also on the number of anion sites eliminated from this fault plane. Ordered distribution of defects is thermodynamically more stable because the decrease of the (ΔH) in the process compensates the entropy decrease which

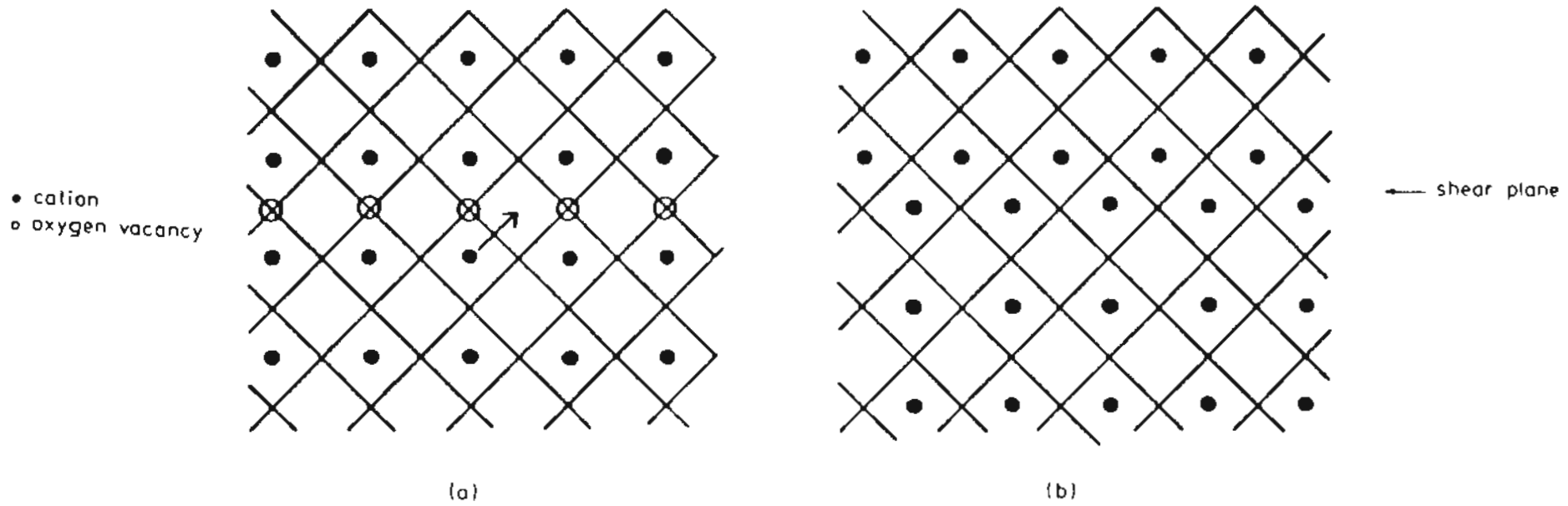

Figure-2. Schematic representation of defect elimination by crystallographic shear. (a) A hypothetical reduced oxide with aligned oxygen vacancies. Shear of bottom half of the crystal in the direction shown superimposes lattice atoms on these vacancies, giving the structure shown in (b) where the vacancies have been eliminated but a fault is present on the cation sublattice.

occurs upon ordering [9-11]. The most notable examples of this behavior are found in oxides of refractory metals, such as TiO_2 [5,12-15], Nb_2O_6 [16-17], WO_3 [18-22] etc., which show considerable deviation from stoichiometry in the direction of deficit of oxygen. In strongly reduced TiO_2, for example, crystallographic shear is a means by which ordered oxygen vacancies are eliminated from the crystal lattice. As a result of this process homologous series of titanium oxides with the general formula Ti_nO_{2n-1} are generated. These homologous series are intermediate phases with the values of $n = 4\text{-}9$ and 16-36 [23]. The difference between the basic structures of the phases lies in the width of the rutile (TiO_2) type slabs and the orientation of the shear planes.

C. Experimental Methods of Investigating Nonstoichiometry

Changes in stoichiometry may be inferred from measurements which are sensitive to composition. Electrical conductivity, electron spin resonance, lattice parameter, seebeck coefficient, density measurements, and optical measurements are all sensitive to composition and provide means of detecting nonstoichiometry. However, with the exception of electrical conductivity, most physical properties are difficult to measure at high temperatures. The electrical conductivity, σ, is given by

$$\sigma = nq\mu \tag{7}$$

where n is the number of charge carriers, q is charge per unit carrier and μ is their mobility. If μ is known from Hall measurements, then n, the concentration of charge carriers, may be calculated from conductivity measurements. The

temperature dependence of the electrical conductivity can give information about the migration energies of defects and their heats of formation. This is because the number of charge carriers is proportional to $\exp(-E_f/2RT)$ and mobility is proportional to $\exp(-E_m/RT)$ where E_f is defect formation energy and E_m is defect migration energy. Hence the eq. 7, can be rewritten in the following manner

$$\sigma = \text{Const} \times \exp - \frac{(E_m + 1/2E_f)}{RT} \tag{8}$$

and plot of log σ vs $1/T$ gives the quantity $(E_m + 1/2E_f)$. The migration energy E_m can be determined from the temperature variation of conductivity of doped crystals where the number of defects is held constant by the addition of impurity atoms. Obtaining E_m in this way enables E_f to be calculated. The departure from stoichiometry at elevated temperatures may also be studied using the thermogravimetric method [24-27] by measuring the percent weight change of a specimen (quenched or in situ) as a function of temperature and oxygen content of the gaseous atmosphere surrounding the specimen. The weight change is recorded as as a function of time; when the new equilibrium is obtained the weight change of the specimen remains constant. The procedure is then repeated for other values of P_{O_2} and temperature. In this type of experiment care must be taken to eliminate various weighing errors (vibration, adsorption and desorption).

D. Titanates

The compositions of most dielectric materials used for ceramic capacitors are based on ferroelectric compounds such as $BaTiO_3$. Recent progress in microwave integrated circuits requires dielectric materials which are stable in these ranges of frequencies. $BaTiO_3$ cannot be used as capacitors in tuned circuits or filters where microwave-frequency stability is needed [28]. Polytitanate compounds from the Ti-rich end of the system $BaO-TiO_2$ were investigated as candidates for microwave applications [29-33]. Two compositions, $BaTi_4O_9$ and $Ba_2Ti_9O_{20}$, in the system $BaO-TiO_2$ exhibited attractive dielectric properties such as low dielectric loss and a dielectric constant which is both high and temperature stable at microwave frequencies. Masse and co-workers [34-35], in their study of microwave measurement of $BaTi_4O_9$, reported that the ceramic has a high dielectric constant (k=39) with a negative temperature coefficient and a low dielectric loss (Q=2500). In investigating the microwave properties of $Ba_2Ti_9O_{20}$, O'Bryan [36] pointed out that it was even more useful than $BaTi_4O_9$ as a microwave dielectric resonator filter. He reported a dielectric constant value of (k=39.8) and a dielectric loss of (Q=8000) at 4 GHz for this material. These properties make this compound suitable for use in microwave dielectric resonators. He also recognized that the dielectric properties of this compound are sensitive to the conditions of fabrications, particularly atmosphere. Optimum properties were obtained when the ceramics were fully dense and oxidized. With the aim of improving the the microwave properties of this ceramic, Nomura et al [37], studied the effect of Mn doping on the dielectric properties. They demonstrated

that the addition of Mn was quite effective in enhancing the value of Q. They attributed this improvement to the oxidizing role of Mn in the sintering process. Roth [38], using O'Bryan's data [36], predicted superior dielectric properties for the compound of composition $BaTi_5O_{11}$ if it could be formed as a single phase ceramic.

A number of investigators have studied the phase equilibria in the TiO_2-rich region of the system $BaO-TiO_2$. The data on the phase relations show many inconsistencies with respect to compound identification and stability. The system was first studied by Rase and Roy [39] and they reported the existence of $BaTiO_3$, $BaTi_2O_5$, $BaTi_4O_9$ and $BaTi_3O_7$. During a microprobe study of barium titanates, Tillmanns [40] assigned $Ba_4Ti_{13}O_{30}$ to the compound previously designated as $BaTi_3O_7$ by Rase and Roy [39]. The crystal structure of $BaTi_2O_5$ was first reported by Harrison [41]. Later Tillmanns [42] refined the crystal structure and described it as an almost close-packed array of barium and oxygen atoms with Ti atoms in octahedral voids. In this compound edge sharing TiO_6 octahedra form planar groups of 3-octahedra each, which are linked by common corners to the other groups in the plane (010). In the direction b, infinite zigzag chains are formed via common octahedral edges. $Ba_6Ti_{17}O_{40}$ is another example of a titanate which can be described in terms of close-packed arrays. The crystal structure of this phase has been reported by several investigators [43-45]. The structure is monoclinic and the unit cell contains 4-formula units of $Ba_6Ti_{17}O_{40}$. Barium and oxygen atoms are arranged in close-packed layers perpendicular to the [103] direction. The unit cell of $Ba_4Ti_{13}O_{30}$ contains six layers of close-packed atoms with four rows of six atoms per each layer [46]. There are 16 barium and

120 oxygen atoms in the unit cell as compared with 144 positions in the close-packed array; 8 of these positions must be vacant. A similar case has been observed in the crystal structure of $Ba_6Ti_{17}O_{40}$ [43], where two barium atoms are next nearest neighbors in the same row of the closest packing and the possible positions between them are not occupied. Of the 144 octahedral voids, 64 are coordinated by one barium and five oxygen atoms, 16 by barium and four oxygen atoms, eight by five oxygen atoms and one vacancy, and four by four oxygens and two vacancies leaving 52 voids coordinated by six oxygen atoms for the 52 titanium atoms. In the barium titanates octahedral interstices coordinated by both O and Ba atoms or five O atoms and one vacancy are never occupied by Ti atoms. The crystal structure of $BaTi_4O_9$ observed for the first time by Rase and Roy [39] is built up of sheets of edge-sharing TiO_6 octahedra [47-49]. The individual sheets share common corners and in between the sheets are tunnels which accommodate the Ba atoms. Jonker and Kwestroo [50] identified two additional phases which they formulated as $Ba_2Ti_5O_{12}$ and $Ba_2Ti_9O_{20}$. They found that the compound (2:9) is stabilized only by minute additions of SnO_2 or ZrO_2. They also classified $BaTi_2O_5$ as a metastable phase which forms only from a cooled liquid. The compound $Ba_2Ti_9O_{20}$ was confirmed by O'Bryan and Thomson [51] in their examination of the subsolidus phase relations in the BaO-TiO_2 system. In disagreement with Jonker & Kwestroo, O'Bryan found that substitutions are not required to stabilize the $Ba_2Ti_9O_{20}$ phase. The crystal structure of this phase was first reported by Tillmanns et al [52]. He described the unit cell as hexagonally close-packed layers of oxygen and barium ions; all Ti ions reside in the octahedral interstices located between these close packed layers. $BaTi_5O_{11}$ is

another compound in this system where the close packing of Ba and O atoms is clearly evident. The monoclinic crystal structure of this compound was reported by Tillmanns [53]. Subsequently the X-ray diffraction pattern of this phase was published by O'Bryan and Thomson [54]. Among the more recent papers on the subject reference should be made to the work done by Negas and Roth [38]. They observed higher polytitanates at Ba/Ti ratios of 6:17, 4:13, 1:4 and 2:9. One objective of the present work is to reinvestigate the phase relations in this system using Raman spectroscopy and compare the results to the most recent work done on this system.

E. Point Defects in Ternary Ionic Crystals

In this section the dependence of native point defect concentration on the oxygen partial pressure will be demonstrated for the case of ternary compound $BaTiO_3$ which is equivalent to ABO_3. First the relations are developed for the thermodynamic situation where the only defects present are V_A , V_B , V_O , $V_A^{'}$, $V_B^{'}$, $V_{\dot{O}}$, n and p and the following relations hold; $[V_A] = [V_B]$ and $[V_A^{'}] = [V_B^{'}]$. These assumptions lead to the following equilibrium constants, for the formation of point defects.

$$K_9 = [V_A][V_B][V_O]^3 \tag{9}$$

$$K_{10} = [V_A^{'}][V_B^{'}][V_{\dot{O}}]^3 \tag{10}$$

$$K_{11} = \frac{n[V_{\dot{O}}]}{[V_O]} \tag{11}$$

$$K_{12} = \frac{p[V_A^{'}]}{[V_A]} \tag{12}$$

$$K_{13} = \frac{p[V_B^{'}]}{[V_B]} \tag{13}$$

$$[n][p] = K_i \tag{14}$$

$$[V_O] = K_{15} P_{O_2}^{-1/2} \tag{15}$$

$$[V_A][V_B] = K_{16} P_{O_2}^{3/2} \tag{16}$$

$$[V_A] = [V_B] = K_{16}^{1/2} P_{O_2}^{3/4} \tag{17}$$

Furthermore the neutrality condition should be fulfilled. This condition may be written as follows:

$$[V_{\dot{O}}]+p = n+[V_B^{'}]+[V_A^{'}] \tag{18}$$

For solving this system of equations the method proposed by Brouwer is applied. This method consists of dividing the whole range of the oxygen pressure into the regions in which the two types of defects occurring in the neutrality condition predominate. At the low values of P_{O_2}, the singly ionized vacancies in the oxygen sublattice are the prevailing defects; in this case the neutrality condition reduces to

$$[V_{\dot{O}}] = [n] \tag{19}$$

For sufficiently large values of oxygen pressure P_{O_2}, $[V_A^{'}]$ and $[V_B^{'}]$ will be much greater than $[V_{\dot{O}}]$ and n. Therefore the neutrality condition assumes the form

$$[V_A'] + [V_B'] = [p] \tag{20}$$

For the intermediate values of oxygen pressures, there are two possible approximate solutions depending on the values of the equilibrium constant. These two conditions are

$$[V_{\dot{O}}] = [V_A'] + [V_B'] \tag{21}$$

and

$$[n] = [p] \tag{22}$$

The solution of the system of equations (15,16,19-22) can be obtained for particular ranges of the oxygen pressure P_{O_2}. These solutions are presented in Table I.

Table-I. P_{O_2} Dependence of Neutral and Singly Ionized Defect Concentrations in the Ternary Oxide ABO_3.

Defect	$[n] = [V_{\dot{O}}]$	$[n] \simeq [p]$	$[V_O'] \simeq [V_A'] + [V_B']$	$[p] \simeq [V_A'] + [V_B']$
$[n]$	-1/4	0	-5/8	-3/8
$[p]$	1/4	0	5/8	3/8
$[V_O]$	-1/2	-1/2	-1/2	-1/2
$[V_A] = [V_B]$	3/4	3/4	3/4	3/4
$[V_{\dot{O}}]$	-1/4	-1/2	1/8	-1/8
$[V_A'] = [V_B']$	1/2	3/4	1/8	3/8

Figs. 3 and 4 show the variation of defect concentrations as a function of oxygen

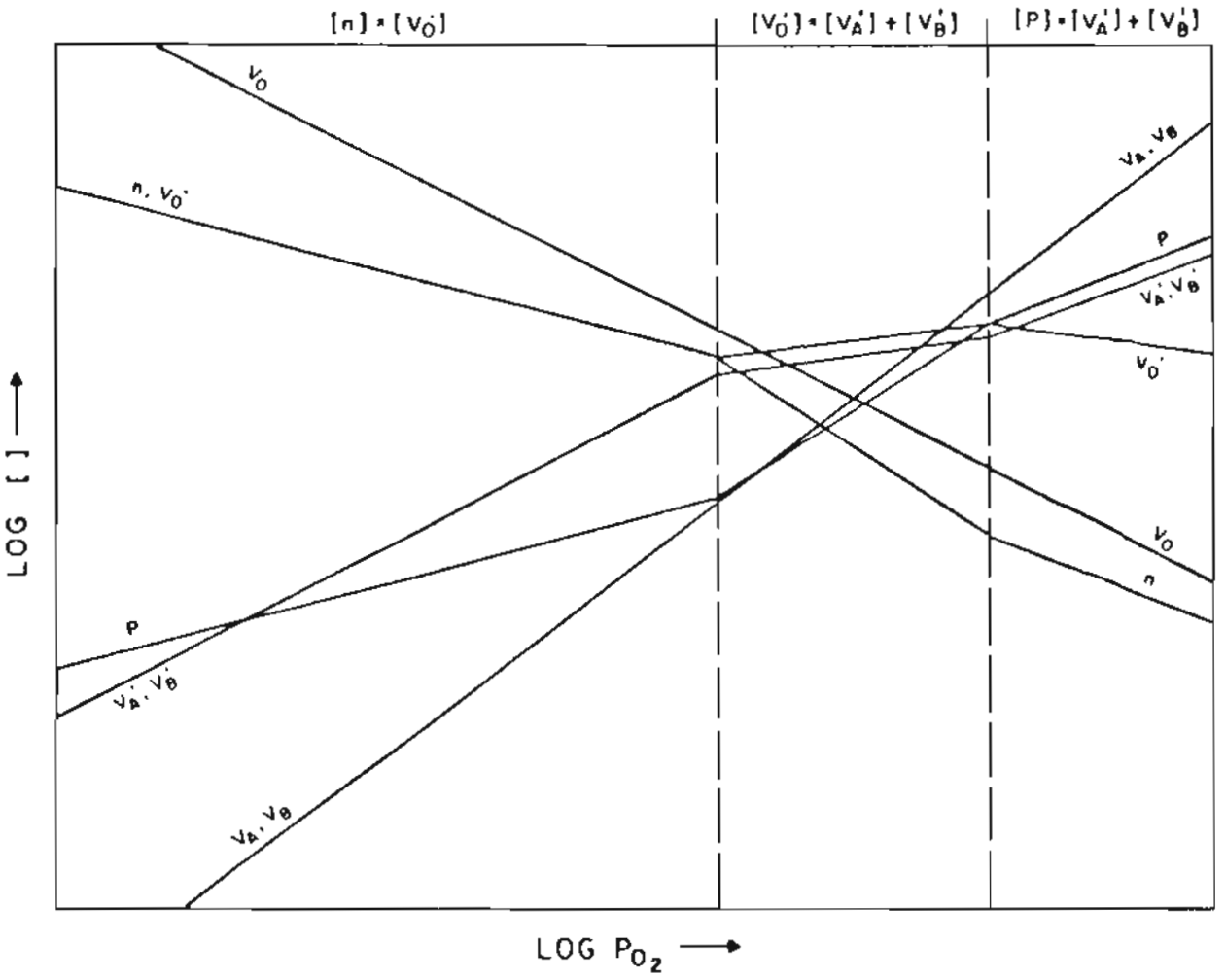

Figure-3. Calculated defect concentration vs. oxygen partial pressure in ABO_3. Neutral and singly charged defects only are considered. The concentrations of the two cations are assumed to be equal. Intermediate neutrality condition is $[V_O^{\cdot}] \simeq [V_A^{'}] + [V_B^{'}]$.

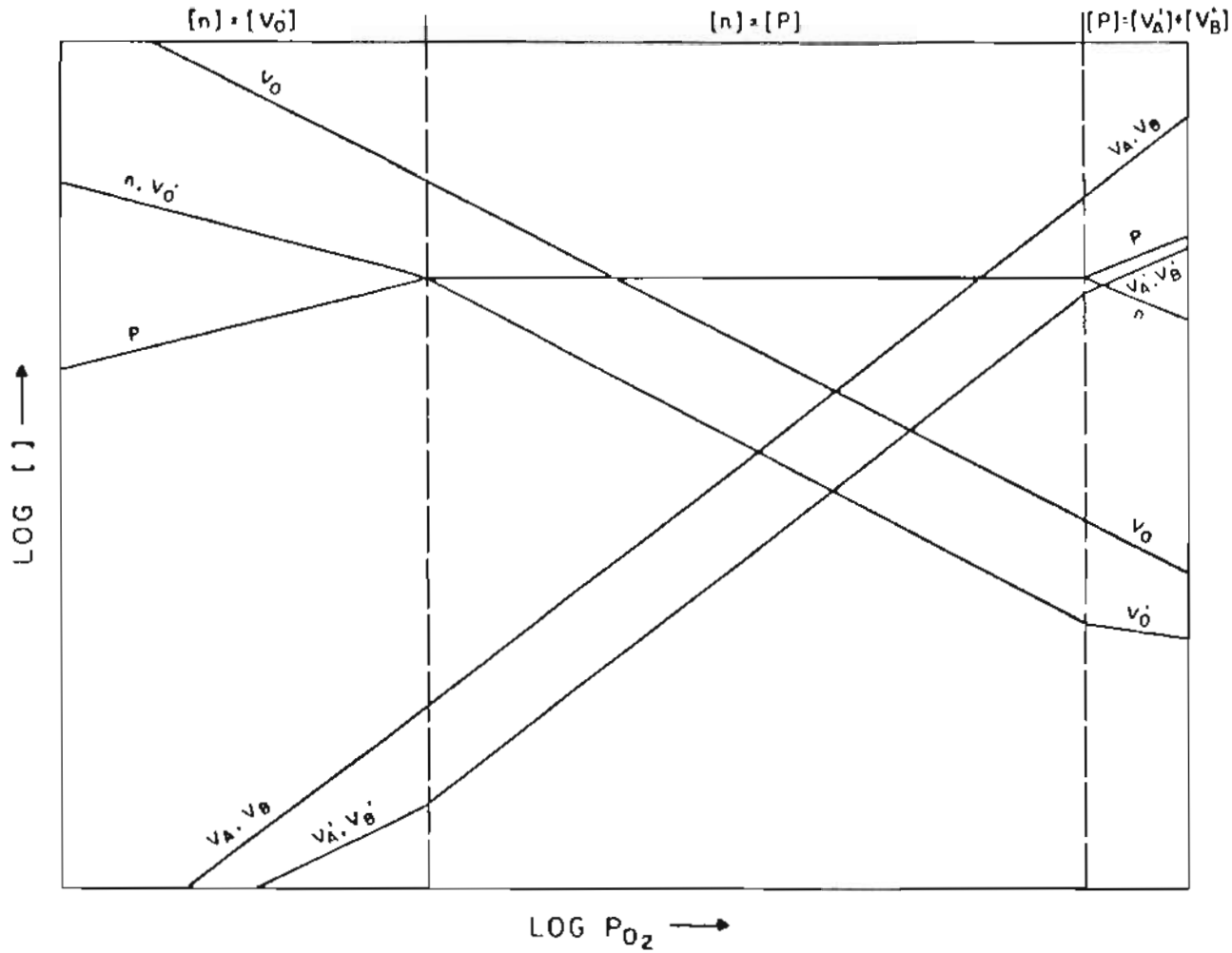

Figure-4. Concentrations of defects as in Figure 3, but with intermediate neutrality condition $|n| \simeq |p|$.

pressure for the two intermediate neutrality conditions. We can also consider the complete ionization of the defects. In this case the following sequence of neutrality conditions are expected with increasing values of oxygen pressure:

$$[n] = [V_{\dot{O}}] \tag{23}$$

$$[n] = 2[V_{\ddot{O}}] \tag{24}$$

$$[V_{\ddot{O}}] = [V_A^{''}] + 2[V_B^{''''}] \tag{25}$$

$$[p] = 2[V_A^{''}] + 4[V_B^{''''}] \tag{26}$$

$$[p] = [V_A^{'}] + 2[V_B^{''}] \tag{27}$$

The calculated P_{O_2} dependence of fully ionized defect concentrations is shown in Table II.

Table-II. P_{O_2} Dependence of Completely Ionized Defect Concentrations in the Ternary Oxide ABO_3.

Defect	$[n] \simeq 2[V_{\ddot{O}}]$	$[V_{\ddot{O}}] \simeq [V_A^{''}] \simeq 2[V_B^{''''}]$	$[n] \simeq [p]$	$[p] \simeq 2[V_A^{''}] + 4[V_B^{''''}]$
$[n]$	-1/6	-1/4	0	-3/16
$[p]$	1/6	1/4	0	3/16
$[V_{\ddot{O}}]$	-1/6	0	-1/2	-1/8
$[V_A^{''}]=[V_B^{''''}]$	5/12	0	3/4	3/16

Figs. 5 and 6 are the isothermal pressure dependence of various defect concentra-

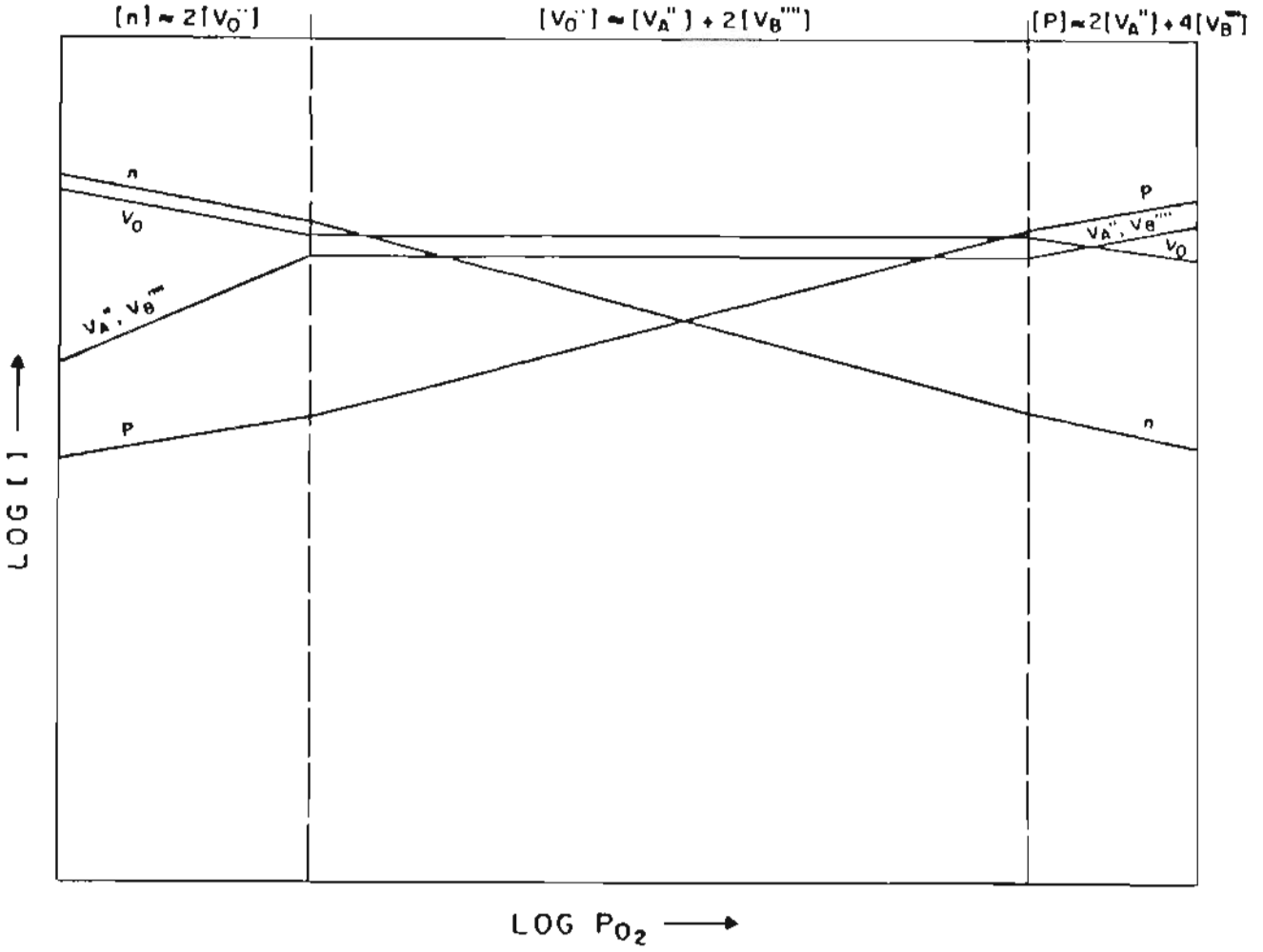

Figure-5. Calculated defect concentrations vs. the oxygen partial pressure. Only the totally ionized defects are shown. Intermediate neutrality condition is $[V_{\ddot{O}}] \simeq [V_A^{\cdot\cdot}] + [V_B^{\cdot\cdot\cdot\cdot}]$.

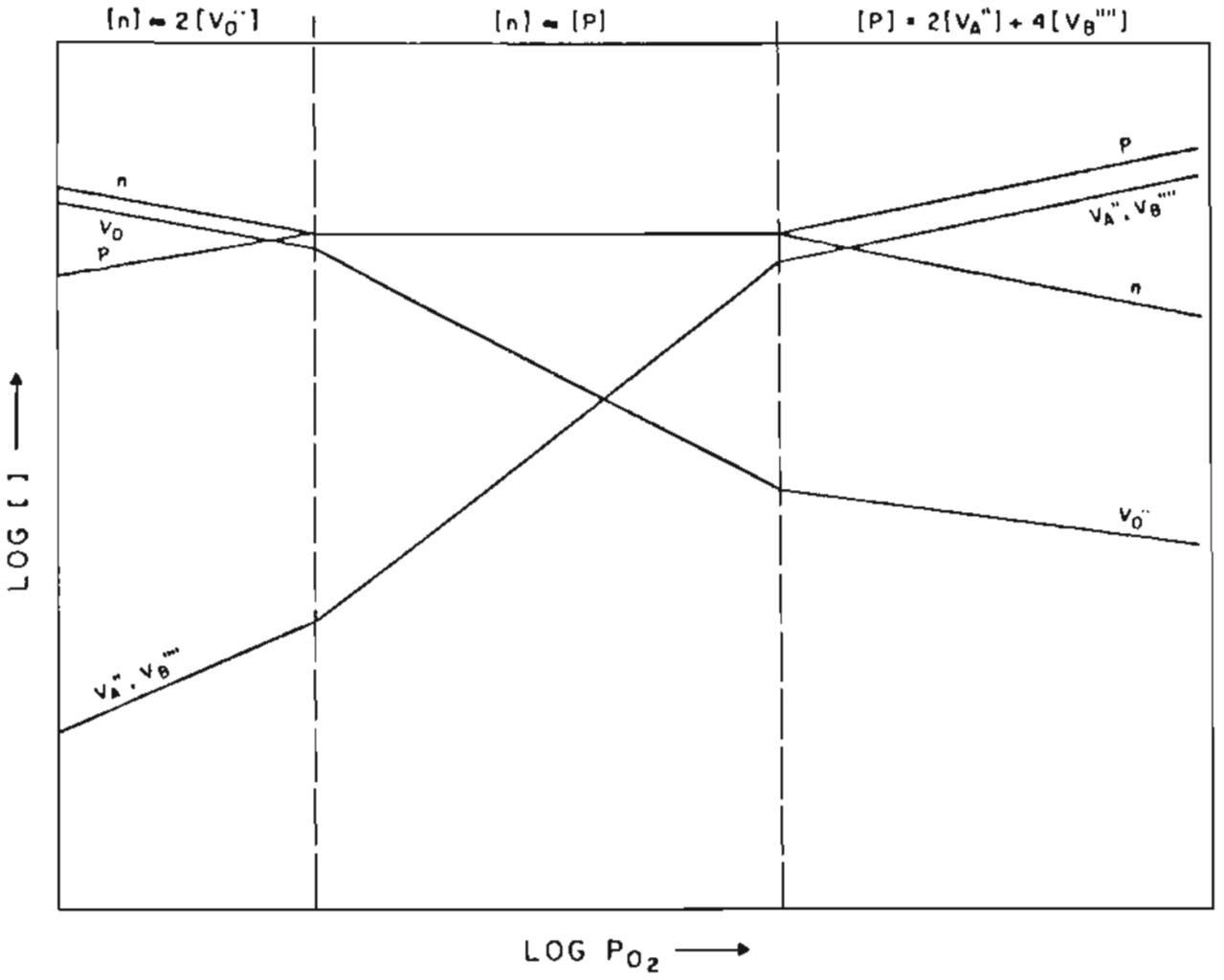

Figure-6. Same as Figure 5 but with [n] ≃ [p] for intermediate neutrality condition.

tions for the neutrality conditions in the intermediate region $[V_{\ddot{O}}] \simeq [V_A^{''}] + 2[V_B^{''''}]$ and $[n] = [p]$ respectively. The electrical properties of ceramic titanates are strongly dependent upon defects generated by deviation from stoichiometry. The defect structure of $BaTiO_3$ has been studied in considerable detail [55-66]. All of these studies indicate that in the P_{O_2} range near 1atm, the conductivity of an undoped sample increases with increasing P_{O_2}. This is characteristic of p-type conduction. As the oxygen partial pressure surrounding the specimen falls, a transition to n-type conduction is observed (conductivity increased with decreasing oxygen pressure). Eror and Smyth [62] studied the equilibrium electrical conductivity of a Ti rich single crystal $BaTiO_3$ over a wide range of oxygen partial pressures between 800 and 1200°C. They observed P-type conductivity at high PO_2 with $\log \sigma \simeq 1/4 \log P_{O_2}$ and n-type conduction at low oxygen partial pressure with log conductivity varying as $P_{O_2}^{-1/6}$. The proposed defect model consisted of doubly ionized oxygen vacancies in the low P_{O_2} region. At high oxygen partial pressure region (p-type) the dominating defects were acceptor impurities and their compensating oxygen vacancies. Daniels and Hardt [67] reported singly ionized oxygen vacancy as being the dominant defect at low oxygen pressures between 700 and 900°C. At higher temperatures, they proposed that the doubly ionized vacancies occurred in appreciable concentrations. Similar results were reported by Chan et al [59,66] on their investigation of polycrystalline sample with Ba/Ti = 0.995 at temperatures 750 to 1000°C and oxygen pressures between 10^{-20} and 10^{-1} atm.

III. EXPERIMENTAL PROCEDURE

A. Sample Preparation

The samples used in this investigation were prepared by a method first described by Pechini [68]. Following this technique, required amounts of barium carbonate and tetraisopropyl titanate solution were dissolved in an ethylene glycol-citric acid solution. The mixture was then heated slowly on a stirring hot plate to remove solvent and to form a solution of increasing viscosity. At this stage the product is amorphous and the ions are mixed on an atomic scale. This material is heated slowly for a few days until a gray, ashy powder is obtained. To remove any remaining organics the powder was calcined at 600°C for four hrs in air atmosphere. This heat treatment produces a white powder of precise stoichiometry and small particle size of around a few hundred angstroms. This low temperature technique of sample preparation enables us to have a much better control over the stoichiometry and homogenuity of the end product.

B. Raman Spectral Measurements

The powdered products of the liquid mix method were placed on platinum foil on an alumina dish. The dishes were placed in a quartz envelope which fit

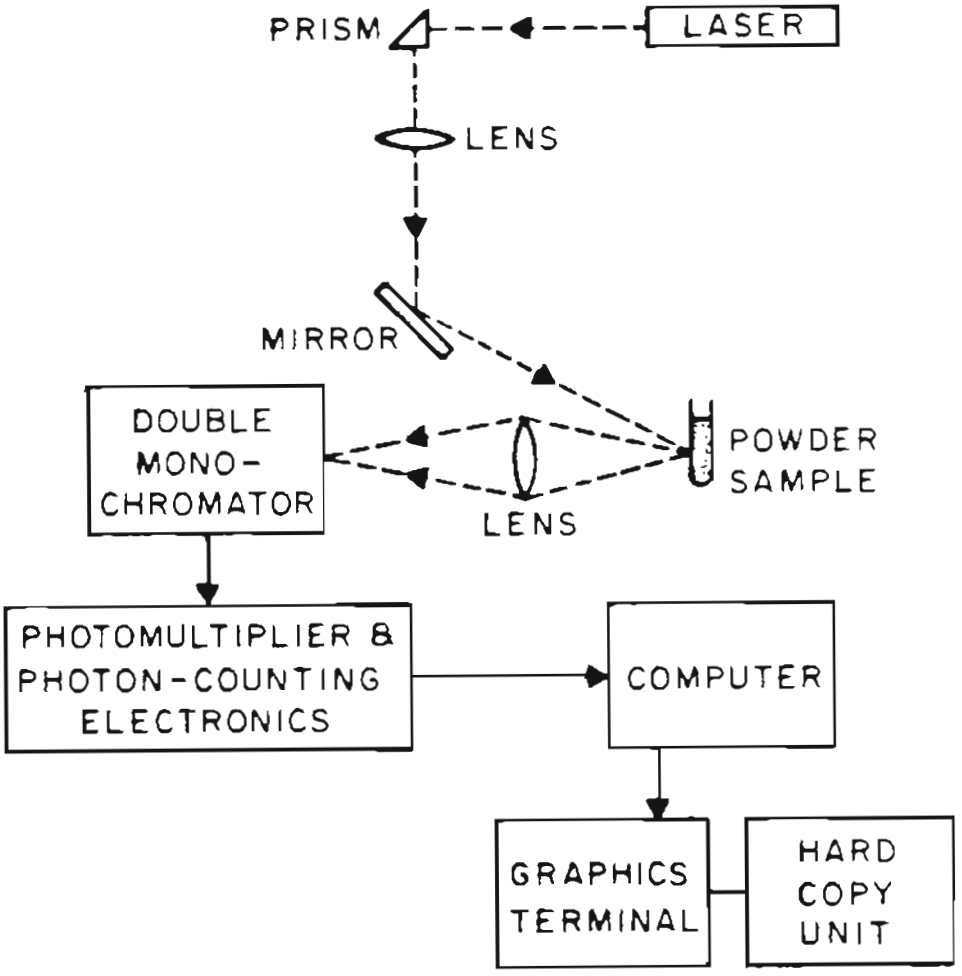

Figure-7. Schematic diagram of the computer-controlled laser Raman spectrometer.

into a muffle furnace. The samples were heat treated at temperatures from 600-1200°C. The higher temperature heat treatments were carried out in a tube furnace. The heated samples were placed in capillary tubes and supported by a sample holder for the back scattering arrangement. The excitation source was an Argon ion laser with an excitation wavelength of 5145A. A Jarrel-Ash 25-300 Raman spectrophotometer equipped with an RCA C3103 (Ga-AS) photomultiplier and an ORTEC amplifier/discriminator was used to analyze the scattered light. Photon counting was carried out with a computer. A schematic diagram of the computer controlled Laser Raman Spectrometer is shown in Fig. 7. The incident power of the laser beam was approximately 20mw and this beam was focussed using a condensing lens to a spot size of $<$ 1mm on the specimens. The Raman spectra were recorded over the range of 50-1150 cm^{-1}. The scattered photons were collected by an F 1.2 objective lens and were focussed onto the entrance slit of a double monochromator. An interactive graphics terminal (Tektronix, model 4010-1) provided rapid and accurate spectral analysis. Each sample was scanned once. Most of the spectra were obtained with a scan rate of $2.5cm^{-1}$/sec and a spectral slit width of $2.5cm^{-1}$.

C. Electrical Conductivity Measurements

The powder samples prepared by the liquid mix method [68] were compressed into pellet form under a pressure of 50,000 psi. The disk shaped pellets were then placed on a platinum sheet in an alumina boat and sintered in air. The sintering times & temperatures for the various compounds are summarized in Table III.

Table-III. Sintering Conditions of Polytitanate Compounds Studied.

sample	Temp(°C)	Time(hrs)
$BaTi_2O_5$	1200	20
$Ba_6Ti_{17}O_{40}$	1300	26
$Ba_4Ti_{13}O_{30}$	1300	4
$BaTi_4O_9$	1300	24
$Ba_2Ti_9O_{20}$	1400	36
$BaTi_5O_{11}$	1000	16

The sintered samples were quenched by being rapidly pulled out of the furnace. The specimens for the electrical conductivity measurements were cut from these sintered pellets into rectangular bars with approximate dimensions of 10mm×5mm×.5mm. A conventional four probe direct current technique [69-70] was employed in measuring the electrical conductivity of polytitanate compounds. If the current, I, through the specimen & the voltage, V, across the two inner probes are measured the specimen conductivity is given by

$$\sigma = \frac{(I)(d)}{(V)(A)} \tag{28}$$

where A is the area of the sample and d is the separation of the two inner probes. The electrical contacts for the four probe conductivity measurements were made by wrapping the sample with platinum wire .016in. in diameter. Four small grooves were cut into the edges of the samples to aid in holding the platinum wires in place. The spacing of the two inner probes and the cross- sectional

area of the specimens were measured. The conductivity was determined by supplying constant current (Keithley 225) in both polarities between the two outer probes and measuring the potential difference across the two inner probes using a high impedance digital multimeter (Keithley 191). In the course of this investigation the specimens were exposed at constant temperature to successively changing oxygen pressures. The change in the voltage drop value between the two inner probes was recorded after each variation of P_{O_2}. The state of equilibrium was assumed when the voltage drop value no longer changed with time.

D. Oxygen Partial Pressure Control

The high range of oxygen partial pressure, 10^0 - 10^{-5} atm, surrounding the samples was established by using pure oxygen and analyzed Argon-oxygen mixtures. The lower values of oxygen partial pressures were obtained by using mixtures of CO and CO_2. For the reaction

$$CO + 1/2O_2 \rightarrow CO_2 \tag{29}$$

the standard Gibbs free energy, ΔG_T, is given by Wicks and Block [71]. The equilibrium constant for the above reaction is

$$\Delta G = -RT\ln K = \frac{RT\ln P_{CO} P_{O_2}^{1/2}}{P_{CO_2}} \tag{30}$$

or

$$\log P_{O_2} = \frac{2\log P_{CO_2}}{P_{CO} + 2\frac{\Delta G_T}{2.303RT}} \tag{31}$$

Thus, the oxygen pressure in equilibrium with a nonstoichiometric oxide can be controlled by passing a gaseous mixture with a known ratio of CO_2 to CO over the sample at a given temperature. A schematic diagram of the glass assembly designed to control the gas flow through the furnace is shown in Fig. 8. Gases are delivered to the capillary flow meters (A) and are passed through the capillary tubes (B). The pressure drop across the capillary tubes is indicated by manometric flow meters (E). This pressure drop was determined by adjusting the level of di-butyl phthalate in the gas blow-off column and the fluid reservoir (D). The flow rates of various capillaries were calibrated as a function of pressure drop by measuring the displacement of a soap bubble in a graduated glass tube. Gases coming out of flow meters are passed through a purification system (C). The oxygen and argon-oxygen mixtures were passed through successive tubes containing magnesium perchlorate, ascarite and magnesium perchlorate. The carbon monoxide gas was purified by passing through the same columns to remove carbon dioxide and moisture. Removal of water vapor from carbon dioxide gas was achieved by passing the gases over drierite. After purification the gases were passed through a mixing column (G) containing glass beads for uniform mixing. The purified gas mixtures were then transferred to the furnace containing the specimen. The kanthal wound furnace used for the electrical conductivity measurements consisted of a mullite tube with tapered pyrex joints at both ends. The temperature inside the furnace was measured with a platinum-platinum 10% rhodium thermocouple.

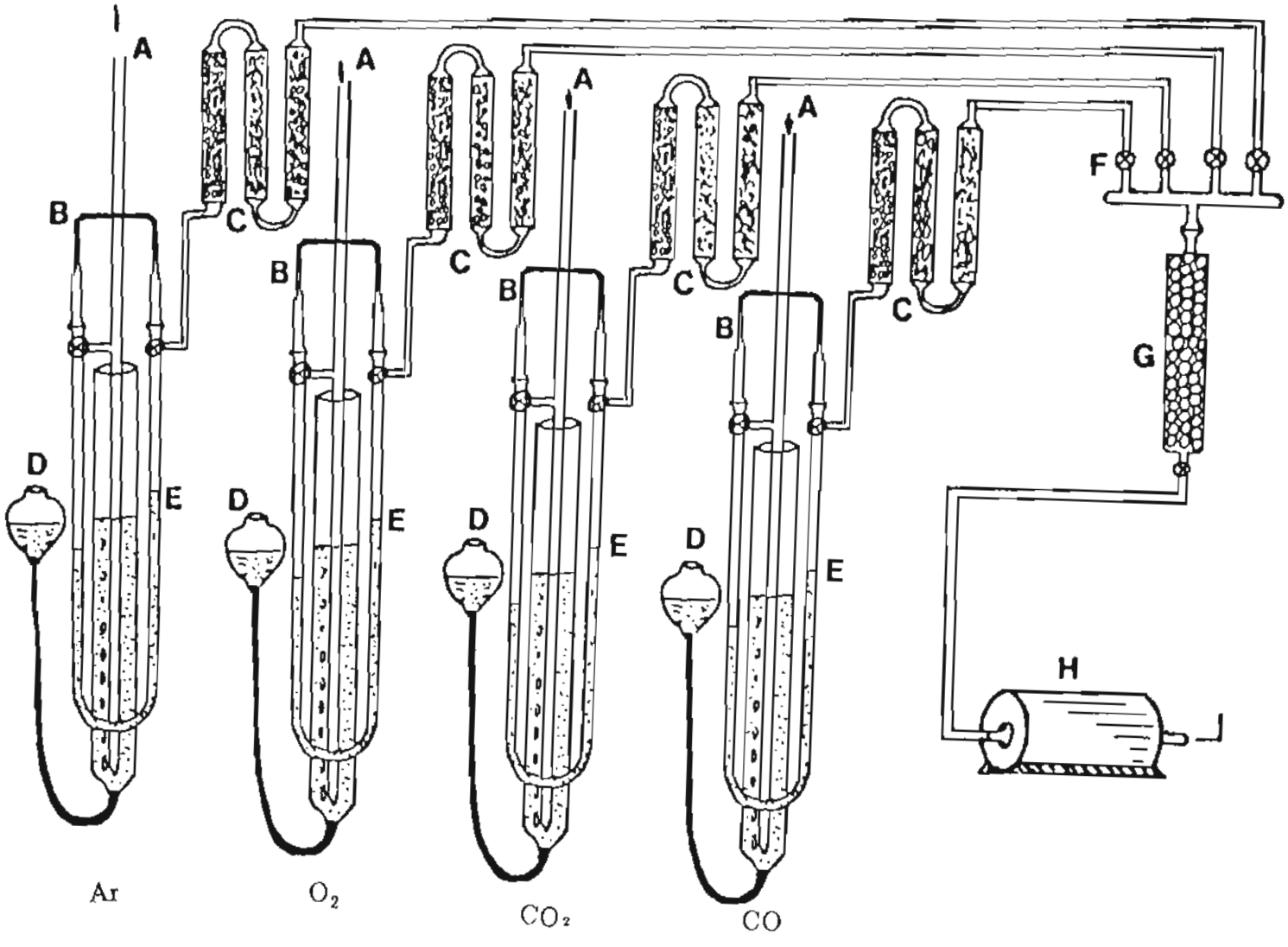

Figure-8. Schematic diagram of the capillary flow meter system to control the oxygen partial pressure.

IV. RESULTS AND DISCUSSIONS

A. Raman Spectral Measurements

Fig. 9 shows the phase diagram obtained by R.S. Roth et al [38], from the specimens prepared by hydrolysis of mixed barium and titanium ethoxide solutions. The phase diagram was constructed from the data obtained by x-ray diffraction analyses of the various heat treatments. One objective of the present study was to compare the phase relations obtained using the hydrolysis method employed by these authors, and liquid mix technique used in this study. The following is a comparison of the two studies on this system.

$BaTi_2O_5$ (1:2)

Roth et al [38] suggested that the specimens of $BaO{:}2TiO_2$ crystallize at ~ 700°C into the known form of $BaTi_2O_5$ which is stable up to 1150°C where it decomposes into $BatiO_3$ and $Ba_6Ti_{17}O_{40}$. Our Raman spectroscopy data on this compound as a function of temperature are shown in Fig. 10. As prepared samples were found to be amorphous when heated at 600°C for 4 hrs. Calcining at 700°C gave rise to a rather noisy spectrum with signs of crystallinity. Our results do not show significant changes in the spectra obtained for the samples

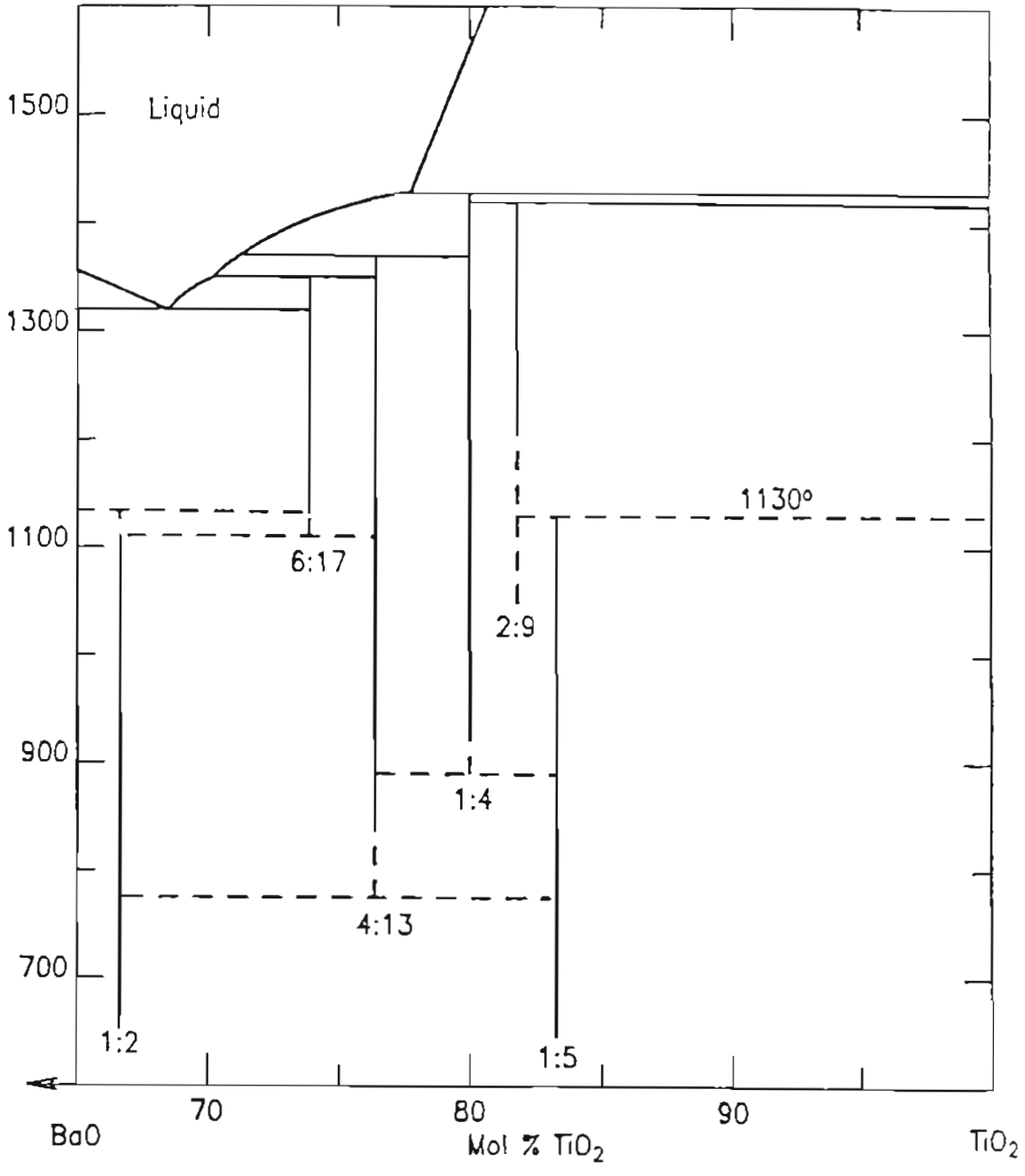

Figure-9. Phase diagram constructed from the data obtained from the heat treatments of the specimens obtained by hydrolyzing mixtures of Ba-and-Ti ethoxide solutions after refluxing at boiling point of ethyl alcohol for at least 30 min. (Courtesy of Roth et al).

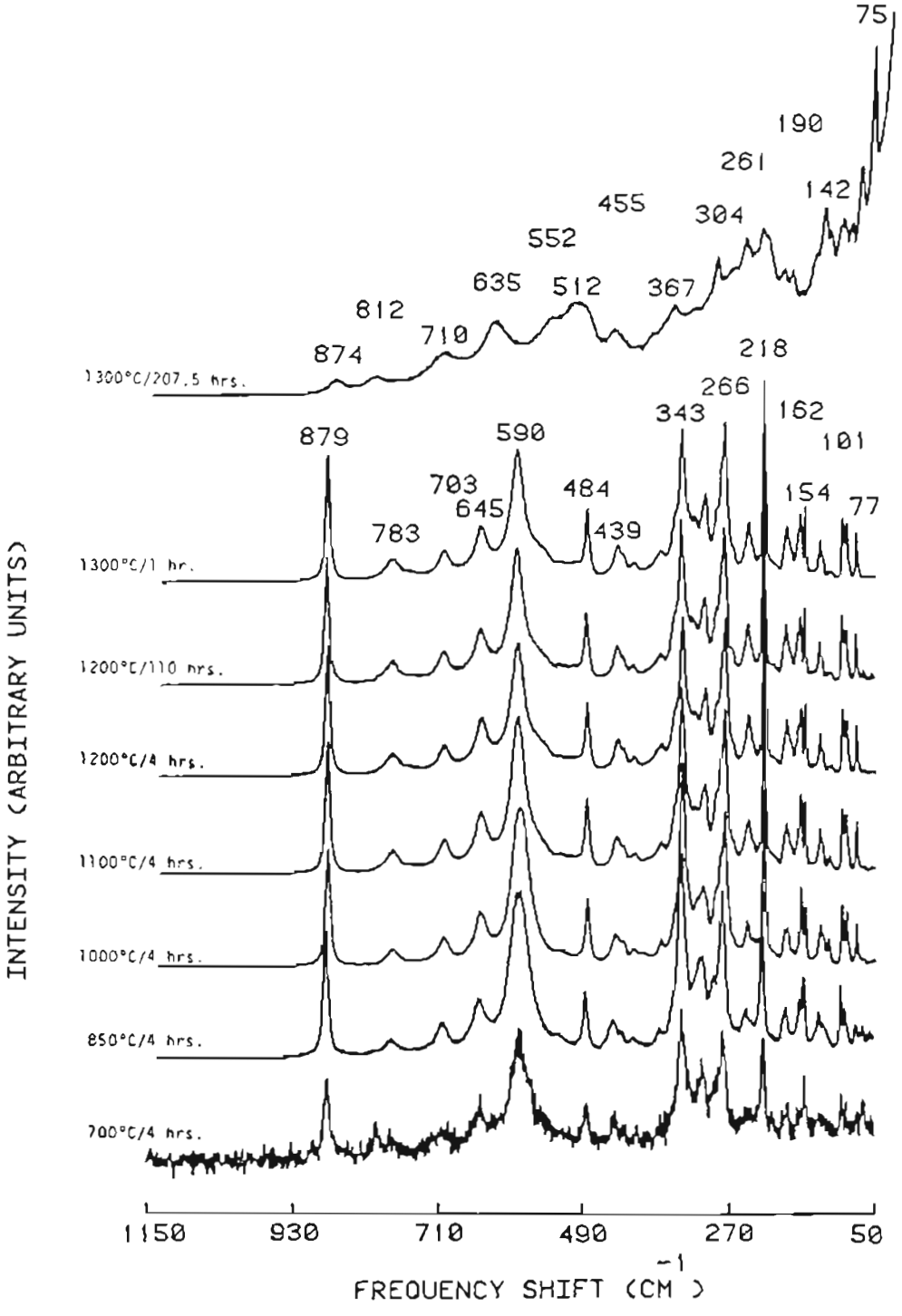

Figure-10. Raman spectra of $BaTi_2O_5$ as a function of temperature.

heated between 850 and 1100°C for 4 hrs, indicating the fact that $BaTi_2O_5$ is a low temperature phase as observed by Roth. To further confirm the uniqueness of the structure, X-ray diffractometry was done on $BaTi_2O_5$ heat treated at 1100°C for 4 hrs. The computed d values and the relative intensities were in good agreement with the powder data of O'Bryan et al [36]. As seen from the Raman results in Fig. 10. this compound shows no evidence of decomposition at 1200°C for 110 hrs. However, decomposition occurs when the sample is held at 1300°C for more than 200 hrs, and the equilibrium compounds formed by solid state reaction are $BaTiO_3$ and $Ba_6Ti_{17}O_{40}$. The Raman spectroscopy results of this phase at 1300°C and those of $BaTiO_3$ and $Ba_6Ti_{17}O_{40}$ are shown in Fig. 11. It is seen from Fig. 11 that the $BaTi_2O_5$ heated at 1300°C for $\sim$ 207 hrs contains all the features belonging to that of $Ba_6Ti_{17}O_{40}$ in addition to the $BaTiO_3$ phase. The contributions from the latter phase modifies the intensities of the peaks at $\sim$ 510cm^{-1} and $\sim$ 303cm^{-1}. The present study agrees well with regard to the products of decomposition reported by Roth, although this decomposition was observed at a higher temperature. This could be due to insufficient heating times at lower temperatures (110 hrs).

$Ba_6Ti_{17}O_{40}$ (6:17)

The experimental results obtained by the present investigation on this compound are in good agreement with the findings of Roth [38]. $Ba_6Ti_{17}O_{40}$ was reported to be a high temperature stable phase which does not exist below about 1100°C. The Raman spectrum of (6:17) as a function of temperature is reported

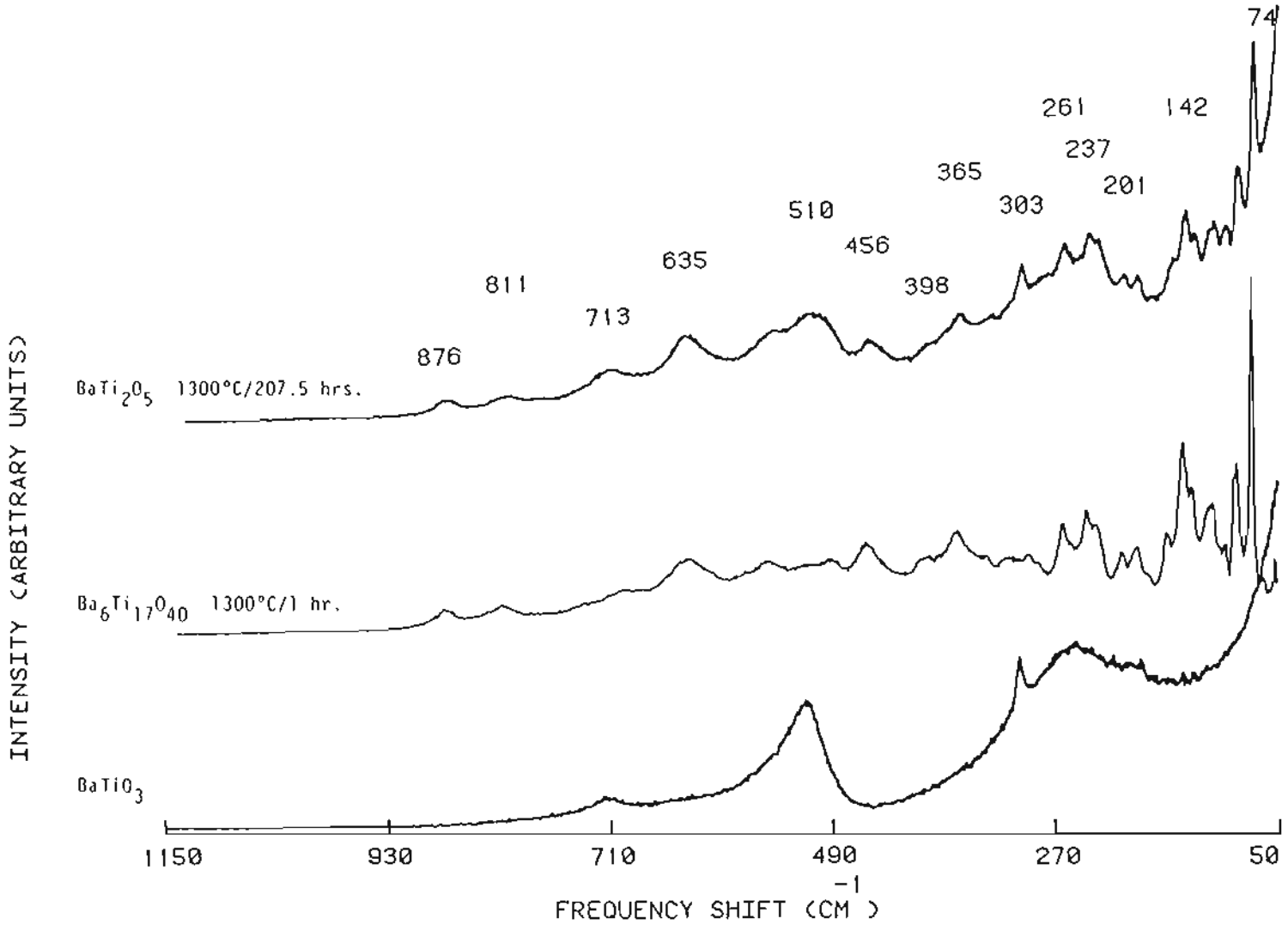

Figure-11. Raman spectra showing the decomposition of $BaTi_2O_5$ into $Ba_6Ti_{17}O_{40}$ and $BaTiO_3$ at 1300°C.

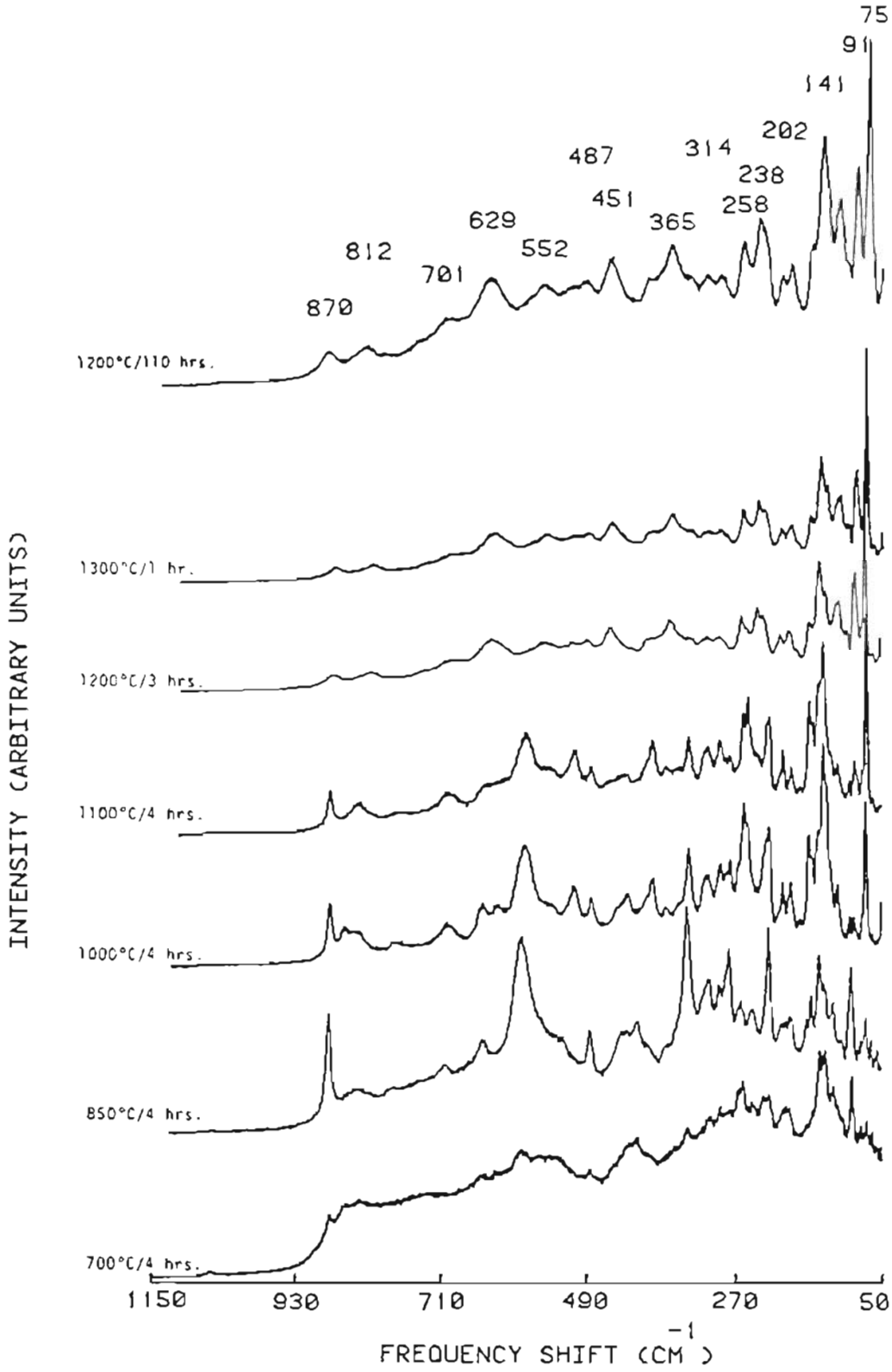

Figure-12. Raman spectra of $Ba_6Ti_{17}O_{40}$ as a function of temperature.

in Fig. 12. When heated at 700°C for four hrs this compound contains three phases, i.e. (1:2), (1:5) and (1:4). This conclusion was drawn after careful comparison of the spectra shown in Fig. 13. At 850°C the (1:4) contribution to the mixture was found to disappear and the compound contains only (1:5) and (1:2). This can be seen in Fig. 14. Further increases in temperature yielded a two phase mixture of $Ba_4Ti_{13}O_{30}$ and $BaTi_2O_5$ for this composition. Raman spectra data describing this effect for (6:17) held at 1000°C for four hrs are presented in Fig. 15. Heat treatment at 1200°C for three hrs resulted in a Raman pattern which did not change even after prolonged heating at this temperature. Therefore, it is suggested that this is the Raman spectrum of the $Ba_6Ti_{17}O_{40}$ compound. This conclusion is also supported by the fact that the X-ray analysis of the quenched sample of $Ba_6Ti_{17}O_{40}$ heated at 1200°C is in good agreement with the reported powder data [45], with respect to d values, although they disagree slightly in intensities. The difference in the X-ray line intensities can be related to preferred orientation effects in the powder sample. Both the study by Roth [38] and the present data indicate the (6:17) is not stable at low temperatures.

$Ba_4Ti_{13}O_{40}$ (4:13)

The Raman spectra data as a function of temperature for $Ba_4Ti_{13}O_{30}$ are given in Fig. 16. This compound crystallizes at 700°C, forming a mixture composed of the (1:5), (1:4) and (1:2) phases. This can be seen from the spectra shown in Fig. 17. Heating $Ba_4Ti_{13}O_{30}$ at 850°C for four hrs led to a pattern consisting of the $BaTi_4O_9$ and the $BaTi_2O_5$ phases. This point is illustrated in Fig.

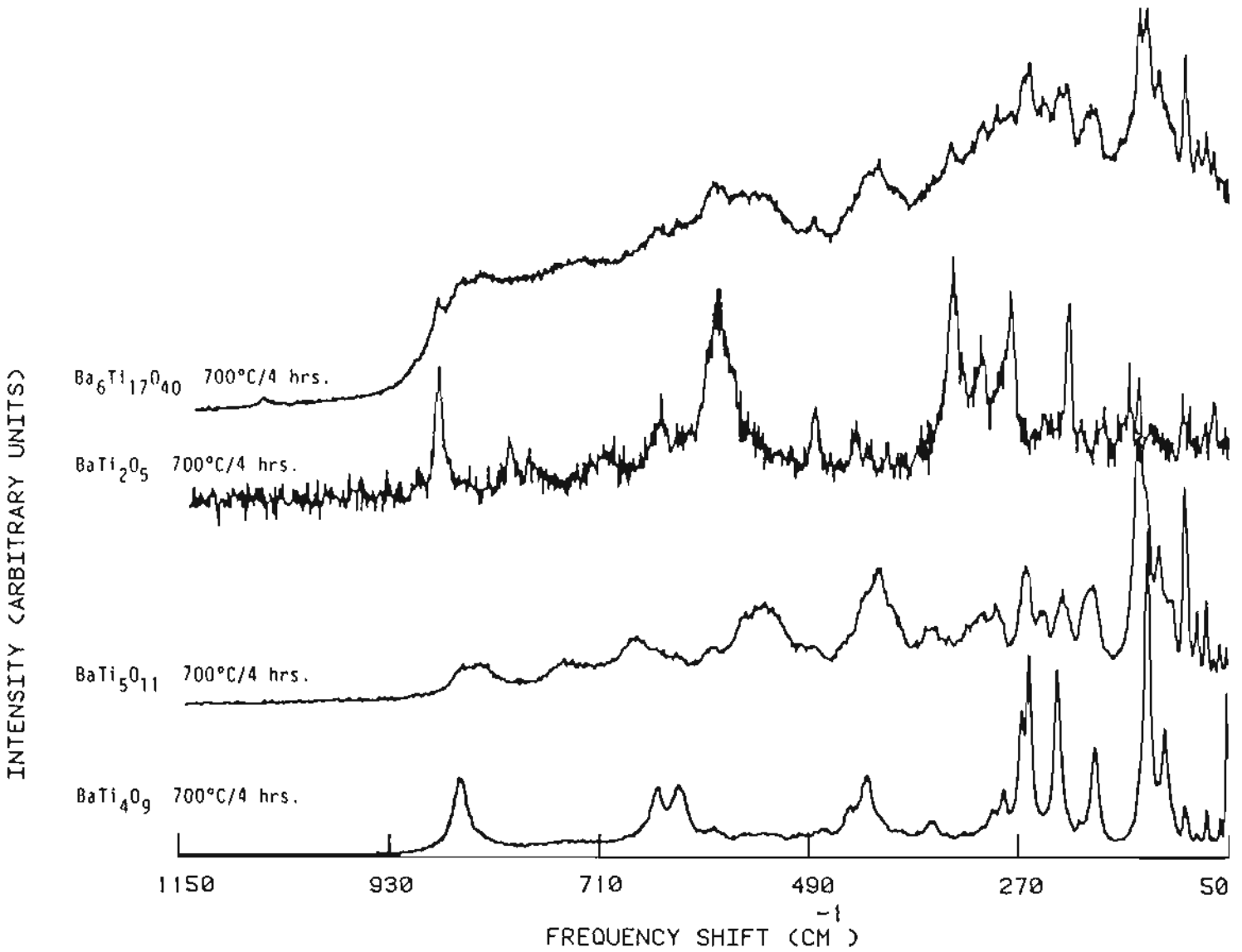

Figure-13. Raman spectrum of $Ba_6Ti_{17}O_{40}$ at 700°C revealing a mixture composed of $BaTi_2O_5$, $BaTi_5O_{11}$ and $BaTi_4O_9$.

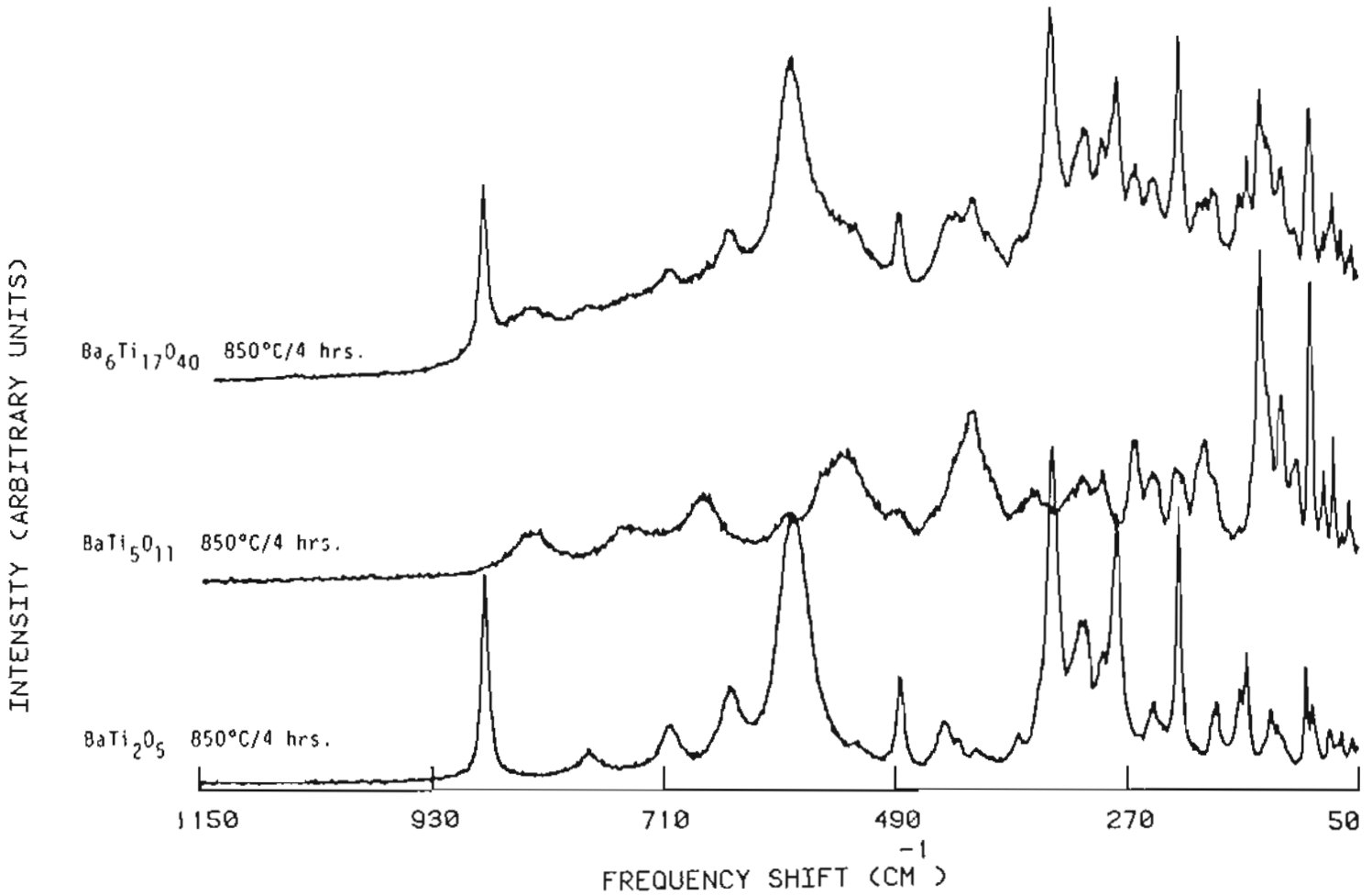

Figure-14. Raman spectrum of $Ba_6Ti_{17}O_{40}$ at 850°C showing a mixture composed only of $BaTi_5O_{11}$ and $BaTi_2O_5$.

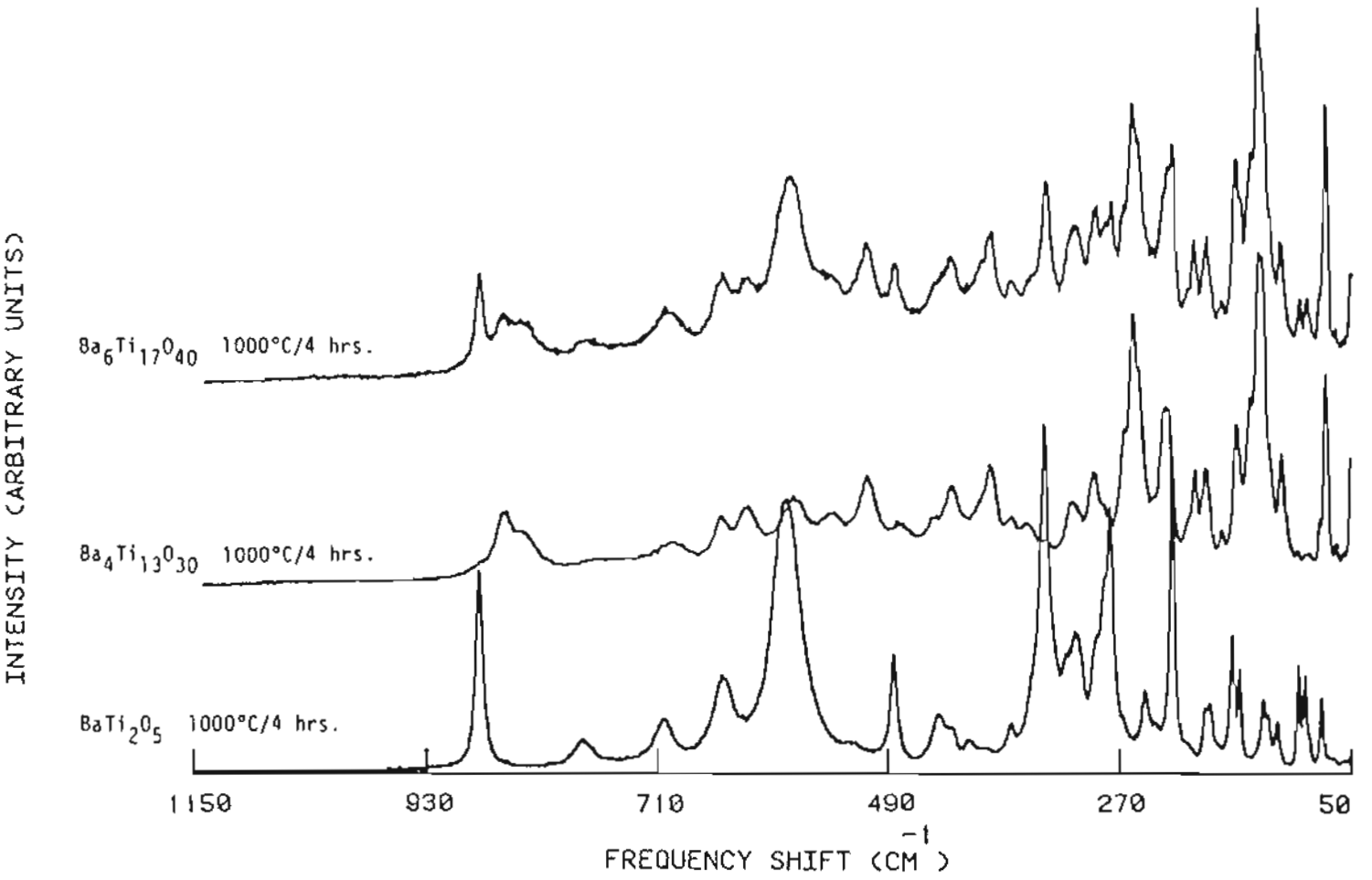

Figure-15. Raman spectrum of $Ba_6Ti_{17}O_{40}$ at 1000°C illustrating a mixture composed of $Ba_4Ti_{13}O_{30}$ and $BaTi_2O_6$.

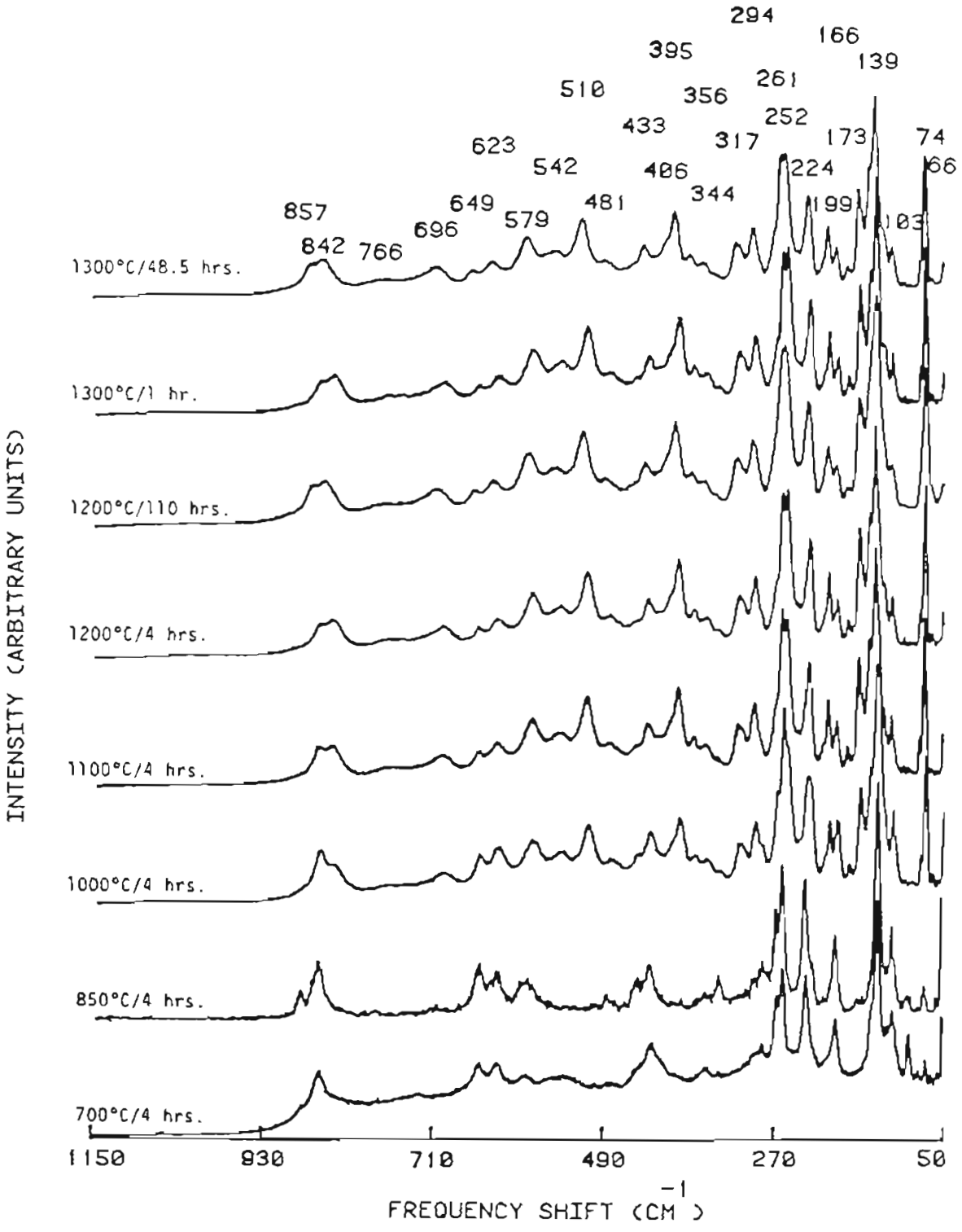

Figure-16. Raman spectra of $Ba_4Ti_{13}O_{30}$ as a function of temperature.

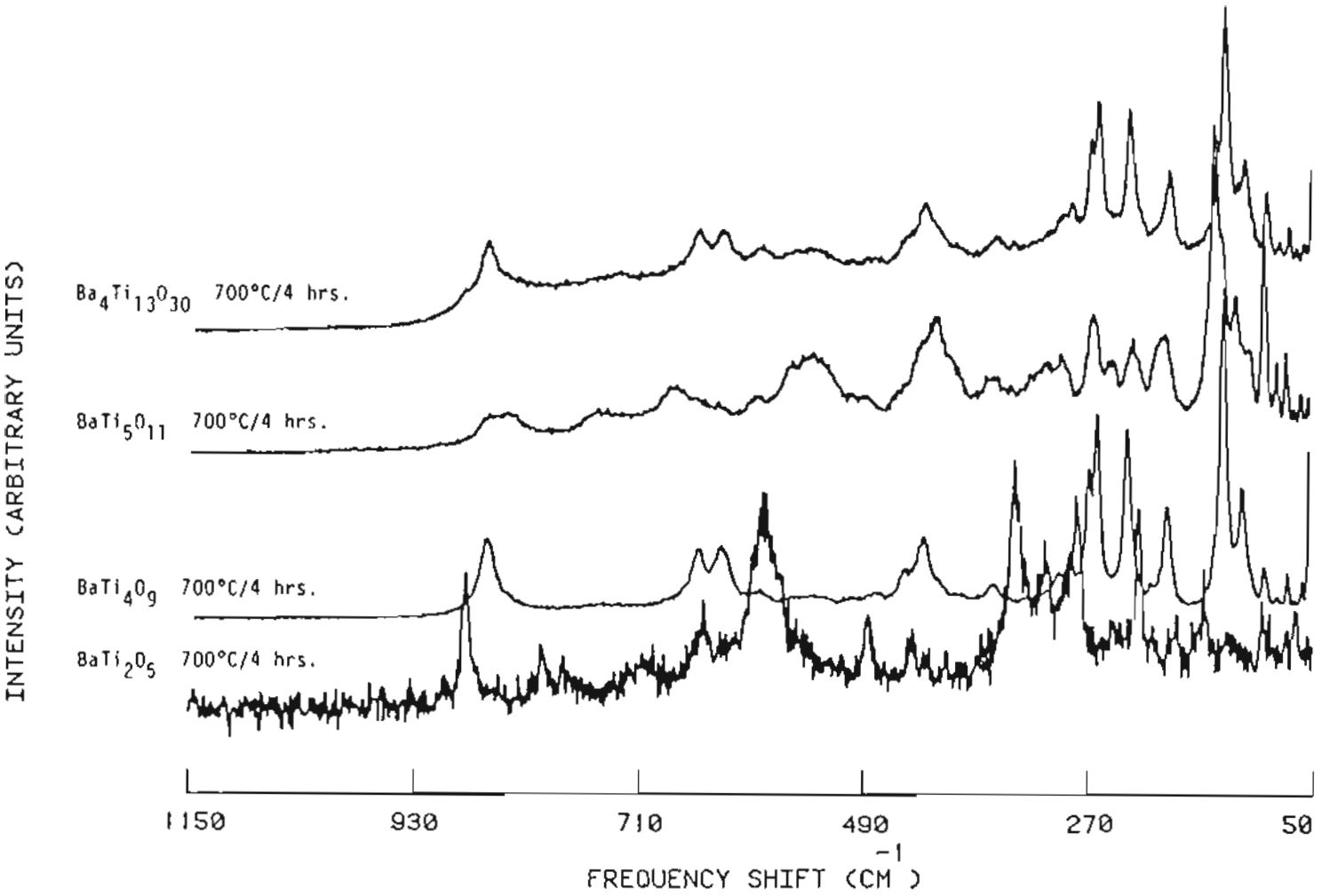

Figure-17. Raman spectrum of $Ba_4Ti_{13}O_{30}$ at 700°C shows a mixture consisting of $BaTi_5O_{11}$, $BaTi_4O_9$ and $Bati_2O_5$.

18. At 1000°C a new structure emerged from the mixture which is stable to at least 1300°C, the highest temperature in the present study. The X-ray diffraction data obtained on $Ba_4Ti_{13}O_{30}$ heated at 1300°C for four hrs is in excellent agreement with the previously published pattern [45]. In his paper, Roth concluded that (4:13) is a very stable phase crystallizing at an even lower temperature than $BaTi_4O_9$. Our observation, however, shows that (1:4) is the only compound in the system which crystallizes when heated at 600°C for four hrs.

$BaTi_4O_9$ (1:4)

At 700°C this phase appears to contain a slight amount of $BaTi_5O_{11}$. This is seen from the Raman spectrum of this compound given in Fig. 19. The broad bands at $\sim$ 740cm^{-1} and 540cm^{-1} and the peak at $\sim$ 94cm^{-1} are due to the (1:5) phase. Unlike the peak at 94cm^{-1}, the bands at 740cm^{-1} and 540cm^{-1} disappear when the material is held at 850°C for four hrs. As shown in Figure 19, with further increase in temperature the 94cm^{-1} band loses its intensity and disappears completely at 1200°C. The X-ray data obtained on this compound heated at 700°C for four hrs showed the presence of $BaTi_5O_{11}$ in addition to the lines for the $BaTi_4O_9$ phase. However, the small amount of (1:5) phase observed by Raman spectroscopy was not detectable by X-ray powder diffraction experiments carried out on the samples heated above 1000°C. The X-ray powder pattern obtained for the single phase $BaTi_4O_9$ is in excellent agreement with the diffraction pattern observed for this compound by O'Bryan et al [36]. The result on this compound differs from those reported by Roth, in that he observed a two

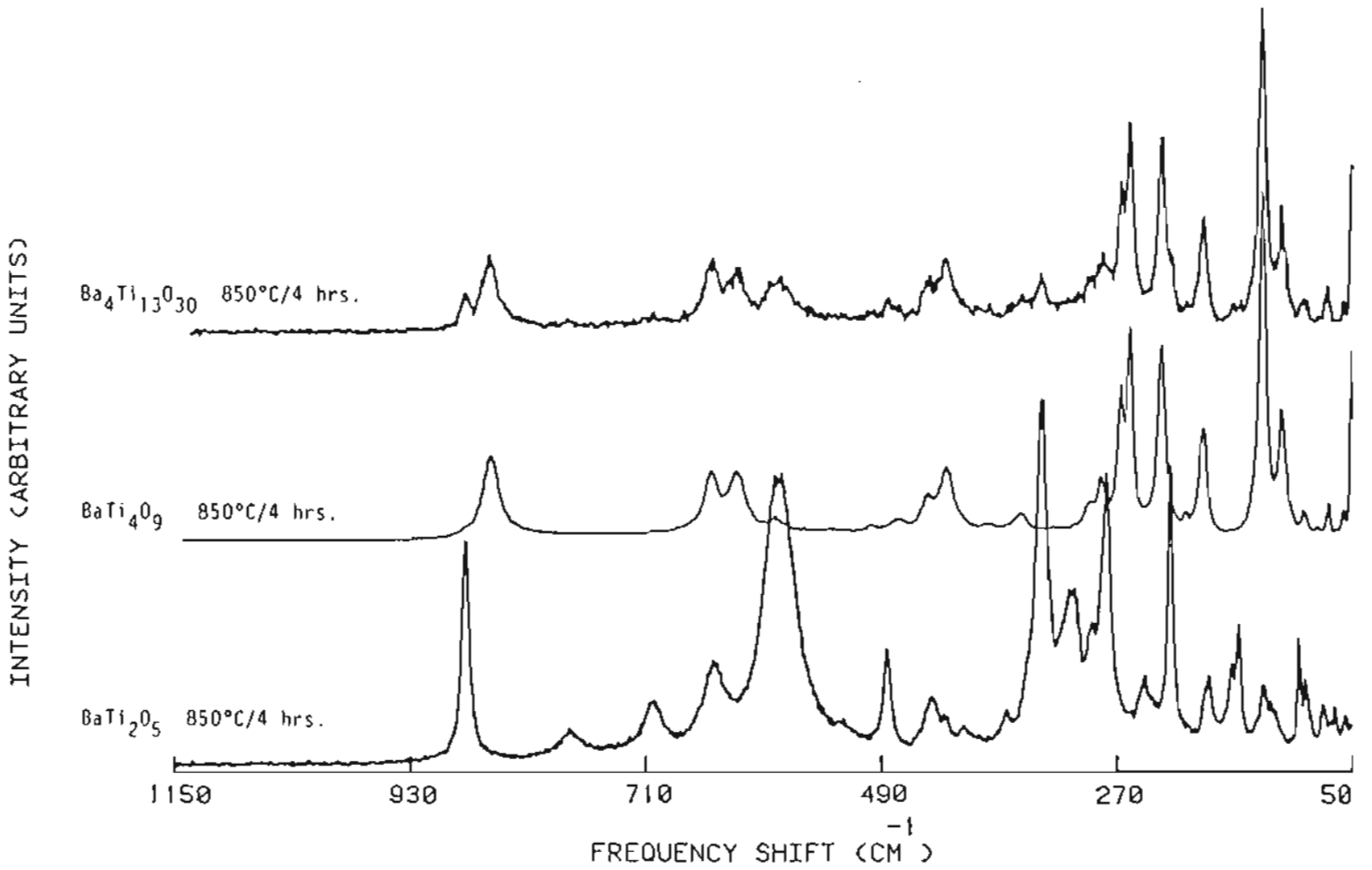

Figure-18. Raman spectrum of $Ba_4Ti_{13}O_{30}$ at 850°C showing a mixture composed only of $BaTi_4O_9$ and $BaTi_2O_5$.

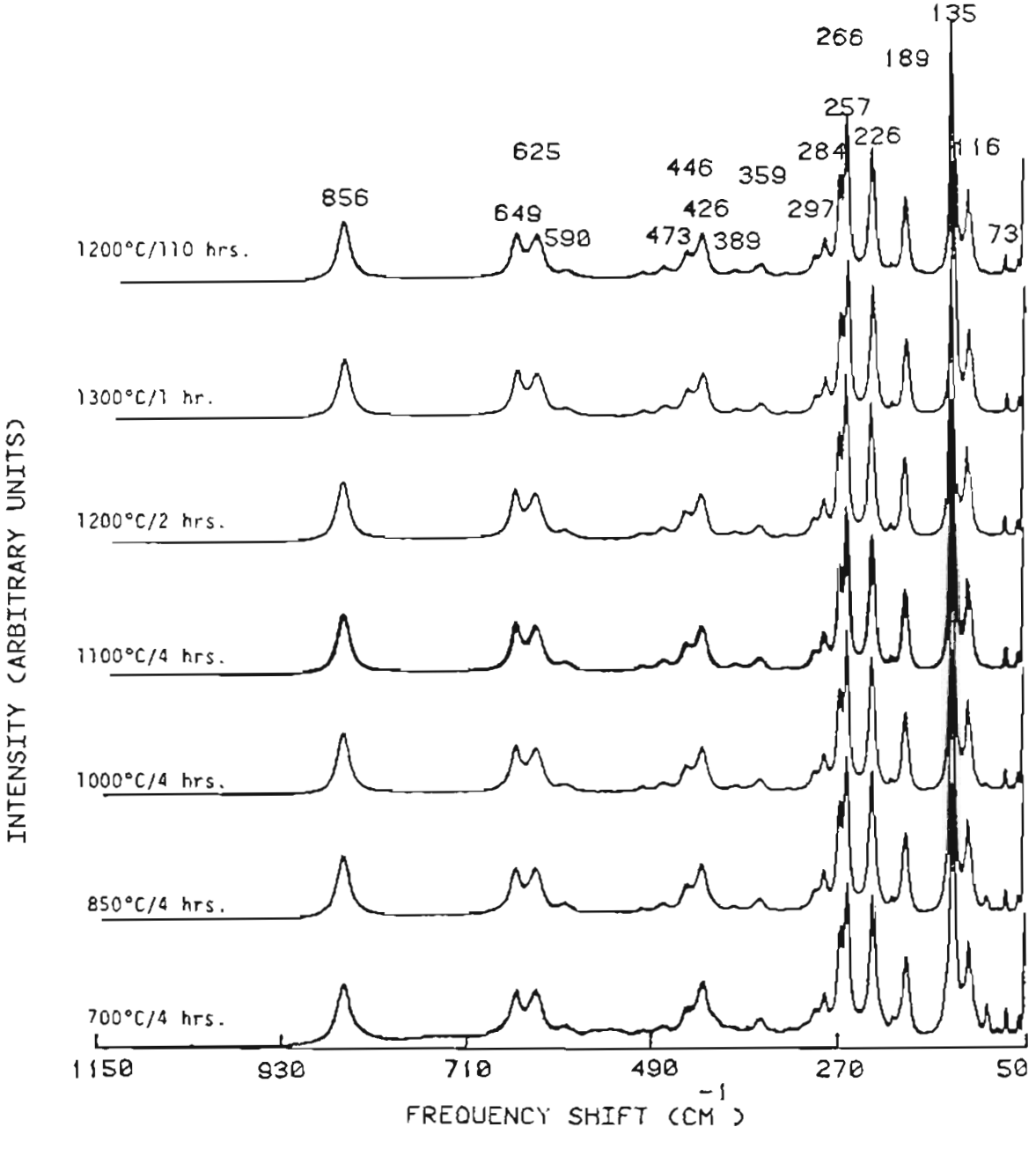

Figure-19. Raman spectra of $BaTi_4O_9$ as a function of temperature.

phase mixture of (1:2) and (1:5) and (4:13) plus (1:5) at 700 and 800°C heat treatments, respectively. He also indicated that the complete pattern of the (1:4) phase does not form from these mixtures until about 1300°C.

$Ba_2Ti_9O_{20}$ (2:9)

Employing hydrolysis of ethoxide precursors, Roth [38] reported that the (2:9) phase does not begin to crystallize until the (1:5) compound begins to dissociate. In his fully refluxed precursor mixture this did not occur until 1200°C. However, if the mixture is hydrolyzed within about five minutes of mixing, the (2:9) phase begins to form at temperatures as low as ~ 900°C. In the present investigation $Ba_2Ti_9O_{20}$ prepared by the liquid mix technique and heat treated between 700 and 1100°C for four hrs crystallizes into a mixture containing the (1:4) and (1:5) phases. The Raman pattern of this compound as a function of temperature is presented in Figure 20. The peaks around 540cm^{-1} and 740cm^{-1} are characteristic of the (1:5) phase. After heating the sample at 1200°C for six hrs the resulting Raman spectrum resembles that of $BaTi_4O_9$. This similarity can be seen in Figure 21, where all the (1:5) characteristics are lost at this temperature. A similar structure was obtained when the sample was held at 1300°C for one hr. A new structure was obtained only after prolonged heat treatment at 1200°C. In comparing the X-ray powder data of Tillmanns et al [52] for $Ba_2Ti_9O_{20}$ with the present X-ray work on the prolonged heated (2:9) sample, good correlation was found between the sets of data with respect to both d values and relative intensities.

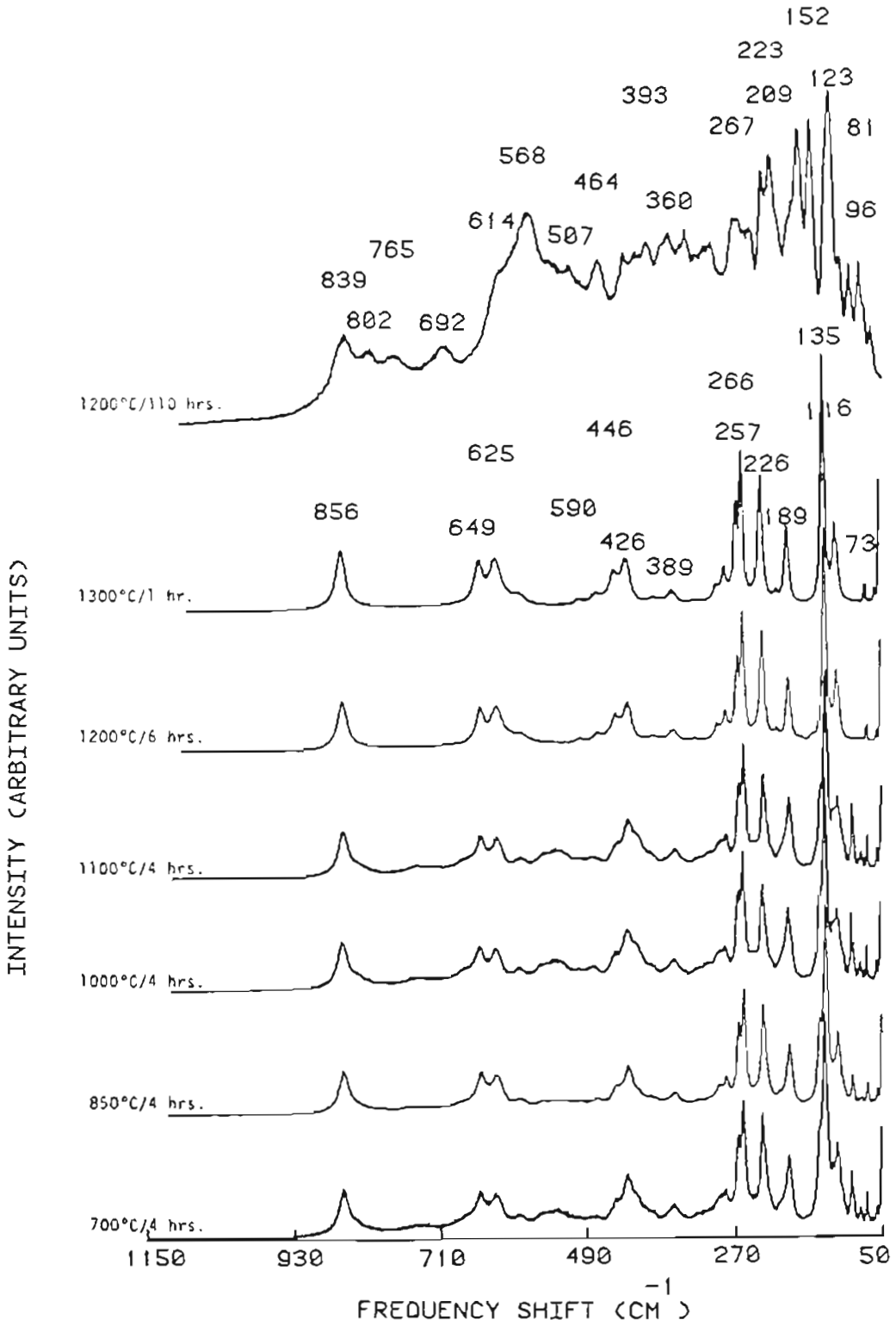

Figure 20. Raman spectra of $Ba_2Ti_9O_{20}$ as a function of temperature.

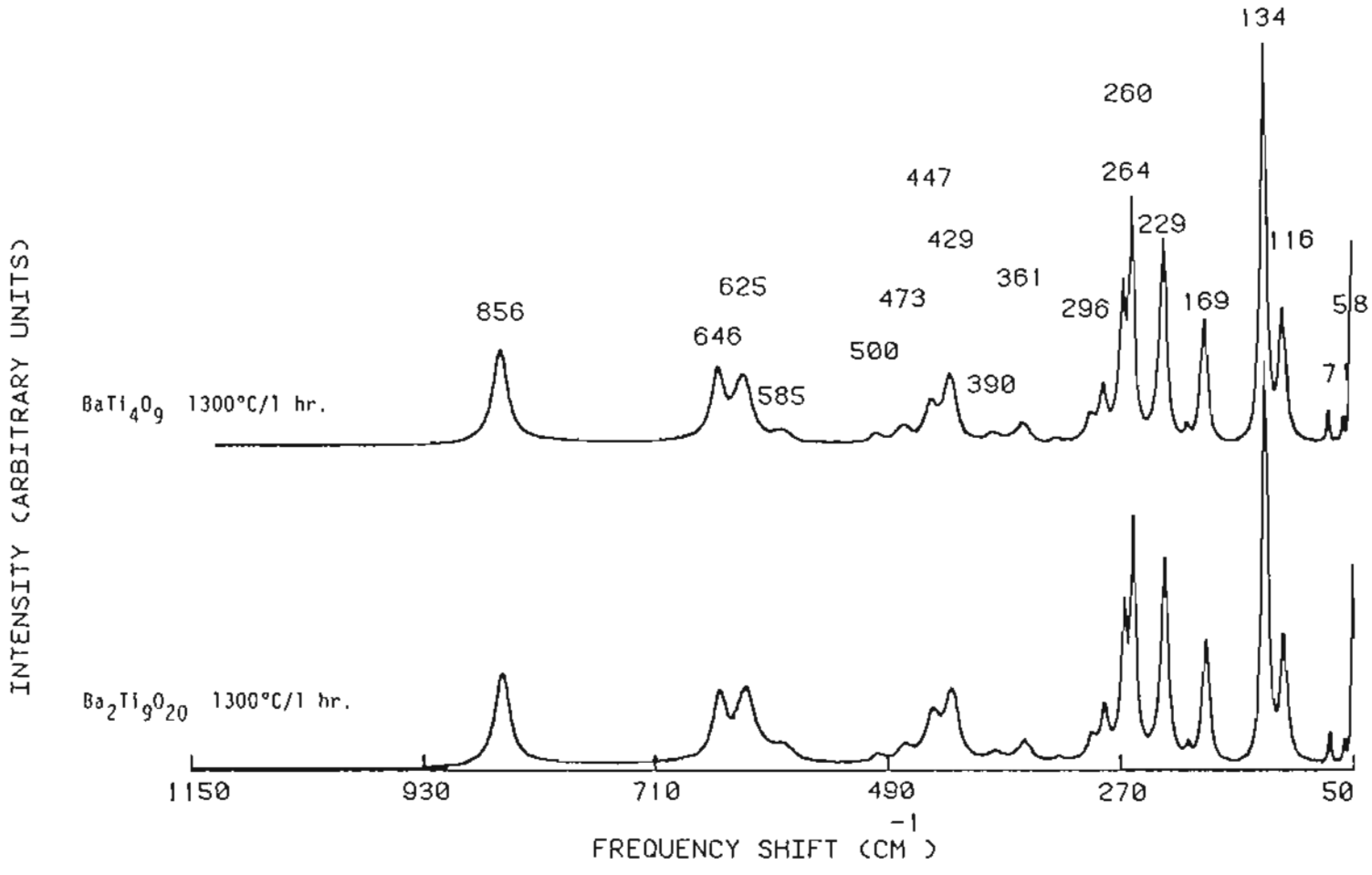

Figure-21. Raman spectra showing identical pattern for $BaTi_4O_9$ and $Ba_2Ti_9O_{20}$ heated at 1300°C for 1hr.

$BaTi_5O_{11}$ (1:5)

The results with regard to the stability range of this compound are consistent with those reported by Roth [38]. The Raman data of Figure 22 shows that the single phase compound is obtained when the powder is heated between 700 and 1100°C for four hrs. However, specimens prepared by Roth required much longer heating times for forming single phase material. He observed quick decomposition of this phase into TiO_2 and $Ba_2Ti_9O_{20}$ and/or $BaTi_4O_9$ at 1200°C. The present experimental data show presence of (1:5) and (1:4) when this composition was heated at 1200°C for four hrs. The peaks for $BaTi_5O_{11}$ ($\sim$ 740cm^{-1}, 540cm^{-1} and 94cm^{-1}) disappeared when the material was heated at 1300°C for one hr. The Raman spectrum that resulted after extensive heat treatment at 1200°C indicated the decomposition of $BaTi_5O_{11}$ into a two phase mixture composed of (2:9) and TiO_2. The decomposition of this compound into these latter phases is illustrated in Figure 23. The X-ray examination of this compound heated at 1100°C for four hrs confirmed the previously reported d values on the single phase $BaTi_5O_{11}$ sample [36].

B. Electrical Conductivity Measurements

$BaTi_2O_5$

The measured electrical conductivity of polycrystalline $BaTi_2O_5$ in the temperature range 1000-1100°C and in equilibrium with oxygen partial pressure between 10^{-18} to 10^0 atm is shown in Fig. 24. As can be seen for all the temperatures investigated, the conductivity of this compound increased with decreasing

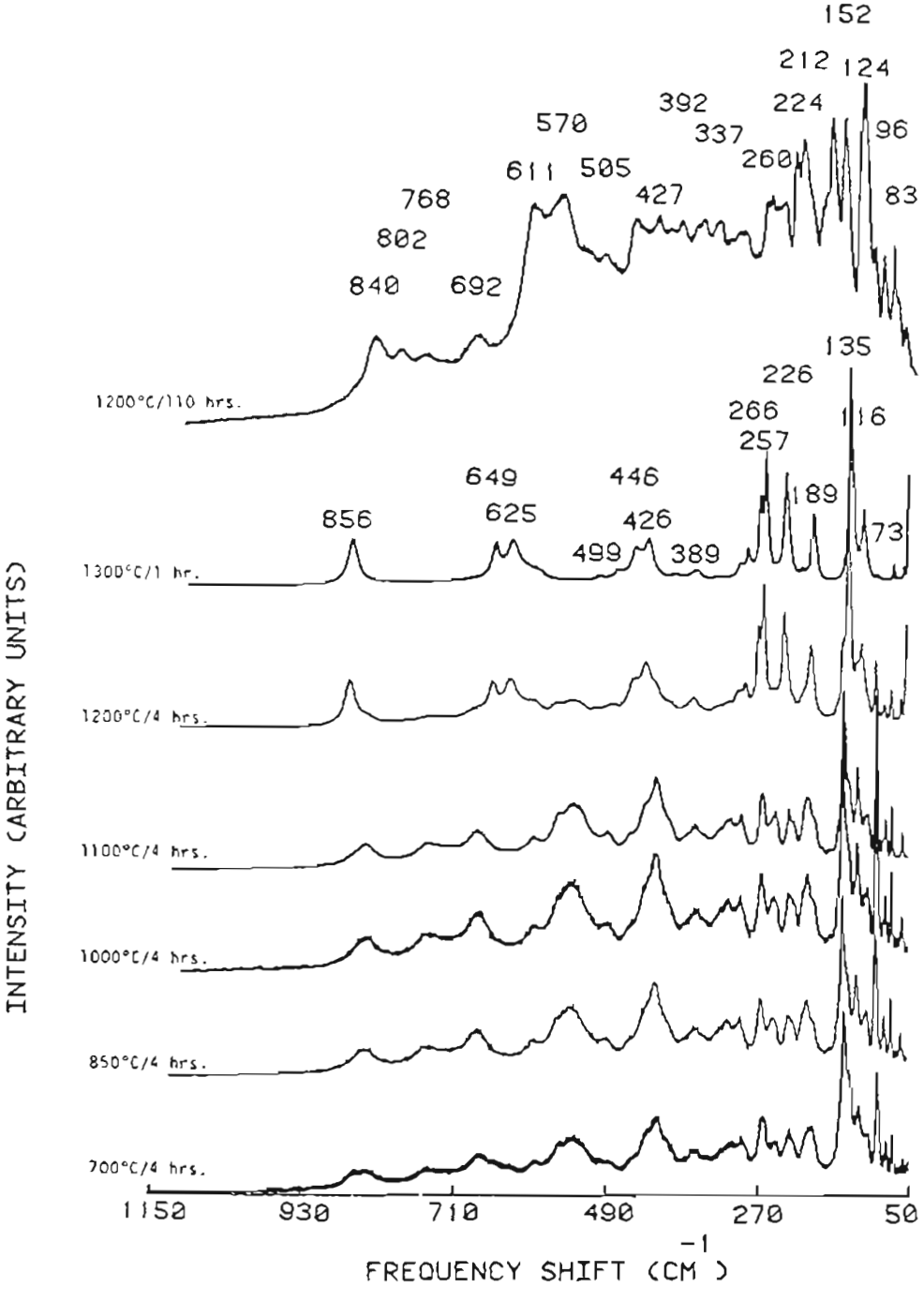

Figure-22. Raman spectra of $BaTi_5O_{11}$ as a function of temperature.

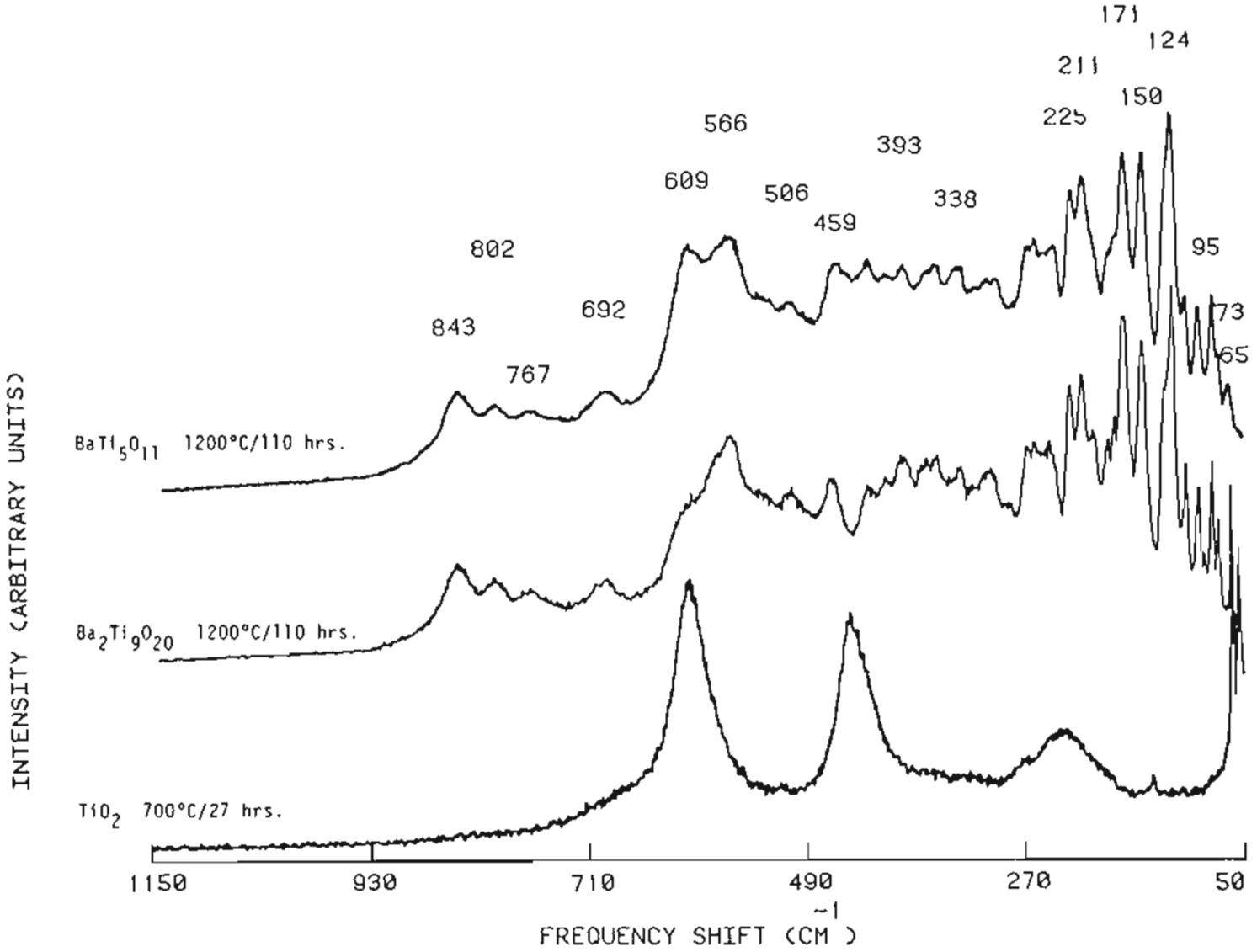

Figure-23. Raman spectra showing the decomposition of $BaTi_6O_{11}$ into $Ba_2Ti_9O_{20}$ and TiO_2.

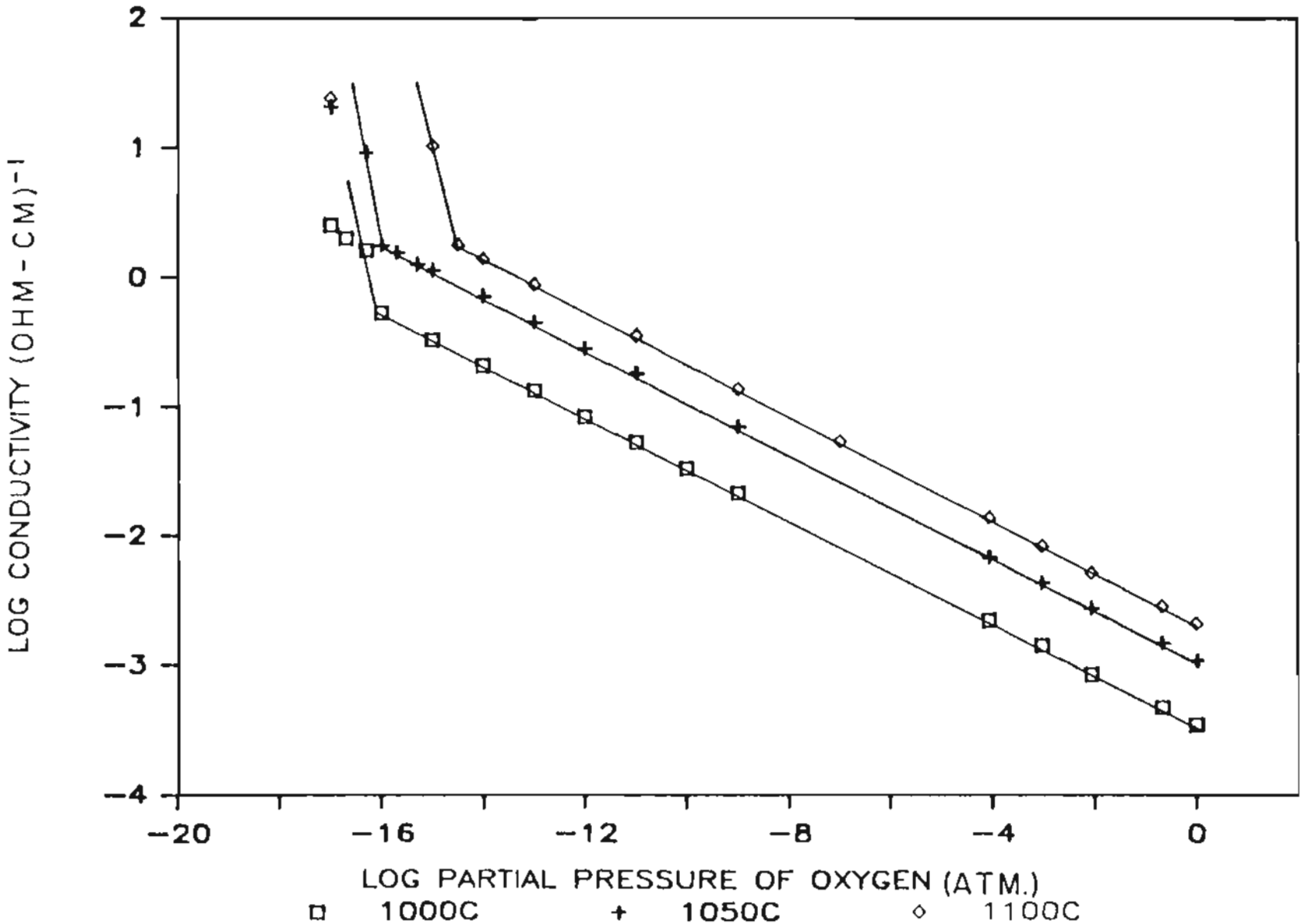

Figure-24. The dependence of the electrical conductivity of $BaTi_2O_5$ on oxygen pressure at 1000, 1050 and 1100°C.

oxygen partial pressure resulting in n-type material throughout the whole P_{O_2} range. This behavior was in contrast to the conductivity data of $BaTiO_3$, which showed a p-type region (conductivity increases with increasing oxygen pressure) in the vicinity of one atm [57,58,61-63,66]. At 1000°C, the oxygen pressure dependence of conductivity can be divided into distinct regions. In region one (10^{-16} to 10^0atm) the plot of log conductivity vs. log P_{O_2} is linear with a slope of $\sim$ -1/5. At the end of this region a sharp increase in the electrical conductivity was observed; the oxygen partial pressure dependence of conductivity in this region was closely approximated by $P_{O_2}^{-1/0.6}$. At 1050°C, over the P_{O_2} range, 10^{-16} to 10^0atm, the conductivity increased linearly with decreasing oxygen pressure showing a slope of nearly -1/5. As the partial pressure of oxygen was decreased, the pressure dependence of conductivity increased to $\sim$ -1/0.5. The conductivity data at 1100°C were proportional to the $\sim$ -1/5 power of the oxygen pressure for the P_{O_2} range $> 10^{-14.5}$atm. This region was followed by a slope of $\sim$ -1/0.4. P_{O_2} dependencies of electrical conductivity for $BaTi_2O_5$ are summarized in Table IV.

Table-IV. P_{O_2} Dependence of Electrical Conductivity for $BaTi_2O_5$.

T(°C)	P_{O_2}(atm)	m for $\sigma \propto P_{O_2}^{-1/m}$
1000	10^{-16} - 10^{0}	5
	$< 10^{-16}$	0.6
1050	10^{-16} - 10^{0}	5
	$< 10^{-16}$	0.5
1100	$10^{-14.5}$ - 10^{0}	5
	$< 10^{-14.5}$	0.4

From the above observation, it is seen that the conductivity plot, e.g. Fig. 24, can be divided into two characteristic regions depending on the P_{O_2} dependence of electronic conduction. The following discussion explains the electrical conductivity behavior in these two regions.

REGIME I: $[\sigma \propto P_{O_2}^{-1/5}]$

As is evident from Fig. 24, the conductivity of $BaTi_2O_5$ increased with decreasing partial pressure of oxygen. This is characteristic of n-type conduction and it is generally agreed that it is due to metal excess defects in non-stoichiometric materials. Two possible metal excess defects are oxygen vacancies and cation interstitials.

(a) OXYGEN VACANCIES

If oxygen vacancies are the predominant nonstoichiometric defects, theoretical equations for the pressure dependence of the isothermal electrical conductivity can be derived. According to the Kroger-Vink notation [3], the formation of a doubly ionized oxygen vacancy can be written as

$$O_O = \frac{1}{2}O_2 + V_{\ddot{O}} + 2e' \tag{32}$$

where O_O is oxygen at a regular site, $V_{\ddot{O}}$ is a doubly ionized oxygen vacancy and e' is an electron. The equilibrium constant for reaction (32) is

$$K_{32} \approx [V_{\ddot{O}}][e']^2 P_{O_2}^{1/2} \tag{33}$$

With the assumption that $V_{\ddot{O}}$ are the dominant defects in the lattice, the approximate condition for charge neutrality is

$$[n] \approx 2[V_{\ddot{O}}] \tag{34}$$

Substituting charge neutrality, Eq. (34), into Eq. (33) yields an expression for the pressure dependence of the electrical conductivity, σ, as given below

$$\sigma \propto P_{O_2}^{-1/6} \tag{35}$$

In a similar manner, for singly ionized oxygen vacancy the defect reaction is

$$O_O = \frac{1}{2}O_2(g) + V_{\dot{O}} + e' \tag{36}$$

With the neutrality condition

$$[n] \approx [V_{\dot{O}}] \tag{37}$$

the pressure dependence for electronic conduction becomes

$$\sigma \propto P_{O_2}^{-1/4} \tag{38}$$

(b) CATION INTERSTITIALS

Formation of fully ionized cation interstitials in $BaTi_2O_5$ can be described using the following reaction

$$Ba_{Ba} + 2Ti_{Ti} + 5O_O \rightleftharpoons Ba_i^{\cdot\cdot} + 2Ti_i^{\cdot\cdot\cdot\cdot} + 10e' + \frac{5}{2}O_2(g) \tag{39}$$

with the equilibrium constant

$$K_{40} \approx [Ba_i^{\cdot\cdot}][Ti_i^{\cdot\cdot\cdot\cdot}]^2[e']^{10}P_{O_2}^{5/2} \tag{40}$$

Using the following neutrality condition

$$[n] \approx 4[Ti_i^{\cdot\cdot\cdot\cdot}] + 2[Ba_i^{\cdot\cdot}] \tag{41}$$

in relation (40), we can write

$$\sigma \propto P_{O_2}^{-1/5.2} \tag{42}$$

The oxygen partial dependence of the electrical conductivity for partially ionized cation interstitials is given in Table V.

Table-V. Summary of the Expected Oxygen Pressure Dependence of Conductivity for the Case of Partially Ionized Cation Interstitials.

Ionization status of barium & titanium		m for $\sigma \propto P_{O_2}^{-1/m}$
$Ba_i^{\cdot\cdot}$	$Ti_i^{\cdot\cdot\cdot}$	4.4
$Ba_i^{\cdot\cdot}$	$Ti_i^{\cdot\cdot}$	3.6
$Ba_i^{\cdot\cdot}$	$Ti_i^{\cdot}$	2.8
$Ba_i^{\cdot\cdot}$	Ti_i	2.0
$Ba_i^{\cdot}$	$Ti_i^{\cdot\cdot\cdot\cdot}$	1.6
$Ba_i^{\cdot}$	$Ti_i^{\cdot\cdot\cdot}$	4.0
$Ba_i^{\cdot}$	$Ti_i^{\cdot\cdot}$	3.2
$Ba_i^{\cdot}$	$Ti_i^{\cdot}$	2.4
$Ba_i^{\cdot}$	Ti_i	1.6
Ba_i	$Ti_i^{\cdot\cdot\cdot\cdot}$	4.4
Ba_i	$Ti_i^{\cdot\cdot\cdot}$	3.6
Ba_i	$Ti_i^{\cdot\cdot}$	2.8
Ba_i	$Ti_i^{\cdot}$	2.0

Consider the experimental electrical conductivity data in this region which, as already indicated, showed a pressure dependency of -1/5. Comparison of the above theoretically predicted oxygen partial pressure dependencies with the experimental result suggests that the possible dominant defects may be fully ionized cation interstitials. However, from a structural point of view it is difficult

to accept that cation interstitials would be the main defects in $BaTi_2O_5$. As mentioned before, this compound belongs to the group of barium titanates which can be described as close-packed layers of barium and oxygen atoms with Ti atoms in octahedral voids. In fact, the structure of all the barium titanate compounds studied in this work are described in this manner [47,72]. The high energy associated with the formation of cation interstitials in a close packed structure [63] makes any defect structure involving the formation of cation interstitials quite unlikely. Therefore, cation interstitials are omitted from further consideration. As an alternative a defect structure is suggested which is based on the simultaneous existence of both singly and doubly ionized oxygen vacancies in approximately equal concentrations. This situation is described in the following relation

$$O_O = \frac{1}{2}O_2(g) + \frac{1}{2}V_{\dot{O}} + \frac{1}{2}V_{\ddot{O}} + 1.5e' \qquad (43)$$

with the equilibrium constant

$$K_{43} \approx [V_{\dot{O}}]^{\frac{1}{2}}[V_{\ddot{O}}]^{\frac{1}{2}}[e']^{1.5}P_{O_2}^{\frac{1}{2}} \qquad (44)$$

Using the following neutrality condition

$$[n] \approx [V_{\dot{O}}] + 2[V_{\ddot{O}}] \qquad (45)$$

in relation (44), we can write

$$\sigma \propto P_{O_2}^{-1/5} \tag{46}$$

This predicted value from equilibrium reaction (43) is consistent with the experimentally observed value.

REGIME II: $[\sigma \propto P_{O_2}^{-1}]$

The striking feature in this regime is that the electrical conductivity increases with a slope of approximately -1. To understand this behavior it should be pointed out that the equilibrium state for the first data point in this regime was reached after $\sim$ 50 hrs. This is significantly different from the $\sim$ three hrs required for each point in regime I. This difference in time could be indicative of a different atomic rearrangement in the lattice. This is not an unreasonable deduction, particularly at low values of oxygen pressures, for which there is now ample evidence for the interaction between point defects and their consequent ordering [73]. Reduced rutile, for example, is known to give rise to a family of ordered phases, with the composition Ti_nO_{2n-1} [4,15,74]. In a self diffusion study of Ti in reduced TiO_2, Akse et al [75] report that for oxygen pressures between 1×10^{-13} and 1×10^{-16}atm, the ln D vs ln P_{O_2} was linear with a slope of approximately -1/5. Decreasing the oxygen pressure below 1×10^{-16}atm caused a large deviation from the expected random point behavior. Instead of continuing to increase with the above slope, the self diffusion coefficient decreased sharply. Since diffusivity is directly proportional to the concentration of random point defects, the sharp descent in the self diffusion coefficient implies reduction of randomly distributed point defects. They explained this reduction in terms of

ordering of point defects and consequent generation of ordered phases. This process reduces the concentration of randomly oriented point defects and in doing so, reduces the diffusivity. An analogous process is believed to take place in $BaTi_2O_5$, when the deviation from stoichiometry is large. With this in mind a defect model is proposed to account for the observed P_{O_2} dependence of electronic conduction in this regime. In writing this model it is assumed that the ordered phase formed in this compound has the general formula $Ba_nTi_{2n}O_{5n-1}$. Formation of 'b' moles of ordered phase in the already reduced matrix can be described by the following reaction

$$\begin{aligned} BaTi_2O_{5-x} = b(Ba_nTi_{2n}O_{5n-1}) + \frac{Z}{2}O_2(g) \\ + Ba_{1-bn}(V_{Ba})_{bn} + Ti_{2-2bn}(V_{Ti})_{2bn} \\ + O_{5-x-b(5n-1)-Z}(V_O)_{Z+b(5n-1)} \end{aligned} \tag{47}$$

Considering site, charge, mass balance and assuming mixed ionization states for oxygen vacancies, the above expression can be written in the following form:

$$\begin{aligned} bnBa_{Ba} + 2bnTi_{Ti} + [(b(5n-1) + Z)]O_O = b(Ba_nTi_{2n}O_{5n-1}) + \frac{Z}{2}O_2(g) \\ + [V_{Ba}]_{bn} + [V_{Ti}]_{2bn} \\ + [V_{\dot{O}}]_{Z+b(5n-1)/2} \\ + [V_{\ddot{O}}]_{Z+b(5n-1)/2} \\ + \frac{3}{2}(Z+b(5n-1))e' \end{aligned} \tag{48}$$

Elimination of a balanced number of vacancy defects and division by b leads to

$$nBa_{Ba} + 2nTi_{Ti} + [(5n-1) + Z/b]O_O = (Ba_nTi_{2n}O_{5n-1}) + \frac{Z}{2b}O_2(g) + [V_{\ddot{O}}]_{Z-b/2b} + [V_{\dot{O}}]_{Z-b/2b} + \frac{3}{2}(Z/b-1)e' \quad (49)$$

In the above reactions Z can be regarded as the total amount of oxygen escaping from the solid into the gas phase and b is the number of oxygen vacancies eliminated in the process of generating shear planes, i.e. (Z-b) = $[V_{\ddot{O}}]+[V_{\dot{O}}]$ and b ≡ [shear structure]. The mass action constant for the reaction (49) can be expressed by

$$K_{49} \approx a_s[V_{\ddot{O}}]^{Z-b/2b}[V_{\dot{O}}]^{Z-b/2b}[e']^{3/2(Z/b-1)}P_{O_2}^{Z/2b} \quad (50)$$

where a_s represents the activity of the shear structure and is assumed to be constant. Since the presence of both singly and doubly ionized oxygen vacancies were assumed the appropriate neutrality condition is

$$[n] \approx 2[V_{\ddot{O}}] + [V_{\dot{O}}] \quad (51)$$

Taking this charge neutrality condition along with the above mass action expression, produces the following relation for the P_{O_2} dependence of electrical conductivity

$$\sigma \alpha P_{O_2}^{-Z/5(Z-b)} \quad (52)$$

or simply

$$\sigma \alpha P_{O_2}^{-1/m'} \quad (53)$$

Where m' = 5(Z-b)/Z. A similar approach was taken by Oh and Eror in their study of TiO_2 system [76]. For various values of Z/b, the predicted values of m' in Eq. (53) and the corresponding ratios of shear structure to isolated oxygen vacacies are shown in Table VI.

Table-VI. The Predicted Values of m' in the Relation (21), for Various Ratios of z/b and Corresponding Values of b/Z-b.

m' in $\sigma \propto P_{O_2}^{-1/m}$	Z/b	b/Z-b
.4	5/4.6	11.5/1
.5	5/4.5	9/1
.6	5/4.4	7.3/1
1	5/4	4/1
1.2	5/3.8	3.2/1
2.5	2	1/1
4	5	1/4
4.5	10	1/9
4.9	50	1/49

From these calculations it is concluded that the large values of slopes seen in this work can be associated with a high concentration of crystallographic shear (CS) structure. Results shown in Table VI. indicate that the latter proposed model can also predict values such as those observed for the exponent of P_{O_2} dependence of electrical conductivity in regime I. However, based on the following

observation, extensive interaction between point defects at higher values of oxygen partial pressures is ruled out. The electrical conductivity measurements in the present investigation were taken at both decreasing and increasing directions of oxygen pressures. The data obtained in regime I was reproducible during the reduction and oxidation cycles. However, in regime II, during the conductivity measurement on the oxidation side, a hysteresis loop was observed. Such behavior has been associated with the excess energy needed in generating new crystallographic shear planes by Merrit & Hyde [77,78]. In a study on TiO_x system they monitored the partial molar free energy of oxygen in the gas atmosphere over the sample during both increasing and decreasing directions of the oxygen partial pressures. The oxidation and reduction paths obtained in this manner were coincident except in the oxygen pressure range corresponding to the following composition; $1.75 < x < 1.90$ and $1.93 < x < 1.98$. In these regions data exhibited gross hysteresis loops. This behavior was attributed to the excess free energy required in generation and subsequent ordering of shear planes to form a new phase. Based on the above observations (present conductivity data, diffusion study by Akse and Merrit & Hyde's work) it is believed that the absence of hysteresis loop in regime I suggests that randomly distributed point defects are predominant in this regime.

$Ba_6Ti_{17}O_{40}$

The observed electrical conductivity behavior for $Ba_6Ti_{17}O_{40}$ is shown in Fig. 25. The data were obtained at 1000, 1050 and 1100°C under oxygen partial pressures from 10^{-17} - 10^{0} atm. As shown in this figure, the electrical

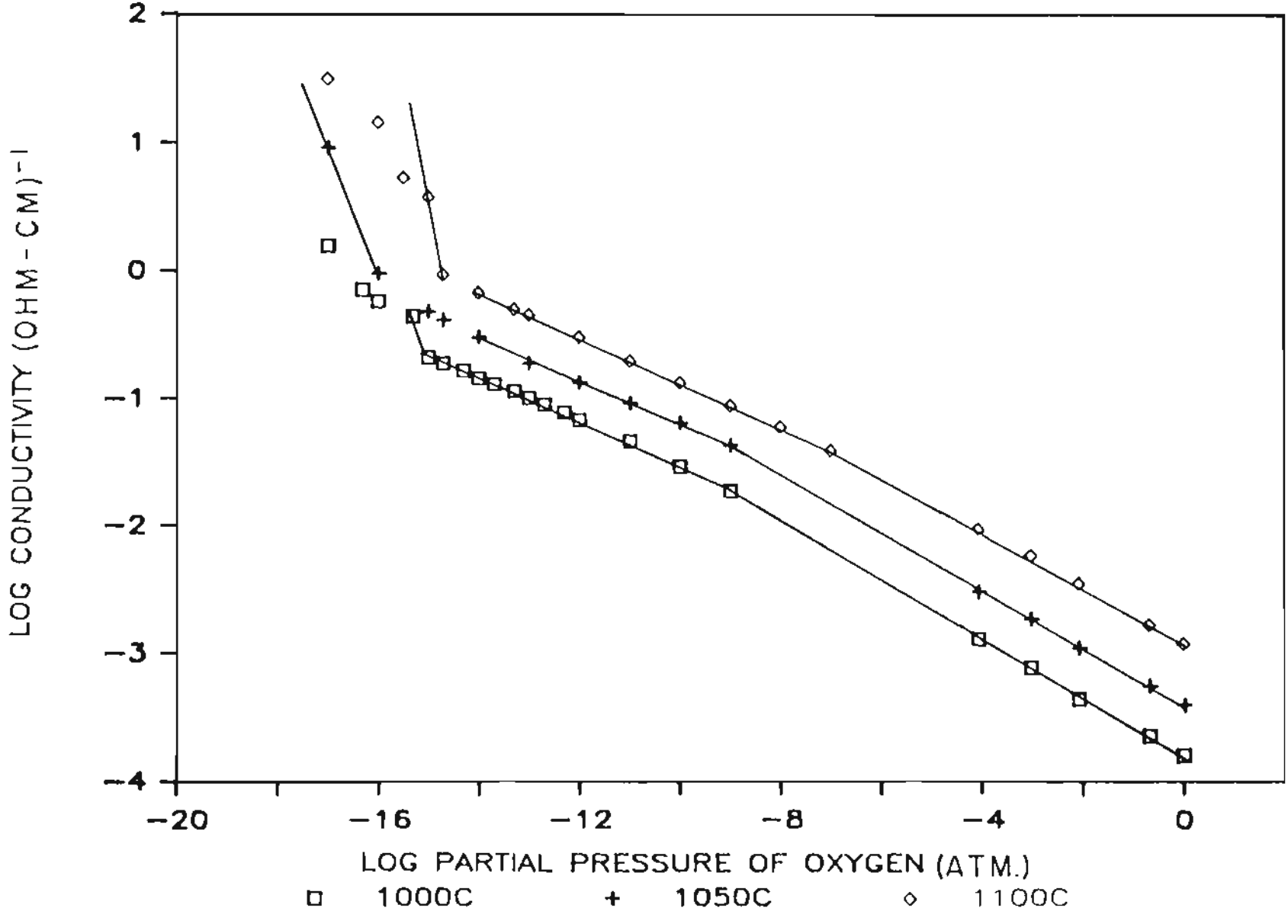

Figure-25. The dependence of the electrical conductivity of $Ba_6Ti_{17}O_{40}$ on oxygen pressure at 1000, 1050 and 1100°C.

conductivity increased with decreasing oxygen partial pressure at constant temperature. At 1000°C the oxygen pressure dependence of the electrical conductivity is characterized by $\sigma \propto P_{O_2}^{-1/4.4}$ for $10^{-9} < P_{O_2} \leq 10^{0}$ and $\sigma \propto P_{O_2}^{-1/5.9}$ for $10^{-15} \leq P_{O_2} < 10^{-9}$. The latter linear region is followed by a slope of nearly -1/0.9. Very similar behavior was observed at 1050°C. However, the sharp rise in conductivity occurred at a slightly higher partial pressure of oxygen. At 1100°C, for oxygen pressures $> 10^{-4}$ atm, the conductivity increased with decreasing P_{O_2} with a slope of -1/4. Over the P_{O_2} range 10^{-14} - 10^{-7} atm, the conductivity dependence varied linearly with a slope of -1/5.7. With further reduction in P_{O_2} the conductivity rose with a slope of $\sim$ -1/0.5 at 1100°C. The summary of experimentally observed slopes is given in Table VII.

Table-VII. P_{O_2} Dependence of Electrical Conductivity for $Ba_8Ti_{17}O_{40}$.

T(°C)	P_{O_2}(atm)	m for $\sigma \propto P_{O_2}^{-1/m}$
1000	10^{-9} - 10^{0}	4.4
	10^{-15} - 10^{-9}	5.9
	$< 10^{-15}$	0.9
1050	10^{-9} - 10^{0}	4.4
	10^{-14} - 10^{-9}	6
	$< 10^{-14}$	1
1100	10^{-4} - 10^{0}	4
	10^{-14} - 10^{-7}	5.7
	$< 10^{-14}$	0.5

Suggested Defect Structures

Regions of the conductivity data characterized by $\sigma \propto P_{O_2}^{-1/4}$ and $P_{O_2}^{-1/4.4}$ can be interpreted in terms of singly ionized oxygen vacancies as was described in eq. (36) and the following reactions respectively

$$O_O = \frac{1}{5}V_{\ddot{O}} + \frac{4}{5}V_{\dot{O}} + 1.2e' + \frac{1}{2}O_2(g) \tag{54}$$

The equilibrium constant is

$$K_{54} \approx [V_{\ddot{O}}]^{1/5}[V_{\dot{O}}]^{4/5}[e']^{1.2}P_{O_2}^{1/2} \tag{55}$$

Assuming the following electrical neutrality

$$[n] \approx 2[V_{\ddot{O}}] + [V_{\dot{O}}] \tag{56}$$

the electrical conductivity σ can be expressed as

$$\sigma \propto P_{O_2}^{-1/4.4} \tag{57}$$

The tendency for the oxygen activity exponent to increase toward -1/5.9 at lower oxygen partial pressure indicates the dominance of completely ionized oxygen vacancies under these atmospheric conditions. This situation is described in the following reaction:

$$O_O = \frac{1}{2}O_2(g) + \frac{19}{20}[V_{\ddot{O}}] + \frac{1}{20}[V_{\dot{O}}] + 1.95e' \tag{58}$$

for which the equilibrium constant is

$$K_{58} \approx [V_{\dot{O}}]^{1/20}[V_{\ddot{O}}]^{19/20}[e']^{1.95}P_{O_2}^{1/2} \tag{59}$$

The condition of electroneutrality is given by the equation

$$[n] \approx [V_{\dot{O}}] + 2[V_{\ddot{O}}] \tag{60}$$

from which it follows

$$\sigma \propto P_{O_2}^{-1/5.9} \tag{61}$$

This predicted value from relation (58) is consistent with the experimentally observed data.

The onset of a sharp rise in the electrical conductivity is described by a defect model incorporating the formation of shear planes as follows:

$$Ba_6Ti_{17}O_{40-x}=b(Ba_{6n}Ti_{17n}O_{40-1}) + \frac{Z}{2}O_2(g)$$
$$+[V_{Ba}]_{6bn} + [V_{Ti}]_{17bn}$$
$$+[V_{\ddot{O}}]_{Z+b(40n-1)} \quad (62)$$

In reaction (62) $Ba_{6n}Ti_{17n}O_{40-1}$ is the assumed composition of the oxygen deficient ordered phase in this compound. This equation can be simplified by elimination of balanced number of vacancy defects and division by b into the following form

$$6nBa_{Ba} + 17nTi_{Ti} + [(40n-1) + Z/b]O_O=(Ba_{6n}Ti_{17n}O_{40n-1}) + \frac{Z}{b}O_2(g)$$
$$+[V_{\dot{O}}^{2\cdot}]_{Z/b-1} + 2(Z/b-1)e' \quad (63)$$

The equilibrium constant for the above reaction takes the form

$$K_{63} \approx a_s[V_{\ddot{O}}]^{Z/b-1}[e']^{2(Z/b-1)}P_{O_2}^{Z/2b} \quad (64)$$

When used with the electroneutrality relation

$$[n] \approx 2[V_{\ddot{O}}] \quad (65)$$

the oxygen partial pressure dependence of electrical conductivity can be expressed in the form of

$$\sigma \propto P_{O_2}^{-Z/6(Z-b)} \quad (66)$$

or

$$\sigma \propto P_{O_2}^{-1/m'} \quad (67)$$

where m' = 6(Z-b)/Z. In the above relations Z and b denote total number of oxygen vacancies and number of oxygen vacancies eliminated in the process of generating shear planes, respectively. For various values of m' the ratios of shear planes and randomly distributed point defects are tabulated in Table VIII.

Table-VIII. The Predicted Values of m' for Various Vatios of Z/b and Corresponding Values of b/Z-b.

m' in $\sigma \propto P_{O_2}^{-1/m'}$	Z/b	b/Z-b
.5	12/11	11/1
.9	6/5.1	5.7/1
1	6/5	5/1
1.5	4/3	3/1
2	3/2	2/1
2.5	6/3.5	1.4/1
3	2	1/1
4	3	1/2
4.5	4	1/3
5	6	1/5
5.5	12	1/11

From Table VIII. it can be seen that the high concentration of shear planes would generate steep slopes such as -1 and -1/0.5 observed in the experimental conductivity data for this compound. It should be mentioned that the Raman spectrum of the $Ba_6Ti_{17}O_{40}$ sample after the electrical conductivity experiment

showed no indication of decomposition.

$Ba_4Ti_{13}O_{30}$

The equilibrium electrical conductivity measurements made on $Ba_4Ti_{13}O_{30}$ over the oxygen pressure range $10^{-18} \leq$ 1atm, at temperatures 1000 and 1100°C is presented in Fig. 26. The conductivity data at 1000°C is characterized by a dependence on oxygen partial pressure of nearly -1/5 for $P_{O_2} > 10^{-15}$. This region is followed by a $P_{O_2}^{-1/4.2}$ slope and finally a gradual transition to $P_{O_2}^{-1/0.5}$ is observed at the lowest experimental P_{O_2} values. The electrical conductivity data at 1100°C also shows three distinct dependencies on oxygen partial pressure. For P_{O_2} from 10^{-10}atm to one atm of oxygen the slope of log σ vs. log P_{O_2} is $\sim$ -1/5. Between 10^{-10} and 10^{-14}atm the P_{O_2} dependence of electrical conductivity is characterized by $\sim$ -1/5.8. At lower values of oxygen partial pressures the conductivity varied with a slope of nearly $P_{O_2}^{-1}$. The above mentioned slopes are summarized in Table IX.

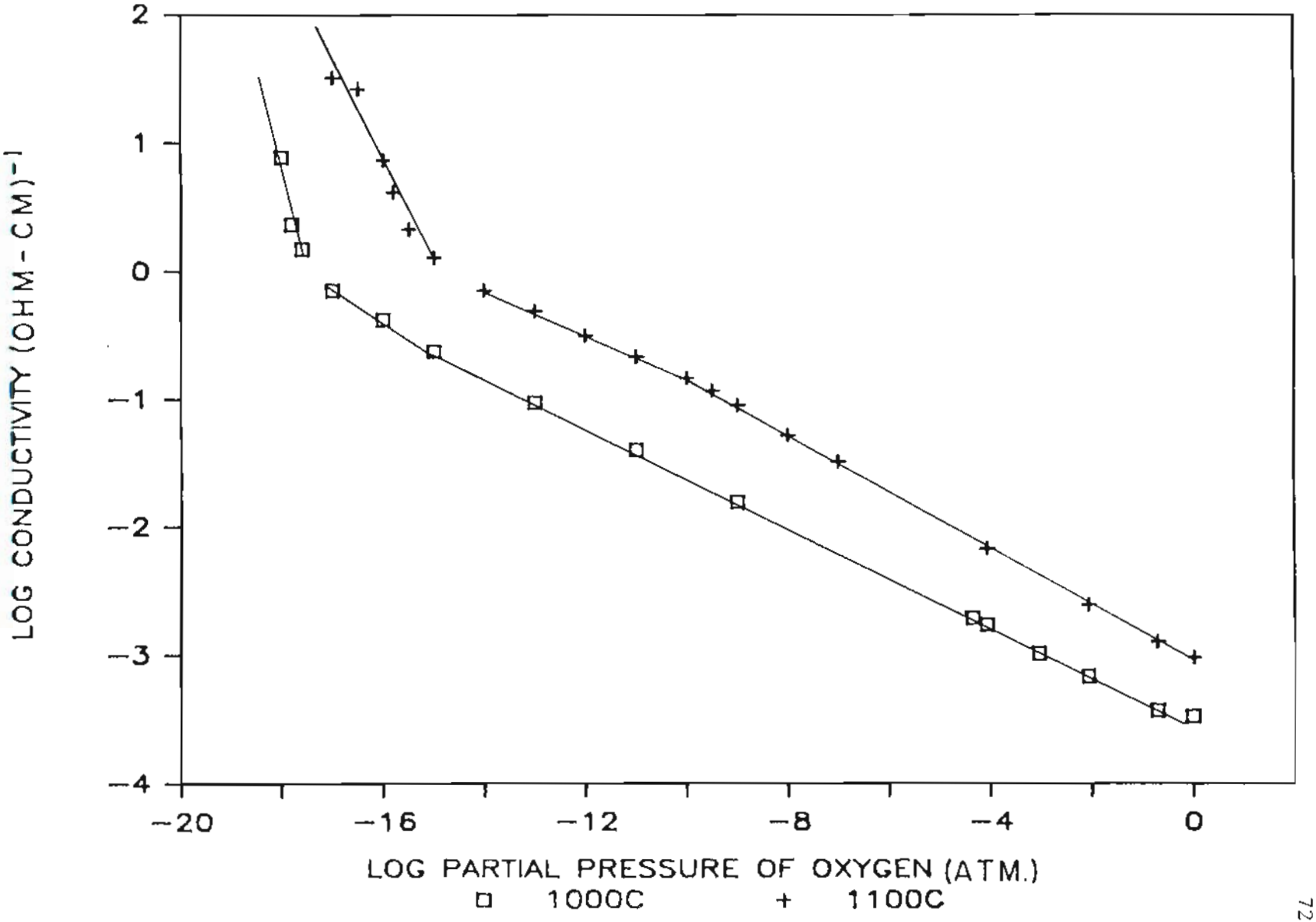

Figure-26. The dependence of the electrical conductivity of $Ba_4Ti_{13}O_{30}$ on oxygen pressure at 1000 and 1100°C.

Table-IX. P_{O_2} Dependence of Electrical Conductivity for $Ba_4Ti_{13}O_{30}$.

T(°C)	P_{O_2}(atm)	m for $\sigma \propto P_{O_2}^{-1/m}$
1000	10^{-15} - 10^{0}	5
	10^{-17} - 10^{-15}	4.2
	$< 10^{-17}$	0.5
1100	10^{-10} - 10^{0}	5
	10^{-14} - 10^{-10}	5.8
	$< 10^{-14}$	1

The experimental $P_{O_2}^{-1/5}$ dependence of conductivity observed both at 1000 and 1100°C can be explained based on the formation of oxygen vacancies in both states of ionization. This type of behavior was also seen in $BaTi_2O_6$ and equations describing the formation of defects of this nature are as follows:

$$O_O = \frac{1}{2}O_2(g) + \frac{1}{2}[V_{\dot{O}}] + \frac{1}{2}[V_{\ddot{O}}] + 1.5e' \tag{68}$$

with an equilibrium constant

$$K_{88} \approx [V_{\dot{O}}]^{1/2}[V_{\ddot{O}}]^{1/2}[e']^{1.5}P_{O_2}^{1/2} \tag{69}$$

and electroneutrality expression

$$[n] \approx [V_{\dot{O}}] + 2[V_{\ddot{O}}] \tag{70}$$

the electrical conductivity σ can be expressed as

$$\sigma \propto P_{O_2}^{-1/5} \tag{71}$$

This electrical conductivity dependence on the oxygen pressure is consistent with the experimental result. At 1000°C the region of 1/5 dependence is followed by an increase in oxygen pressure dependence to ~ -1/4.2. This break in the slope of electrical conductivity plot can be rationalized in terms of suppression of doubly ionized oxygen vacancies due to an increase in electron concentration at lower values of oxygen pressures. The slope of -1/4.2 agrees with the following reaction

$$O_O = \frac{9}{10}V_{\dot{O}} + \frac{1}{10}V_{\ddot{O}} + 1.1e' + \frac{1}{2}O_2(gas) \tag{72}$$

with the chemical equilibrium constant

$$K_{72} \approx [V_{\dot{O}}]^{9/10}[V_{\ddot{O}}]^{1/10}[e']^{1.1}P_{O_2}^{1/2} \tag{73}$$

and charge neutrality condition of

$$|n| \approx [V_{\dot{O}}] + 2|V_{\ddot{O}}| \tag{74}$$

the oxygen pressure dependence of the electrical conductivity is given by

$$\sigma \propto P_{O_2}^{-1/4.2} \tag{75}$$

in agreement with our results. At 1100°C the tendency for the exponent to decrease from -1/5 to -1/5.8 (between 10^{-14} and 10^{-10}atm) indicates more complete ionization of oxygen vacancies at higher temperatures. The following defect model can account for the observed value of $P_{O_2}^{-1/5.8}$ in this region.

$$O_O = \frac{1}{10}V_{\dot{O}} + \frac{9}{10}V_{\ddot{O}} + 1.9e' + \frac{1}{2}O_2(gas) \tag{76}$$

By applying the mass action law to the above relation the equation for the equilibrium constant can be written as follows

$$K_{78} \approx [V_{\dot{O}}]^{1/10}[V_{\ddot{O}}]^{9/10}[e']^{1.9}P_{O_2}^{1/2} \tag{77}$$

With the electroneutrality condition

$$[n] \approx [V_{\dot{O}}] + 2[V_{\ddot{O}}] \tag{78}$$

the expression for the P_{O_2} dependence of σ is written as

$$\sigma \propto P_{O_2}^{-1/5.8} \tag{79}$$

The continuous rise in the conductivity at lower values of oxygen pressures is explained in terms of the existence of an ordered shear phase. With the assignment of the general formula $Ba_{4n}Ti_{13n}O_{30n-1}$, the following are the equilibrium expressions for the formation of b moles of this phase.

$$\begin{aligned} 4nbBa_{Ba} + 13nbTi_{Ti} + [(b(30n-1) + Z)]O_O = b(Ba_{4n}Ti_{13n}O_{30n-1}) + \frac{Z}{2}O_2(gas) \\ +(V_{Ba})_{4nb} + (V_{Ti})_{13nb} \\ +(V_O)_{Z+b(30n-1)} \end{aligned} \tag{80}$$

With the removal of equivalent number of vacancy defects, division by b and dominance of singly ionized oxygen vacancies the above equation can be simplified into the following form

$$4nBa_{Ba} + 13nTi_{Ti} + [(30n-1) + Z/b]O_O = (Ba_{4n}Ti_{13n}O_{30n-1}) + \frac{Z}{2b}O_2(gas)$$

$$+(V_{\dot{O}})_{Z/b-1} + (Z/b-1)e' \qquad (81)$$

The expression for the equilibrium constant is

$$K_{s1} \approx a_s[V_{\dot{O}}]^{Z/b-1}[e']^{Z/b-1}P_{O_2}^{Z/2b} \qquad (82)$$

The electroneutrality condition can be written as follows

$$[n] \approx [V_{\dot{O}}] \qquad (83)$$

Combination of eq. (82) and eq. (83) leads to

$$\sigma \propto P_{O_2}^{-Z/4(Z-b)} \qquad (84)$$

or simply

$$\sigma \propto P_{O_2}^{-1/m'} \qquad (85)$$

where $m' = 4(Z\text{-}b)/Z$. In the above relations Z can be viewed as the total number of oxygen leaving the solid into the gas phase and b is the number of oxygen vacancies eliminated in the process of generating shear planes. The predicted ratios of shear plane concentration and random point defect for some values of m' in eq. (85) are summarized in Table X.

Table-X. The Predicted Values of m′ for Various Ratios of Z/b and Corresponding Values of b/Z-b.

m′ in $\sigma \propto P_{O_2}^{-1/m'}$	Z/b	b/Z-b
.3	4/3.7	12.4/1
.5	4/3.5	7/1
.9	4/3.1	3.5/1
1	4/3	3.5/1
1.6	4/2.4	1.5/1
2	2	1
3	4	1/3
3.5	8	1/7
3.9	40	1/39

This Table suggests that the above model predicts sharp breaks in the log σ vs. log P_{O_2} as the concentration of shear planes increases.

$BaTi_4O_9$

The electrical conductivity dependencies on P_{O_2} for $BaTi_4O_9$ are presented in Fig. 27. The measurements were carried out at temperatures 1000, 1050 and 1100°C under oxygen partial pressure of 10^{-18} - 10^{0}atm. The exponent m in the expression $\sigma \propto P_{O_2}^{-1/m}$ at 1000°C attains values of 4.7 for $P_{O_2} > 10^{-13}$ and 5.4 for $10^{-17} < P_{O_2} < 10^{-13}$ and 0.2 for $P_{O_2} < 10^{-17}$. The oxygen pressure dependence of the electrical conductivity has three different values at 1050°C. These

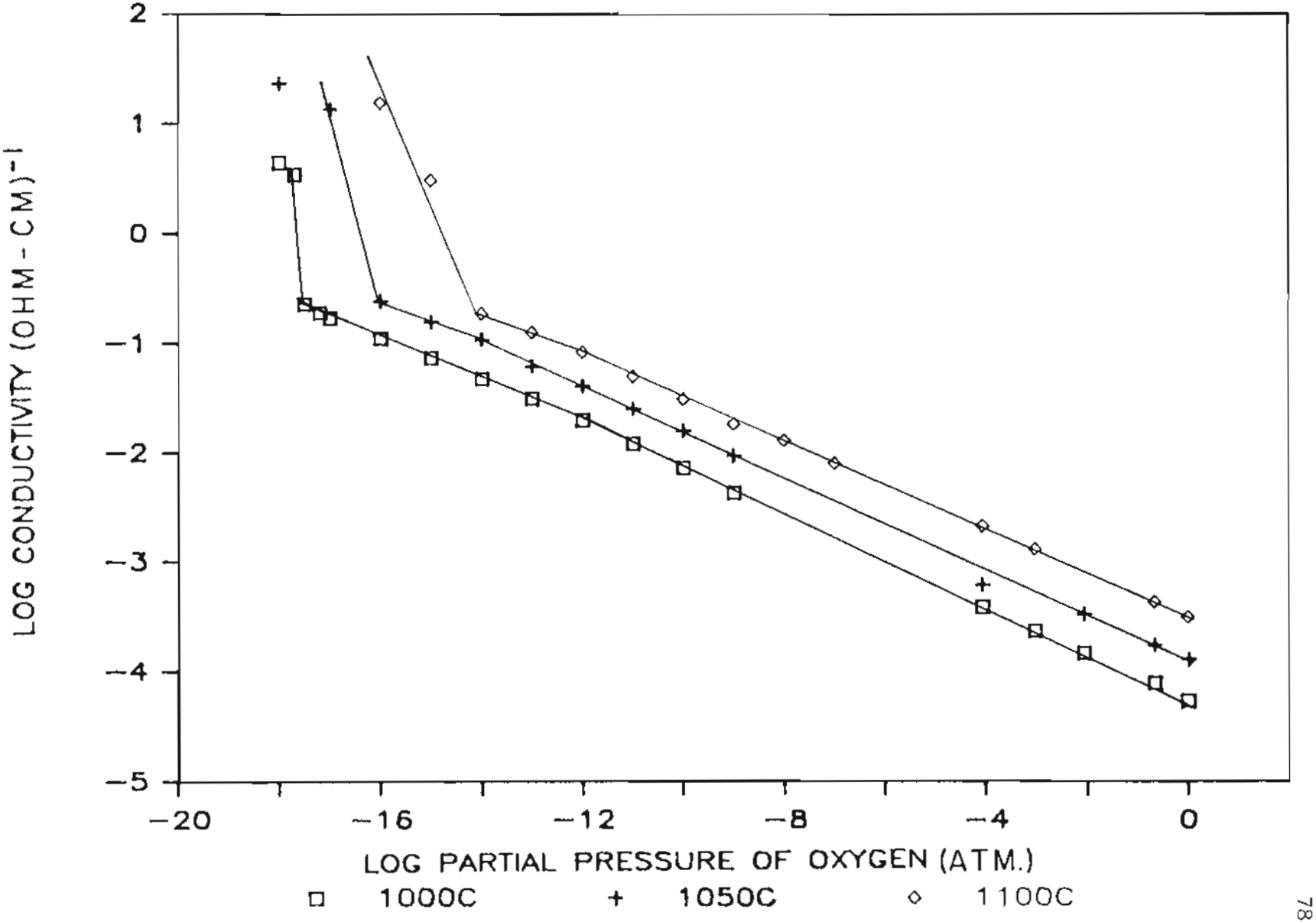

Figure-27. The dependence of the electrical conductivity of $BaTi_4O_9$ on oxygen pressure at 1000, 1050 and 1100°C.

are ~ -1/4.8 in the P_{O_2} region above 10^{-14}, ~ -1/5.7 in the range 10^{-16} - 10^{-14} atm and ~ -1/.6 below 10^{-16}atm. The conductivity at 1100°C increased with decrease in P_{O_2}, showing slopes of ~ -1/5 for $10^{-12} \leq P_{O_2} \leq 10^{0}$atm, ~ -1/5.7 for oxygen partial pressures between 10^{-14} and 10^{-12}atm and ~ -1 for lower values of oxygen partial pressure. The summary of P_{O_2} dependencies is shown in Table XI.

Table-XI. P_{O_2} Dependence of Electrical Conductivity for $BaTi_4O_9$.

T(°C)	P_{O_2}(atm)	m for $\sigma \propto P_{O_2}^{-1/m}$
1000	10^{-13} - 10^{0}	4.7
	10^{-17} - 10^{-13}	5.4
	$< 10^{-17}$	0.2
1050	10^{-14} - 10^{0}	4.8
	10^{-16} - 10^{-14}	5.7
	$< 10^{-16}$	0.6
1100	10^{-12} - 10^{0}	5
	10^{-14} - 10^{-12}	5.7
	$< 10^{-14}$	1

The experimental oxygen partial pressure dependence value -1/4.7 seen at 1000°C can be analyzed in terms of an ideal point defect model involving isolated singly and doubly ionized oxygen vacancies as follows

$$O_O = \frac{1}{2}O_2(g) + \frac{13}{20}V_{\dot{O}} + \frac{7}{20}V_{\ddot{O}} + 1.35e' \tag{86}$$

Applying the mass action law to the above equation results in

$$K_{86} \approx [V_{\dot{O}}]^{13/20}[V_{\ddot{O}}]^{7/20}[e']^{1.35}P_{O_2}^{1/2} \tag{87}$$

The electroneutrality condition in this case can be written as

$$[n] \approx [V_{\dot{O}}] + 2[V_{\ddot{O}}] \tag{88}$$

and from relations (87) and (88) the P_{O_2} dependence of conductivity can be expressed as

$$\sigma \propto P_{O_2}^{-1/4.7} \tag{89}$$

Therefore, both singly and doubly ionized oxygen vacancies are responsible for the electronic n-type conduction of this material. The shallower P_{O_2} dependencies at lower oxygen partial pressures and/or higher temperatures signifies the increasing number of divalent oxygen vacancies.

As can be seen from the plot of log σ vs log P_{O_2} for this compound, the break from random point defects (onset of ordering) occurs at higher values of oxygen partial pressures as temperature increases. This I think indicates that the ordering of random point defects takes place when a certain fraction of available oxygen sites in the lattice are left vacant; and since this fraction is reached sooner as temperature increases, the break in the curve is observed earlier. The process of ordering of defects leads to segregation of a new phase with an

assumed composition of $Ba_nTi_{4n}O_{9n-1}$. The formation of b moles of this phase from reduced parent phase can be expressed as follows:

$$BaTi_4O_{9-x}=b(Ba_nTi_{4n}O_{9n-1}) + \frac{Z}{2}O_2(gas)$$
$$+Ba_{1-bn}(V_{Ba}^{''})_{bn} + Ti_{4-4bn}(V_{Ti}^{''''})_{4bn}$$
$$+O_{9-x-b(9n-1)-z}(V_{\ddot{O}}) + 2(Z-b)e' \quad (90)$$

The above relation can be simplified into the following form:

$$bnBa_{Ba} + 4bnTi_{Ti} + [(b(9n-1) + Z]O_O=b(Ba_nTi_{4n}O_{9n-1}) + \frac{Z}{2}O_2(gas)$$
$$+[V_{Ba}^{''}]_{bn} + [V_{Ti}^{''''}]_{4bn}$$
$$+[V_{\ddot{O}}]_{Z+b(9n-1)} + 2(Z-b)e' \quad (91)$$

Equation (91) can be further simplified by elimination of equivalent numbers of defects and division by b

$$nBa_{Ba} + 4nTi_{Ti} + [(9n-1) + Z/b]O_O=(Ba_nTi_{4n}O_{9n-1}) + \frac{Z}{2b}O_2(gas)$$
$$+[V_{\ddot{O}}]_{z/b-1} + 2(Z/b-1)e' \quad (92)$$

The equilibrium constant for this reaction is

$$K_{92} \approx a_s[V_{\ddot{O}}]^{(z/b-1)}[e']^{2(z/b-1)}P_{O_2}^{z/2b} \quad (93)$$

For all the three temperatures investigated the appropriate electroneutrality expression in this region of low P_{O_2} is

$$[n] \approx 2[V_{\ddot{O}}] \tag{94}$$

By combining the last two relations the pressure dependence of electrical conductivity takes the following form:

$$\sigma \propto P_{O_2}^{-Z/6(Z-b)} \tag{95}$$

Replacing 6(Z-b)/Z by m' leads to the following expression for the electrical conductivity

$$\sigma \propto P_{O_2}^{-1/m'} \tag{96}$$

Table XII. contains predicted ratios of shear structure concentration to isolated divalent oxygen vacancies for some values of m'.

Table-XII. The Predicted Values of m′ for Various Ratios of Z/b and Corresponding Values of b/Z-b.

m′ in $\sigma \propto P_{O_2}^{-1/m'}$	Z/b	b/Z-b
.2	30/29	29/1
.6	30/27	9/1
.8	30/26	6.5/1
1	6/5	5/1
2	6/4	2/1
3	2	1/1
4	3	1/2
5	6	1/5
5.5	12	1/11
5.9	60	1/59

As can be seen from the above Table the small values of m′ are associated with higher concentration of shear planes.

$Ba_2Ti_9O_{20}$

The measured electrical conductivity of polycrystalline $Ba_2Ti_9O_{20}$ in the temperature range 1050-1150°C and in equilibrium with oxygen partial pressures between 10^{-18}-1atm is shown in Fig. 28. As can be seen for all the temperatures investigated, the conductivity of this compound increased with decreasing oxygen partial pressure resulting in n-type material throughout the whole P_{O_2} range. At

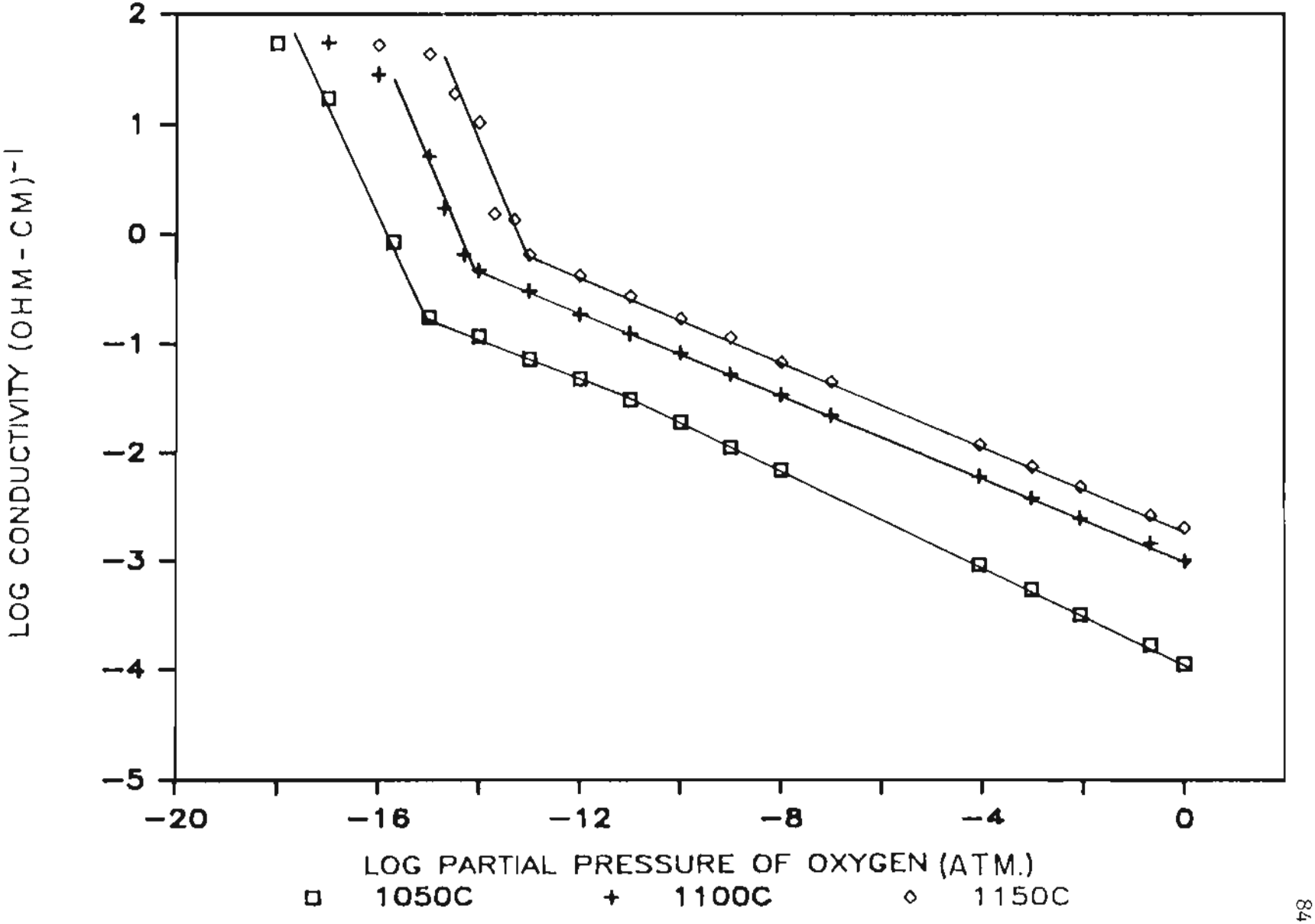

Figure-28. The dependence of the electrical conductivity of $Ba_2Ti_9O_{20}$ on oxygen pressure at 1050, 1100 and 1150°C.

1050°C, the oxygen pressure dependence of conductivity can be divided into three distinct regions. In region one (10^{-11} to 10^{0}atm) the plot of log σ vs. log P_{O_2} is linear with a slope of -1/4.5. Between 10^{-11} and 10^{-15} atm (region 2) the measured conductivity was proportional to the -1/5.3 power of P_{O_2}. At the end of this region a sharp increase in the electrical conductivity was observed; the oxygen pressure dependence of conductivity in this region was closely approximated by $P_{O_2}^{-1}$. At higher temperatures no region with -1/4.5 dependence for conductivity on oxygen activity was observed. At 1100°C over the P_{O_2} range, 10^{-14} to 10^{0}atm, the conductivity increased linearly with decreasing oxygen pressures showing a slope of -1/5.2. As the partial pressure of oxygen was decreased, the pressure dependence of conductivity increased to $\sim$ -1/0.8. The conductivity data at 1150°C were proportional to the -1/5.1 power of the oxygen pressure for the P_{O_2} range $> 10^{-13}$atm. This region was followed by a discontinuous rise in the conductivity with the P_{O_2} dependence of $\sim$ -1/0.9. The slopes observed in the log σ vs. log P_{O_2} are summarized in Table XIII.

Table-XIII. P_{O_2} Dependence of Electrical Conductivity for $Ba_2Ti_9O_{20}$.

T(°C)	P_{O_2}(atm)	m for $\sigma \propto P_{O_2}^{-1/m}$
1050	10^{-11} - 10^{0}	4.5
	10^{-15} - 10^{-11}	5.3
	$< 10^{-15}$	1
1100	10^{-14} - 10^{0}	5.2
	$< 10^{-14}$	0.8
1150	10^{-13} - 10^{0}	5.1
	$< 10^{-13}$	0.9

The following is the discussion on the nature of defect structures dominating in the three regions of interest.

REGION I: [$\sigma \propto P_{O_2}^{-1/4.5}$]

As has already been mentioned, due to structural restrictions the most favorable choice of defects in these compounds are oxygen vacancies. The experimental slope of -1/4.5 can be interpreted in terms of a defect model based on a simultaneous presence of $V_{\dot{O}}$ and $V_{\ddot{O}}$. The process of defect formation can be written as

$$O_O = \frac{3}{4}V_{\dot{O}} + \frac{1}{4}V_{\ddot{O}} + 1.25e' + \frac{1}{2}O_2(g) \qquad (97)$$

With the equilibrium constant

$$K_{97} \approx [V_{\dot{O}}]^{3/4}|V_{\ddot{O}}|^{1/4}|e'|^{1.25}P_{O_2}^{1/2} \tag{98}$$

the charge neutrality can be expressed as

$$[n] \approx [V_{\dot{O}}] + 2[V_{\ddot{O}}] \tag{99}$$

Combination of the relations (98) and (99) leads to the following expression for the electrical conductivity:

$$\sigma \propto P_{O_2}^{-1/4.5} \tag{100}$$

REGION II. [$\sigma \propto P_{O_2}^{-1/5.1} - P_{O_2}^{-1/5.3}$]

The electrical conductivity in this region is characterized by an oxygen partial pressure dependence, $P_{O_2}^{-1/m}$, with the values of 1/m near -1/5.3 at 1050°C, -1/5.2 at 1100°C and -1/5.1 at 1150°C. In this region, a defect structure which incorporates both singly and doubly ionized oxygen vacancies is also assumed. The values of P_{O_2} dependencies indicated above are proposed to reflect the dominance of doubly ionized oxygen vacancies. For example, the observed slope of -1/5.2 at 1100°C for $P_{O_2} > 10^{-14}$ can be explained through the following reaction

$$O_O = + \frac{2}{5}V_{\dot{O}} + \frac{3}{5}V_{\ddot{O}} + 1.6e' + \frac{1}{2}O_2(g) \tag{101}$$

The equilibrium constant for the above reaction is

$$K_{101} \approx [V_{\dot{O}}]^{2/5}[V_{\ddot{O}}]^{3/5}|e'|^{1.6}P_{O_2}^{1/2} \tag{102}$$

using the following neutrality condition in eqn (102)

$$[n] \approx [V_{\dot{O}}] + 2[V_{\ddot{O}}] \tag{103}$$

the conductivity dependence on oxgen partial pressure becomes

$$\sigma \propto P_{O_2}^{-1/5.2} \tag{104}$$

REGION III. $[\, \sigma \propto P_{O_2}^{-1} \,]$

The sharp change in the slope of electrical conductivity in this region is explained by a model involving the formation of a new ordered structure within the matrix. Following are the equilibrium reactions describing the formation of b moles of this new ordered phase.

$$\begin{aligned} Ba_2Ti_9O_{20-x} = b(Ba_{2n}Ti_{9n}O_{20n-1}) + \frac{Z}{2}O_2(g) \\ + Ba_{2-2bn}(V_{Ba}^{''})_{2bn} + Ti_{9-9bn}(V_{Ti}^{''''}) \\ + O_{20-x-b(20n-1)-Z}(V_{\ddot{O}})_{Z+b(20n-1)} + 2(Z-b)e' \end{aligned} \tag{105}$$

In the above relation, $Ba_{2n}Ti_{9n}O_{20-1}$ is the assumed general formula for the new phase. Considering site, charge and mass balance, the eq. (105) can be restated as

$$\begin{aligned} 2bnBa_{Ba} + 9bnTi_{Ti} + [(b(20n-1) + Z)]O_O = b(Ba_{2n}Ti_{9n}O_{20n-1}) + \frac{Z}{2}O_2(gas) \\ + [V_{Ba}]_{2bn} + [V_{Ti}]_{9bn} \\ + [V_{\ddot{O}}]_{Z+b(20n-1)} + 2(Z-b)e' \end{aligned} \tag{106}$$

The above eq. can be further simplified by elimination of equivalent number of

vacancy defects and division by b

$$2nBa_{Ba} + 9nTi_{Ti} + |(20n-1) + \frac{Z}{b}|O_O = (Ba_{2n}Ti_{9n}O_{20n-1}) + \frac{Z}{2b}O_2(gas) + |V_{\ddot{O}}|_{Z/b-1} + 2(Z/b-1)e' \quad (107)$$

The mass action constant for the above reaction is expressed as

$$K_{107} \approx a_n[V_{\ddot{O}}]^{(Z/b-1)}[e']^{2(Z/b-1)}P_{O_2}^{Z/2b} \quad (108)$$

Since the dominance of $V_{\ddot{O}}$ was assumed the appropriate neutrality condition is

$$[n] \approx 2[V_{\ddot{O}}] \quad (109)$$

Taking this charge neutrality condition along with the above mass action expression, produces the following relation for the P_{O_2} dependence of electrical conductivity

$$\sigma \propto P_{O_2}^{-Z/6(Z-b)} \quad (110)$$

or simply

$$\sigma \propto P_{O_2}^{-1/m'} \quad (111)$$

where $m' = 6(Z\text{-}b)/Z$. In the above reactions Z can be regarded as the total number of oxygen escaping from the solid into the gas phase and b is the number of oxygen vacancies eliminated in the process of generating shear planes. For some values of m', the predicted ratios of Z/b and the corresponding ratios of shear planes to isolated oxygen vacancies (b/Z-b) are shown in Table XIV.

Table-XIV. The Predicted Values of m' for Various Ratios of Z/b and Corresponding Values of b/Z-b.

m' in $\sigma \propto P_{O_2}^{-1/m'}$	Z/b	b/Z-b
.5	12/11	11/1
.8	15/13	13/2
.9	6/5.1	5.67/1
1	6/5	5/1
1.2	5/4	4/1
1.5	4/3	3/1
2.5	12/7	7/5
3.5	12/5	5/7
4	3/1	1/2
4.5	4/1	1/3
5	6/1	1/5

As can be seen from Table XIV. higher concentration of shear planes correspond to lower values of m'. The Raman spectrum of the $Ba_2Ti_9O_{20}$ sample after the electrical conductivity experiment showed no sign of decomposition in this material.

$BaTi_5O_{11}$

Figure 29 shows the conductivity data for $BaTi_5O_{11}$. The measurements were carried out at temperatures 850, 900 and 950°C under oxygen partial

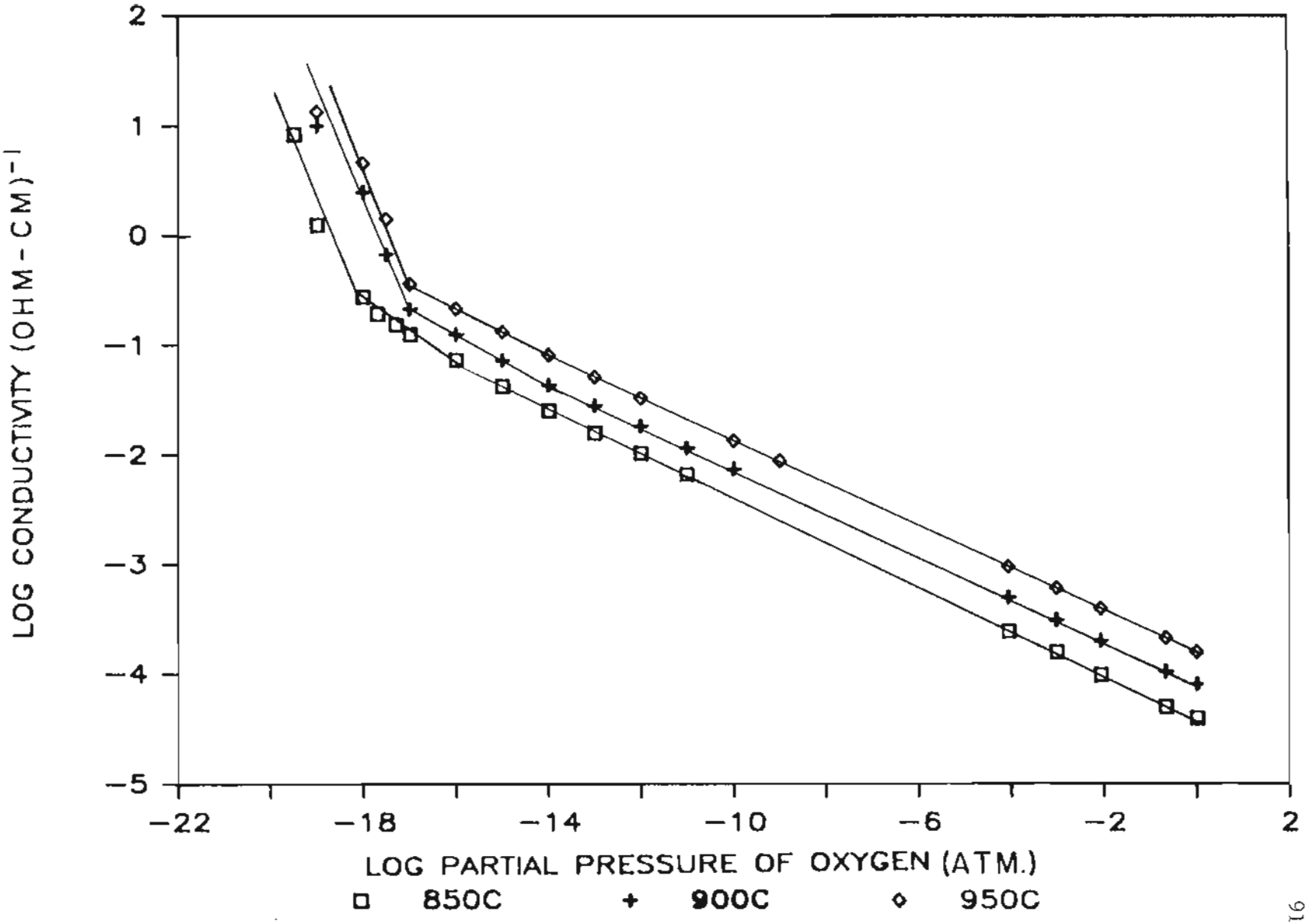

Figure-29. The dependence of the electrical conductivity of $BaTi_6O_{11}$ on oxygen pressure at 850, 900 and 950°C.

pressures from $10^{-19.5}$ to one atm. At any constant temperature the electrical conductivity seems to follow three different oxygen pressure dependencies. At 850°C the P_{O_2} dependence of electrical conductivity can be expressed as $P_{O_2}^{-1/4.9}$ for oxygen pressures $> 10^{-15}$, $P_{O_2}^{-1/4.1}$ for $10^{-15} \leq P_{O_2} \leq 10^{-17.7}$ and $\sigma \propto P_{O_2}^{-1/1.4}$ for $P_{O_2} < 10^{-17.7}$. At 900°C, the conductivity is characterized by $\sigma \propto P_{O_2}^{-1/5.2}$ for $10^{-14} \leq P_{O_2} \leq$ 1atm, $\sigma \propto P_{O_2}^{-1/4.4}$ for $10^{-17} \leq p_{O_2} \leq 10^{-14}$ and $\sigma \propto P_{O_2}^{-1/0.9}$ for $P_{O_2} < 10^{-17}$. At 950°C the observed slopes are -1/5.2 for $P_{O_2} > 10^{-14}$, -1/4.7 for $10^{-17} \leq P_{O_2} \leq 10^{-14}$ and -1/0.85 for $P_{O_2} \leq 10^{-17}$. The summary of observed slopes is given in Table XV.

Table-XV. P_{O_2} Dependence of Electrical Conductivity for $BaTi_6O_{11}$.

T(°C)	P_{O_2}(atm)	m for $\sigma \propto P_{O_2}^{-1/m}$
850	$10^{-15} - 10^{0}$	4.9
	$10^{-17.7} - 10^{-15}$	4.1
	$< 10^{-17.7}$	1.4
900	$10^{-14} - 10^{0}$	5.2
	$10^{-17} - 10^{-14}$	4.4
	$< 10^{-17}$	0.9
950	$10^{-14} - 10^{0}$	5.2
	$10^{-17} - 10^{-14}$	4.7
	$< 10^{-17}$	0.85

The experimental -1/4.9 slope observed at 850°C can be explained by means of a model, whose basic assumption is the simultaneous existence of singly and doubly ionized oxygen vacancies according to the following equilibrium reaction

$$O_O = \frac{1}{2}O_2(g) + \frac{11}{20}V_{\dot{O}} + \frac{9}{20}V_{\ddot{O}} + 1.45e' \qquad (112)$$

The equilibrium constant for the above reaction is

$$K_{112} \approx [V_{\dot{O}}]^{11/20}[V_{\ddot{O}}]^{9/20}[e']^{1.45}P_{O_2}^{1/2} \qquad (113)$$

Substituting the following electroneutrality condition

$$[n] \approx [V_{\dot{O}}] + 2[V_{\ddot{O}}] \tag{114}$$

back in eq. (113) gives

$$\sigma \propto P_{O_2}^{-1/4.9} \tag{115}$$

At lower values of P_{O_2} the concentration of singly ionized oxygen vacancies becomes appreciable, causing σ to tend toward a $P_{O_2}^{-1/4.1}$ dependence. This situation can be represented by the following defect reaction

$$O_O = \frac{1}{2}O_2(g) + \frac{19}{20}V_{\dot{O}} + \frac{1}{20}V_{\ddot{O}} + 1.05e' \tag{116}$$

The equilibrium constant for reaction (116) is

$$K_{116} \approx [V_{\dot{O}}]^{19/20}[V_{\ddot{O}}]^{1/20}[e']^{1.05}P_{O_2}^{1/2} \tag{117}$$

Assuming the following electrical neutrality condition

$$[n] \approx 2[V_{\ddot{O}}] + [V_{\dot{O}}] \tag{118}$$

the electrical conductivity σ can be expressed as

$$\sigma \propto P_{O_2}^{-1/4.1} \tag{119}$$

Formation of shear planes is believed to be responsible for the steep rise in the conductivity for $P_{O_2} < 10^{-17.7}$. Defect notation for the formation of shear planes in $BaTi_5O_{11}$ is as follows

$$BaTi_5O_{11-x}=b(Ba_nTi_{5n}O_{11n-1}) + \frac{Z}{2}O_2(g)$$
$$+Ba_{1-bn}(V_{Ba})_{bn} + Ti_{5-5bn}(V_{Ti})_{5bn}$$
$$+O_{11-x-b(11n-1)-Z}(V_O)_{Z+b(11n-1)} \qquad (120)$$

Considering site, charge, mass balance and assuming mixed ionization states for oxygen vacancies, the above relation can be written in the following form:

$$bnBa_{Ba} + 5bnTi_{Ti} + |(b(11n-1) + Z)]O_O=b(Ba_nTi_{5n}O_{11n-1}) + \frac{Z}{2}O_2(g)$$
$$+[V_{Ba}]_{bn} + [V_{Ti}]_{5bn}$$
$$+1.9[V_{\dot{O}}]_{Z+b(11n-1)/2}$$
$$+.1[V_{\ddot{O}}]_{Z+b(11n-1)/2} \qquad (121)$$
$$+(1.05Z + 1.05b(11n-1))e'$$

Elimination of a balanced number of vacancy defects and division by b leads to

$$nBa_{Ba} + 5nTi_{Ti} + [(11n-1) + Z/b]O_O=(Ba_nTi_{5n}O_{11n-1}) + \frac{Z}{2b}O_2(g)$$
$$+1.9[V_{\dot{O}}]_{Z-b/2b} + .1[V_{\ddot{O}}]_{Z-b/2b}$$
$$+1.05(Z/b-1)e' \qquad (122)$$

In the above reactions Z can be regarded as the total amount of oxygen escaping from the solid into the gas phase and b is the number of oxygen vacancies eliminated in the process of generating shear planes. The mass action constant for the relation (122) is

$$K_{122} \approx a_s[V_{\dot{O}}]^{1.9(Z-b/2b)}[V_{\ddot{O}}]^{.1(Z-b/2b)}[e']^{1.05(Z/b-1)}P_{O_2}^{Z/2b} \quad (123)$$

Since the presence of both singly and doubly ionized oxygen vacancies were assumed the appropriate neutrality condition is

$$|n| \approx [V_{\dot{O}}] + 2|V_{\ddot{O}}| \quad (124)$$

Combination of eqns (123) and (124) leads to the following relation for the pressure dependence of electrical conductivity

$$\sigma \propto P_{O_2}^{-Z/4.1(Z-b)} \quad (125)$$

or simply

$$\sigma \propto P_{O_2}^{-1/m'} \quad (126)$$

where $m' = 4.1(Z\text{-}b)/Z$. For various values of Z/b, the predicted values of m' in eq. (126) and the corresponding ratios of shear structure to isolated oxygen vacancies are give in Table XVI.

Table-XVI. The Predicted Values of m' for Various Ratios of Z/b and Corresponding Values of b/Z-b.

m' in $\sigma \propto P_{O_2}^{-1/m'}$	Z/b	b/Z-b
.3	4.1/3.8	12.6/1
.5	4.1/3.6	7.2/1
.7	4.1/3.4	4.85/1
.8	4.1/3.3	4.1/1
.9	4.1/3.2	3.5/1
1.2	4.1/2.9	2.4/1
1.4	4.1/2.7	1.9/1
2	4.1/2.1	1.05/1
3	4.1/1.1	1/2.7
3.5	4.1/0.6	1/5.8
4	41	1/40

The electrical conductivity data exhibited a very similar pattern at higher temperatures (900 and 950°C). The shallower slopes observed at these temperatures suggest that a higher proportion of oxygen vacancies are fully ionized. For example, to account for the experimentally observed slope of -1/5.2 at 950°C for $P_{O_2} > 10^{-14}$, the following model is proposed

$$O_O = \frac{4}{10} V_{\dot{O}} + \frac{6}{10} V_{\ddot{O}} + 1.6e' + \frac{1}{2} O_2(g) \qquad (127)$$

With mass action constant given by

$$K_{127} \approx [V_{\dot{O}}]^{4/10}[V_{\ddot{O}}]^{6/10}[e']^{1.6}P_{O_2}^{1/2} \tag{128}$$

Using the following neutrality condition

$$[n] \approx [V_{\dot{O}}] + 2[V_{\ddot{O}}] \tag{129}$$

in relation (128), one can write

$$\sigma \propto P_{O_2}^{-1/5.2} \tag{130}$$

V. SUMMARY AND CONCLUSIONS

In order to reinvestigate the phase relations in the TiO_2- rich region of BaO-TiO_2 system, the compositions of $BaTi_2O_5$, $Ba_6Ti_{17}O_{40}$, $Ba_4Ti_{13}O_{30}$, $BaTi_4O_9$ and $Ba_2Ti_9O_{20}$ were prepared using the Pechini method. The resultant amorphous powders were heated from 600 to 1300°C. Raman spectroscopy was used to determine phase transformations as a function of temperature. The following are the conclusions based on this study:

1- The compound $BaTi_2O_5$ is a low temperature stable phase and it decomposes slowly into $BaTiO_3$ and $Ba_6Ti_{17}O_{40}$ at 1300°C.

2- $Ba_6Ti_{17}O_{40}$ forms after short heat treatment at 1200°C.

3- The phase $Ba_4Ti_{13}O_{30}$ was observed at 1000°C and was stable at higher temperatures.

4- The $BaTi_4O_9$ structure forms at temperatures as low as 600°C, but in addition there is some indication of (1:5) phase. This small amount of (1:5) phase is not detectable by x-ray diffraction experiments for samples heated above 1000°C. The trace of (1:5) compound disappears from Raman pattern of $BaTi_4O_9$ at 1200°C.

5- The $Ba_2Ti_9O_{20}$ structure forms only after long heat treatment at 1200°C.

6- $BaTi_5O_{11}$ was stable between 700 and 1100°C. This phase decomposes into (2:9) and TiO_2 after prolonged heating times at 1200°C.

7- Although there are some differences in the results obtained from the two low temperature preparation techniques (the liquid mix technique used in the present study and hydrolysis method used by Roth), in general there is a fairly good agreement between the two sets of data with regard to stability conditions for the studied polytitanates.

In the second part of this work, the electrical conductivities of these materials were measured as a function of temperature (850 to 1150°C) and oxygen activity (10^{-19} to 1atm). The polytitanates investigated exhibited n-type conduction for the entire range of oxygen partial pressures at any constant temperature. The observed variation of log conductivity with log P_{O_2} matched the predicted value for a defect structure consisting of simultaneous presence of singly and doubly ionized oxygen vacancies. The onset of abrupt change in the electrical conductivity at low values of oxygen activity was related to the formation of shear structures. Thus, the major contributions of this research were the identification of the Raman spectra and defect structures of Ti-rich compounds in the $BaTiO_3$-TiO_2 system.

Bibliography

[1] C. Wagner and W. Schottky: Z.Phys.Chem. B11, 163 (1931).

[2] C. Wagner: Z.Phys.Chem. B22, 181 (1933).

[3] F. A. Kroger and H. J. Vink: Solid State Physics, 3 307-435 (1956).

[4] S. Anderson, B. Collen, U. Kuylenstierna and A. Magneli: Acta.Chem.Scand. 11, 164 (1957).

[5] L. A. Bursill and B. G. Hyde: Acta.Crysta. B27, 210 (1971).

[6] For a review see: J. S. Anderson in "Surface and Defect Properties of Solids" (M. W. Roberts and J. M. Thomas, eds.) Vol. 1, P.1 The Chemical Society London, (1972).

[7] S. Anderson: Acta.Chem.Scand. 14, 1161 (1960).

[8] A. D. Wadsley: Rev.Pure.Appl.Chem. 5, 165 (1955).

[9] A. L. G. Ress: Trans.Faraday.Soc. 50, 335 (1954).

[10] M. Atlas: J.Phys.Chem.Solids. 29, 91 (1968).

[11] N. N. Greenwood in "Ionic Crystal Lattice Defects, Nonstoichiometry" ButterWorth and Co. London (1970).

[12] S. Anderson and L. Jahnberg: Ark.Kemi 21, 413 (1963).

[13] R. M. Gibb and J. S. Anderson: J. Solid State Chem. 4, 379 (1972).

[14] R. M. Gibb and J. S. Anderson: J. Solid State Chem. 5, 212 (1972).

[15] J. Vanlanduyt and S. Amelincky: Mat.Res.Bull. 5, 267 (1970).

[16] J. S. Anderson and B. G. Hyde: Bull.Soc.Chim. France 1215 (1965).

[17] S. Anderson and B. G. Hyde: J. Phys.Chem.Solids. 28, 1393 (1967).

[18] R. J. D. Tilley: Mat.Res.Bull. 5, 813 (1970).

[19] J. G. Allpress and P. Gados: Cryst.Latti.Defec. 1, 331 (1970).

[20] J. G. Allpress, R. J. D. Tilley and M. J. Sienko: J. Solid State Chem. 4, 440 (1971).

[21] L. A. Bursill and B. G. Hyde: J. Solid State Chem. 4, 430 (1972).

[22] T. Ekstrom and R. J. D. Tilley: Mat. Res. Bull. 9 705-714 (1974).

[23] J. S. Anderson in "Defects and Transport in Oxides" (M. S. Seltzer and R. I. Jaffee, eds.) P. 42, Plenum Press, N.Y. (1973).

[24] N. G. Eror: Ph.D. Thesis, Northwestern University, (1965).

[25] P. Kofstad: Phys.Chem.Solids. 23, 1579 (1962).

[26] K. Forland: Acta.Chem.Scand. 18, 1267 (1964).

[27] R. J. Panlener and R. N. Blumenthal: J.Amer.Ceram.Soc. 54 610 (1971).

[28] F. S. Glasso in "Structure, Properties and Preparation of Perovskite-type Compounds" P. 105, Pergamon Press, London (1969).

[29] H. M. O'Bryan, J. K. Plourde, J. Thomson, Jr., and D. F. Linn:

[30] S. Nomura: Ferroelectrics. 49, 61 (1983).

[31] S. Kawashima, M. Nishida, I. Veda and H. Ouchi: National Tech.Report. 28, 1108 (1982).

[32] S. Nomura, K. Toyama and K. Kaneta: Jpn.J.Appl.Phys. 21, L624 (1982).

[33] J. K. Plourde, D. F. Linn, H. M. O'Bryan and J. Thomson, Jr.: J.Amer.Ceram.Soc. 58, 418 (1975).

[34] D. J. Masse, R. A. Purcel, D. W. Readey, E. A. Maguire and C. P. Hartwig: Proc.IEEE. 59, 11, 1628 (1971).

[35] D. W. Readey, E. A. Maguire, C. P. Hartwig and D. J. Masse: Tech.Rept. ECOM-0455-F, June (1971).

[36] H. M. O'Bryan, Jr., J. K. Plourde, J. Thomson, Jr., and D. F. Linn: J.Amer.Ceram.Soc. 57, 10 450 (1974).

[37] S. Nomura, K. Tomaya and K. Kaneta: Jpn.J.Appl.Phys. 22, 1125 (1983).

[38] J. J. Ritter, R. S. Roth and J. E. Blendell: J.Amer.Ceram.Soc. 69, 2 155 (1986).

[39] D. E. Rase and R. Roy: J.Amer.Ceram.Soc. 38, 3 102 (1955).

[40] E. Tillmanns: Cryst.Struct.Comm. 11, 2087 (1982).

[41] F. W. Harrison: Acta Cryst. 9, 495 (1956).

[42] E. Tillmanns: Acta.Cryst. B30, 2894 (1974).

[43] E. Tillmanns and W. H. Baur: Acta.Cryst. B26, 1645 (1970).

[44] W. Hofmeister and E. Tillmanns: Acta.Cryst. C40, 1510 (1984).

[45] T. Negas, R. S. Roth, H. S. Parker and D. Minor: J. Solid State Chem. 9, 297 (1974).

[46] E. Tillmanns: Crysta.Struct.Comm. 11, 2087 (1982).

[47] E. Tillmanns, W. Hofmeiser and W. H. Baur: J. Solid State Chem. 58, 14 (1985).

[48] M. Herviev, G. Desgardin and B. Raveau: J. Solid State Chem. 30, 375 (1979).

[49] K. Lukaszewicz: Rocz.Chemi. 31, 1111 (1957).

[50] G. H. Jonker and W. Kwestroo: J.Amer.Ceram.Soc. 41, 10 390 (1958).

[51] H. M. O'Bryan, Jr., and J. Thomson, Jr.: J.Amer.Ceram.Soc. 57, 12 522 (1974).

[52] E. Tillmanns, W. G. Hofmeister and W. H. Baur: J.Amer.Ceram. Soc. 66, 268 (1983).

[53] E. Tillmanns: Acta.Cryst. B25, 8 1444 (1969).

[54] H. M. O'Bryan and J. Thomson: J. Amer.Ceram.Soc. 58, 9-10 454 (1975).

[55] H. Veith and Z. Angew: Phys. 20, 16 (1965).

[56] F. Kosek and H. Arend: Phys.Status.Solidi. 24, K69 (1967).

[57] S. A. Long and R. N. Blumenthal: J.Amer.Ceram.Soc. 54, 515 (1971).

[58] S. A. Long and R. N. Blumenthal: J.Amer.Ceram.Soc. 54, 577 (1971).

[59] N. H. Chan and D. M. Smyth: J.Amer.Ceram.Soc. 67, 4 285 (1984).

[60] W. Heywang: J.Amer.Ceram.Soc. 47, 484 (1964).

[61] A. M. J. H. Seuter: Philips Res. Rep. Suppl. 3, 36 (1974).

[62] N. G. Eror and D. M. Smyth: J. Solid State Chem: 24, 235 (1978).

[63] G. V. Lewis and C. R. A. Catlow: J. Phys. Chem. Solids. 47, 89-97 (1986).

[64] L. C. Walters and R. E. Grace: J.Phys.Chem.Solids. 28, 239 (1967).

[65] A. S. Shaikh and R. W. West: J.Amer.Ceram.Soc. 69, 689 (1986).

[66] N. H. Chan and D. M. Smyth: J. Electrochem.Soc. 123 1585 (1976).

[67] J. Daniels and K. H. Hardt: Philips Res. Repts. 31, 489 (1976).

[68] M. Pechini, U.S. Patent,3,330,697, "Method of preparing Lead and Alkaline Earth Titanates and Niobates Coating Method Using the Same to Form a Capacitor", July 11, 1967.

[69] L. J. Vander Pauw: Philips Res. Rept. 13, (1958).

[70] L. B. Valdes: Proc.Ire. 42, 420 (1954).

[71] C. E. Wicks and F. E. Block: Bureau of Mines, Bulletin No. 605, U.S. Govt. Printing Office , Washington D.C. (1963).

[72] M. Herviev, G. Desgardin and B. Raveau: J.Solid State Chem. 30, 375 (1979).

[73] L. Eyring and M. O'Keeffe in "The Chemistry of Extended Defects in Non-metallic Solids", North Holland, Amsterdam, (1970).

[74] L. A. Bursill, B. G. Hyde, O. Terasaki and A. Watanabe: Phil.Mag. 20, 347 (1969).

[75] J. R. Akse and H. B. White Hurst: J.Phys.Chem.Solids. 39, 457 (1978).

[76] T. I. Oh and N. G. Eror: To be published.

[77] L. A. Bursill and B. G. Hyde in "Progress in Solid State Chemistry" Vol. 7 Pergamon, London (1972).

[78] R. R. Merritt and B. G. Hyde: Phil.Trans.Roy.Soc.London Ser.A 274, 627 (1973).

APPENDIX

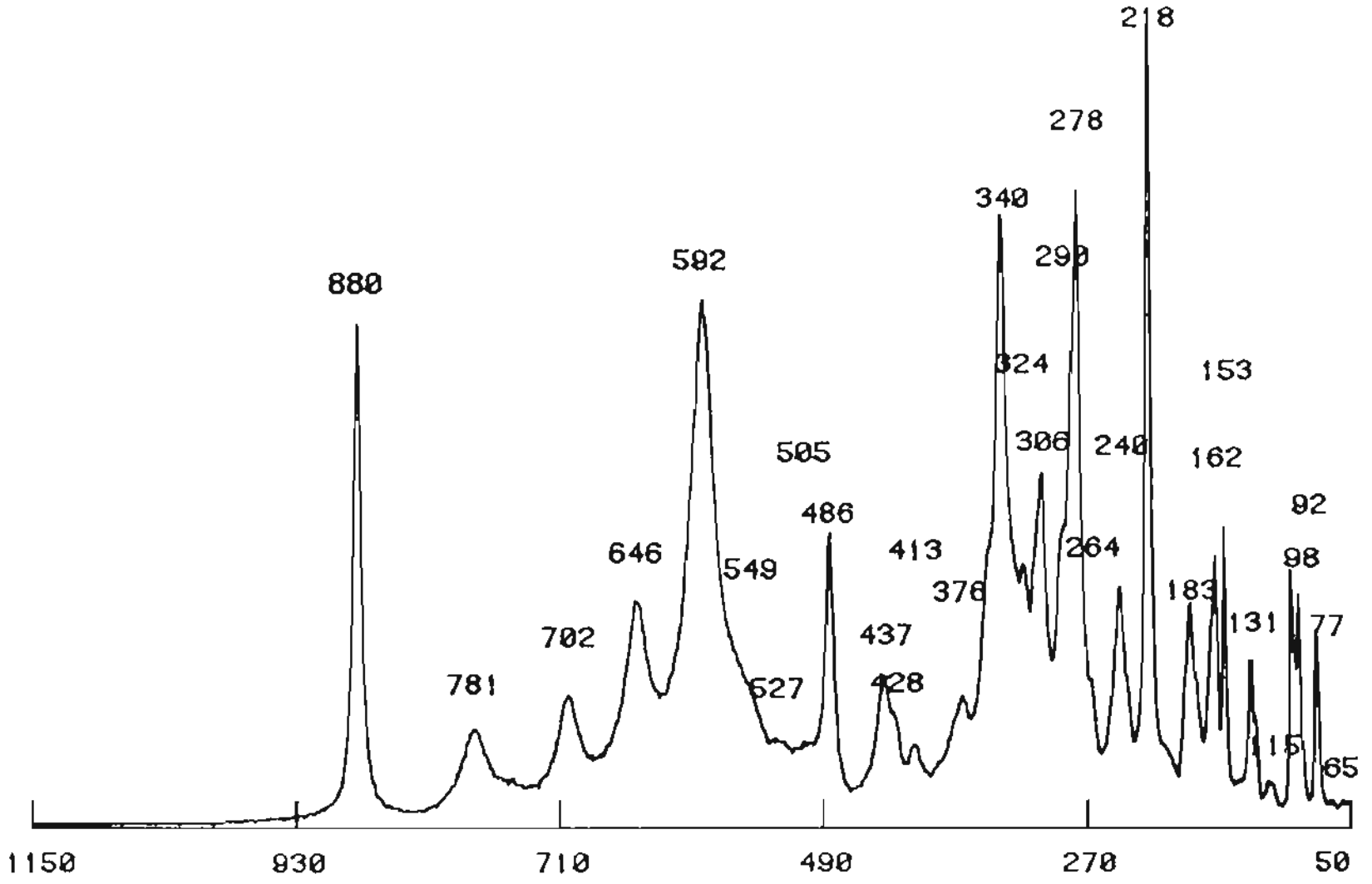

Figure 30. Raman spectrum of $BaTi_2O_5$ heated at 1300°C for one hr.

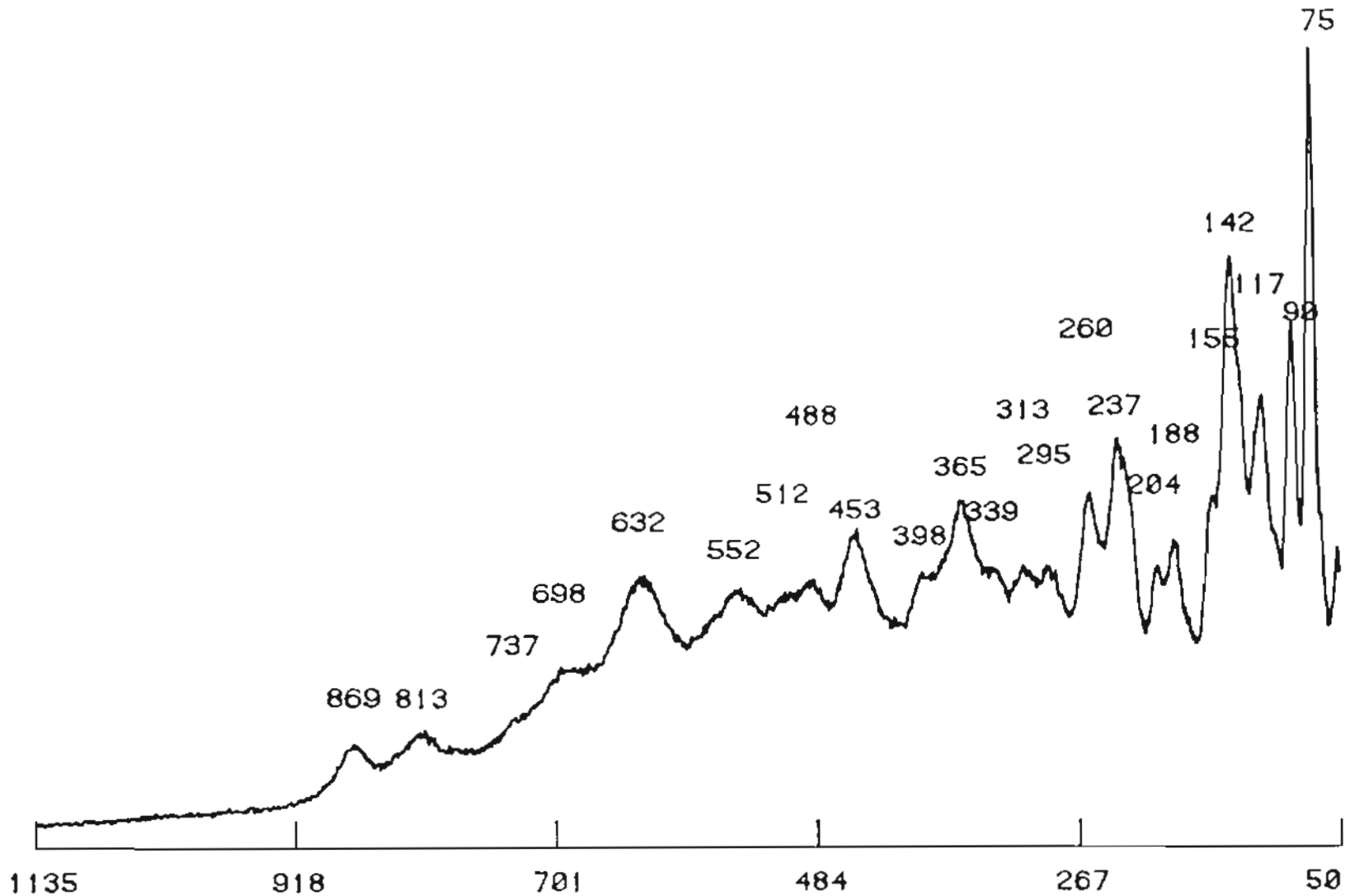

Figure 31. Raman spectrum of $Ba_6Ti_{17}O_{40}$ heated at 1200°C for 110 hrs.

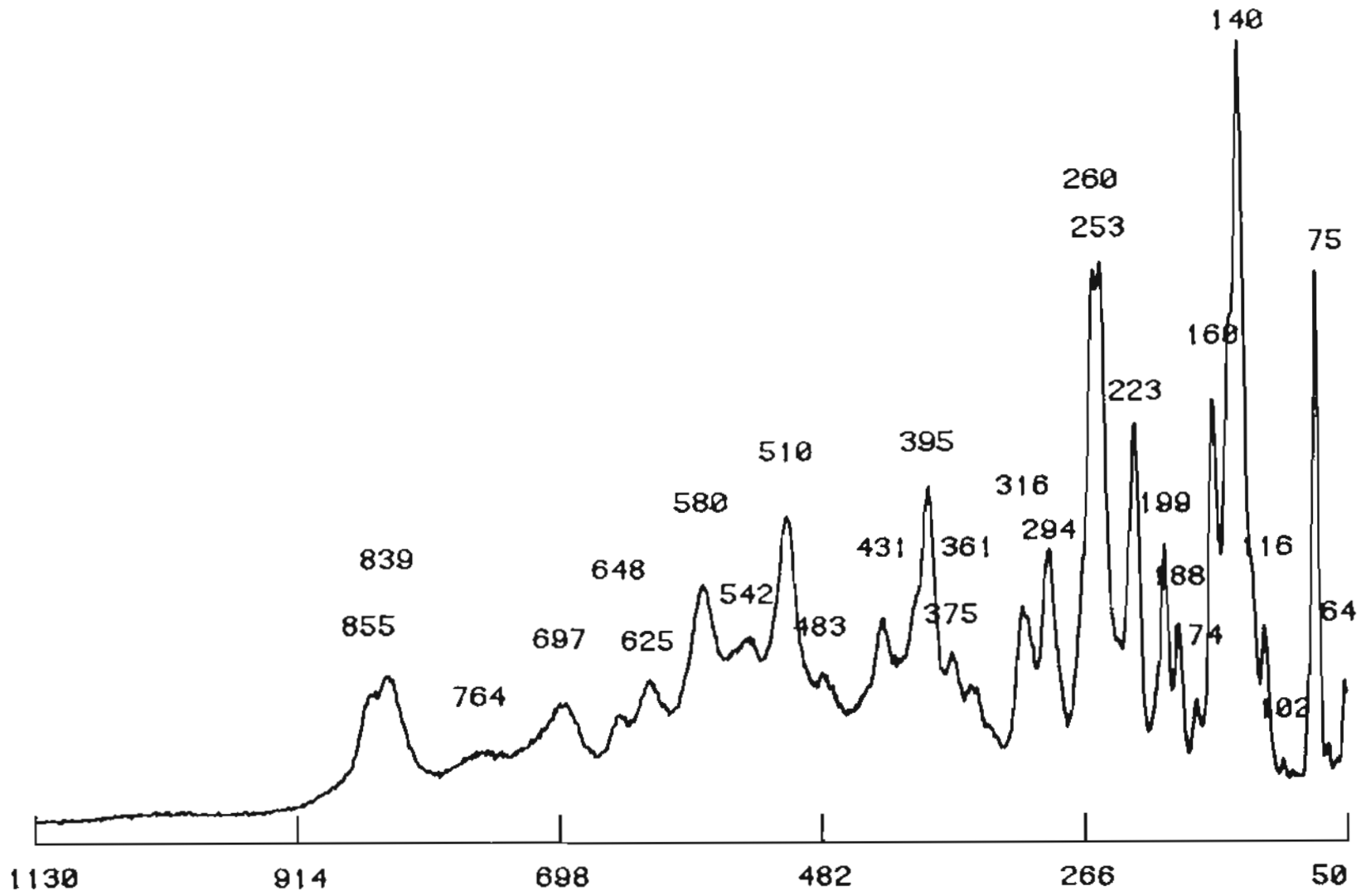

Figure 32. Raman spectrum of $Ba_4Ti_{13}O_{30}$ heated at 1300°C for 48 hrs.

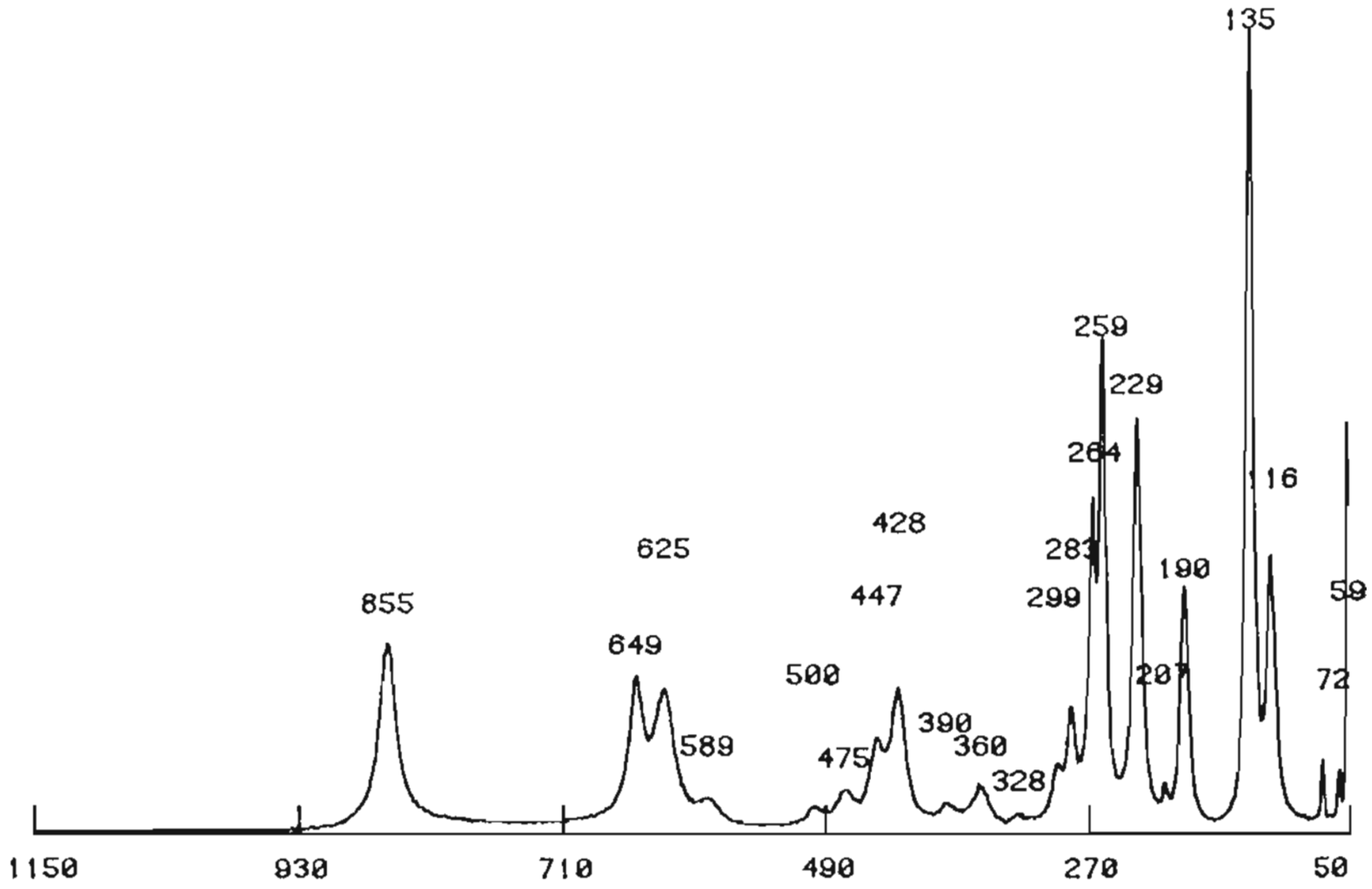

Figure 33. Raman spectrum of $BaTi_4O_9$ heated at 1300°C for one hr.

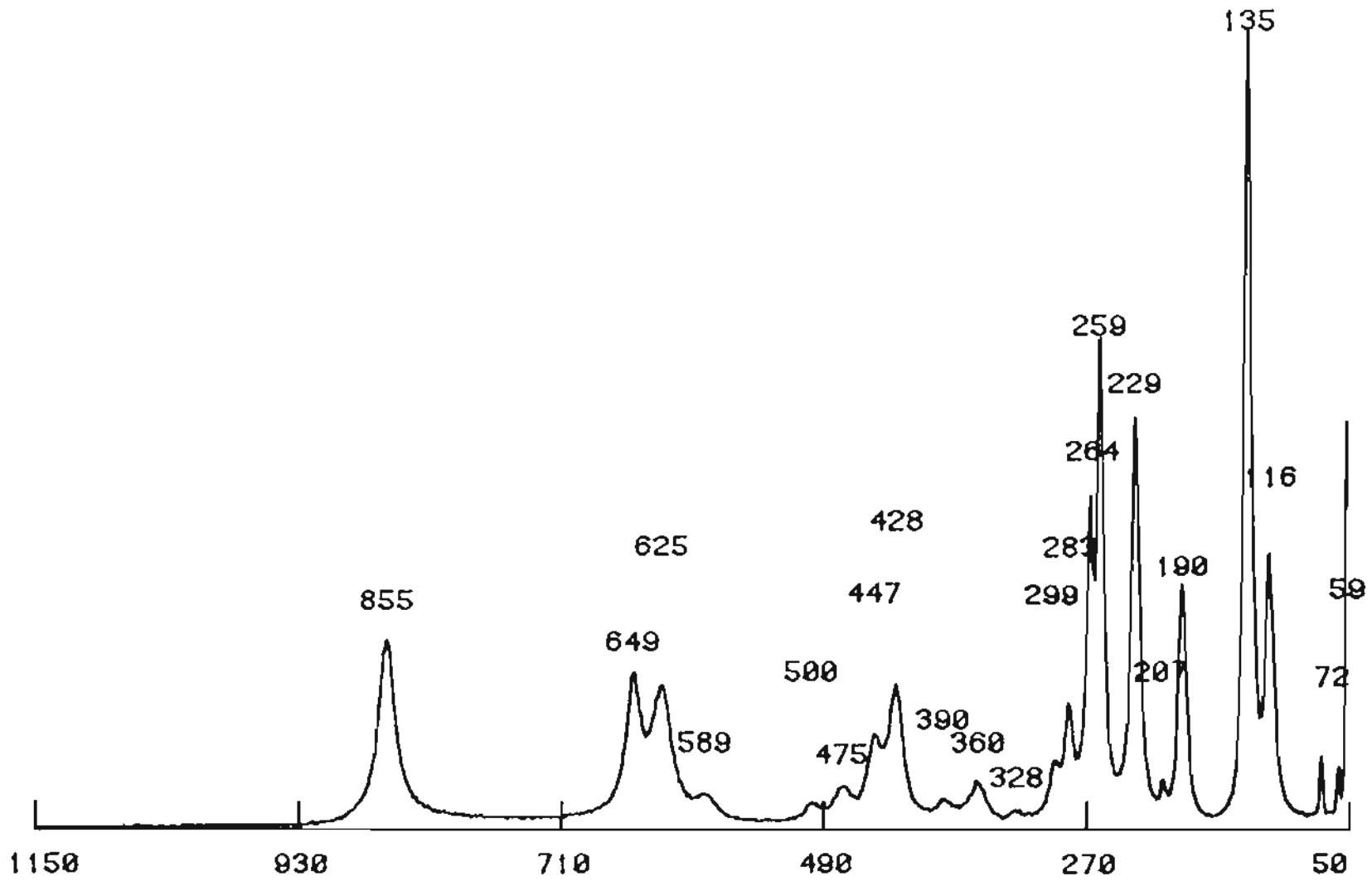

Figure 33. Raman spectrum of $BaTi_4O_9$ heated at 1300°C for one hr.

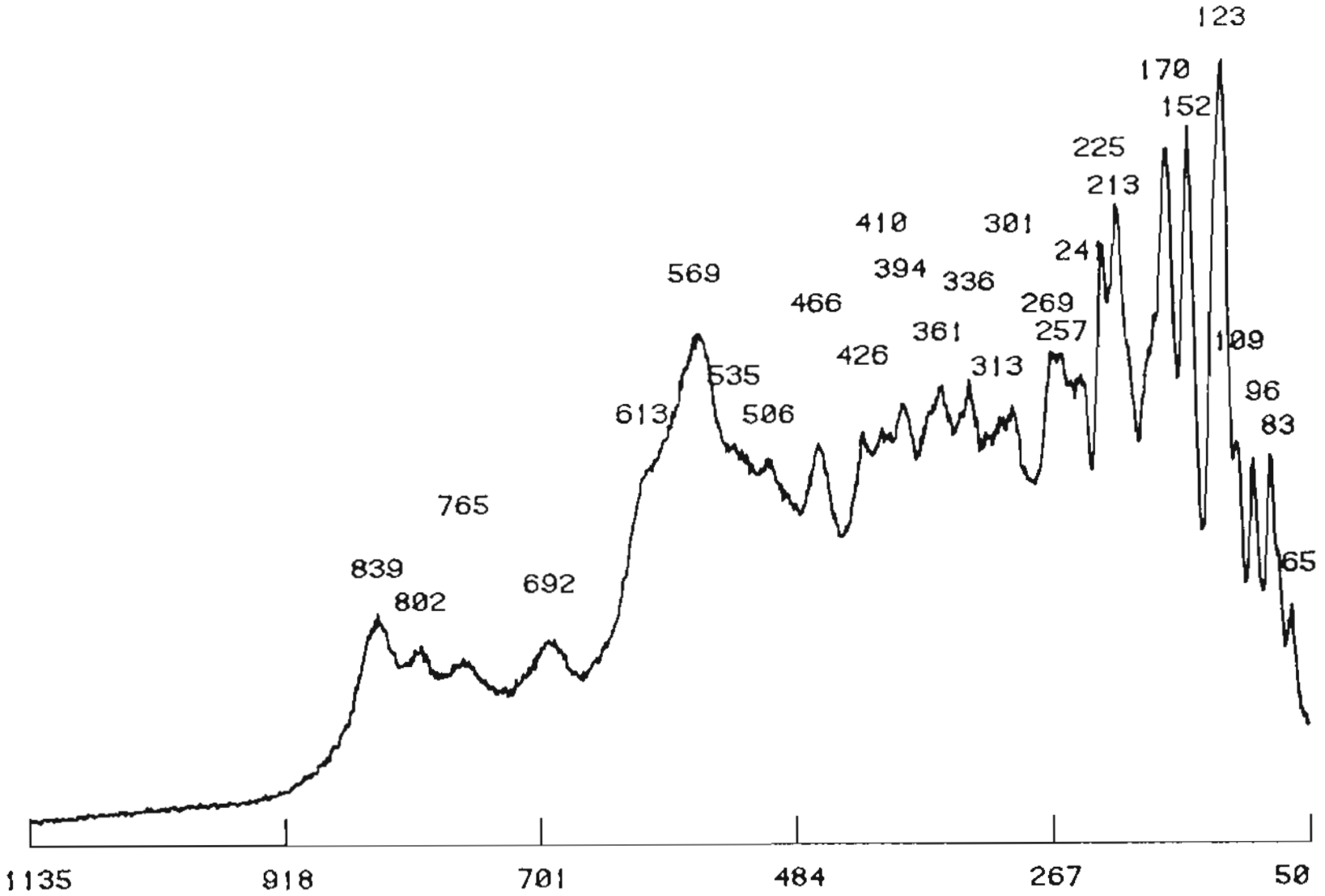

Figure 34. Raman spectrum of $Ba_2Ti_9O_{20}$ heated at 1200°C for 110 hrs.

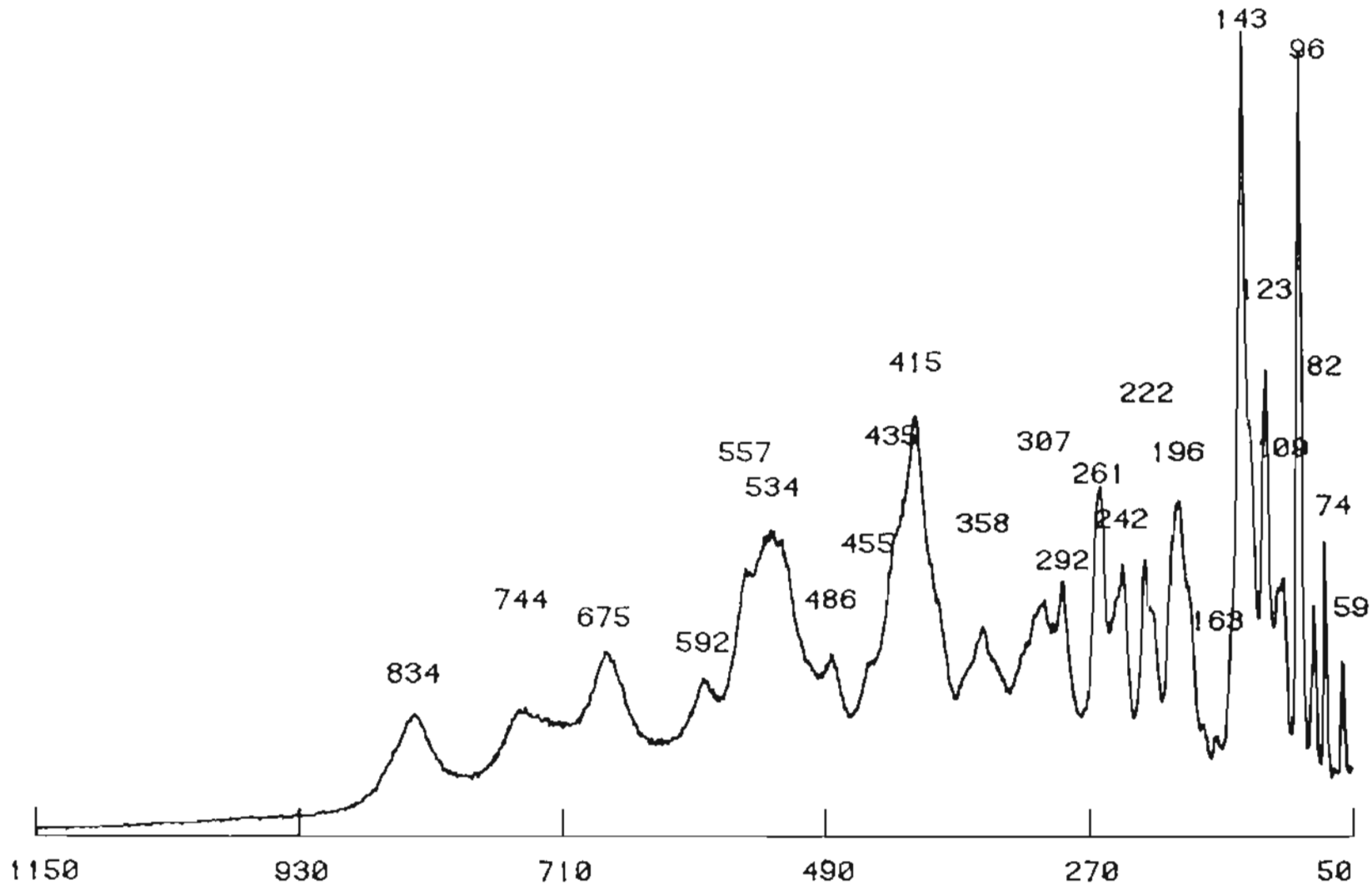

Figure 35. Raman spectrum of $BaTi_6O_{11}$ heated at 1100°C for 4 hrs.

VITA

The author was born on March 28, 1958 in Ardebil, Iran. He graduated from Nathan Hale High School in Seattle, Wash. in 1977. The author received his Bachelor and Master of Science degrees from State University of New York at Stony Brook in 1980 and 1983 respectively. In Sepember, 1983 he began his studies at Oregon Graduate Center where he completed the requirements for the Ph.D. degree in Materials Science and Engineering in January 1988.